NUREG/CR-4667, Vol. 31
ANL-01/09

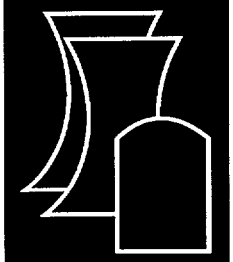

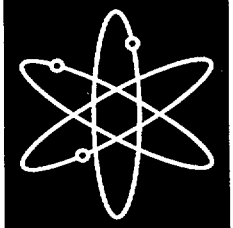

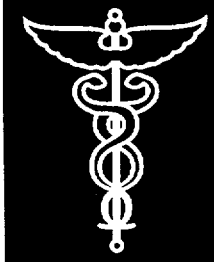

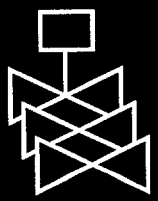

Environmentally Assisted Cracking in Light Water Reactors

Semiannual Report
July 2000 – December 2000

Argonne National Laboratory

U.S. Nuclear Regulatory Commission
Office of Nuclear Regulatory Research
Washington, DC 20555-0001

AVAILABILITY OF REFERENCE MATERIALS IN NRC PUBLICATIONS

NRC Reference Material

As of November 1999, you may electronically access NUREG-series publications and other NRC records at NRC's Public Electronic Reading Room at www.nrc.gov/NRC/ADAMS/index.html. Publicly released records include, to name a few, NUREG-series publications; *Federal Register* notices; applicant, licensee, and vendor documents and correspondence; NRC correspondence and internal memoranda; bulletins and information notices; inspection and investigative reports; licensee event reports; and Commission papers and their attachments.

NRC publications in the NUREG series, NRC regulations, and *Title 10, Energy*, in the Code of *Federal Regulations* may also be purchased from one of these two sources.

1. The Superintendent of Documents
   U.S. Government Printing Office
   Mail Stop SSOP
   Washington, DC 20402–0001
   Internet: bookstore.gpo.gov
   Telephone: 202-512-1800
   Fax: 202-512-2250
2. The National Technical Information Service
   Springfield, VA 22161–0002
   www.ntis.gov
   1–800–553–6847 or, locally, 703–605–6000

A single copy of each NRC draft report for comment is available free, to the extent of supply, upon written request as follows:

Address: Office of the Chief Information Officer,
Reproduction and Distribution
Services Section
U.S. Nuclear Regulatory Commission
Washington, DC 20555-0001
E-mail: DISTRIBUTION@nrc.gov
Facsimile: 301–415–2289

Some publications in the NUREG series that are posted at NRC's Web site address www.nrc.gov/NRC/NUREGS/indexnum.html are updated periodically and may differ from the last printed version. Although references to material found on a Web site bear the date the material was accessed, the material available on the date cited may subsequently be removed from the site.

Non-NRC Reference Material

Documents available from public and special technical libraries include all open literature items, such as books, journal articles, and transactions, *Federal Register* notices, Federal and State legislation, and congressional reports. Such documents as theses, dissertations, foreign reports and translations, and non-NRC conference proceedings may be purchased from their sponsoring organization.

Copies of industry codes and standards used in a substantive manner in the NRC regulatory process are maintained at—

The NRC Technical Library
Two White Flint North
11545 Rockville Pike
Rockville, MD 20852–2738

These standards are available in the library for reference use by the public. Codes and standards are usually copyrighted and may be purchased from the originating organization or, if they are American National Standards, from—

American National Standards Institute
11 West 42nd Street
New York, NY 10036–8002
www.ansi.org
212–642–4900

Legally binding regulatory requirements are stated only in laws; NRC regulations; licenses, including technical specifications; or orders, not in NUREG-series publications. The views expressed in contractor-prepared publications in this series are not necessarily those of the NRC.

The NUREG series comprises (1) technical and administrative reports and books prepared by the staff (NUREG–XXXX) or agency contractors (NUREG/CR–XXXX), (2) proceedings of conferences (NUREG/CP–XXXX), (3) reports resulting from international agreements (NUREG/IA–XXXX), (4) brochures (NUREG/BR–XXXX), and (5) compilations of legal decisions and orders of the Commission and Atomic and Safety Licensing Boards and of Directors' decisions under Section 2.206 of NRC's regulations (NUREG–0750).

NUREG/CR-4667, Vol. 31
ANL-01/09

Environmentally Assisted Cracking in Light Water Reactors

Semiannual Report
July 2000 – December 2000

Manuscript Completed: October 2001
Date Published: April 2002

Prepared by
O.K. Chopra, H.M. Chung, E.E. Gruber,
W.J. Shack, W.K. Soppet, and R.V. Strain

Argonne National Laboratory
9700 South Cass Avenue
Argonne, IL 60439

M.B. McNeil, NRC Project Manager

Prepared for
Division of Engineering Technology
Office of Nuclear Regulatory Research
U.S. Nuclear Regulatory Commission
Washington, DC 20555-0001
NRC Job Code W6610

Previous Documents in Series

Environmentally Assisted Cracking in Light Water Reactors Semiannual Report
April—September 1985, NUREG/CR–4667 Vol. I, ANL–86–31 (June 1986).
October 1985—March 1986, NUREG/CR–4667 Vol. II, ANL–86–37 (September 1987).
April—September 1986, NUREG/CR–4667 Vol. III, ANL–87–37 (September 1987).
October 1986—March 1987, NUREG/CR–4667 Vol. IV, ANL–87–41 (December 1987).
April—September 1987, NUREG/CR–4667 Vol. V, ANL–88–32 (June 1988).
October 1987—March 1988, NUREG/CR–4667 Vol. 6, ANL–89/10 (August 1989).
April—September 1988, NUREG/CR–4667 Vol. 7, ANL–89/40 (March 1990).
October 1988—March 1989, NUREG/CR–4667 Vol. 8, ANL–90/4 (June 1990).
April—September 1989, NUREG/CR–4667 Vol. 9, ANL–90/48 (March 1991).
October 1989—March 1990, NUREG/CR–4667 Vol. 10, ANL–91/5 (March 1991).
April—September 1990, NUREG/CR–4667 Vol. 11, ANL–91/9 (May 1991).
October 1990—March 1991, NUREG/CR–4667 Vol. 12, ANL–91/24 (August 1991).
April—September 1991, NUREG/CR–4667 Vol. 13, ANL–92/6 (March 1992).
October 1991—March 1992, NUREG/CR–4667 Vol. 14, ANL–92/30 (August 1992).
April—September 1992, NUREG/CR–4667 Vol. 15, ANL–93/2 (June 1993).
October 1992—March 1993, NUREG/CR–4667 Vol. 16, ANL–93/27 (September 1993).
April—September 1993, NUREG/CR–4667 Vol. 17, ANL–94/26 (June 1994).
October 1993—March 1994, NUREG/CR–4667 Vol. 18, ANL–95/2 (March 1995).
April—September 1994, NUREG/CR–4667 Vol. 19, ANL–95/25 (September 1995).
October 1994—March 1995, NUREG/CR–4667 Vol. 20, ANL–95/41 (January 1996).
April—December 1995, NUREG/CR–4667 Vol. 21, ANL–96/1 (July 1996).
January 1996—June 1996, NUREG/CR–4667 Vol. 22, ANL–97/9 (June 1997).
July 1996—December 1996, NUREG/CR–4667 Vol. 23, ANL–97/10 (October 1997).
January 1997—June 1997, NUREG/CR–4667 Vol. 24, ANL–98/6 (April 1998).
July 1997—December 1997, NUREG/CR–4667 Vol. 25, ANL–98/18 (September 1998).
January 1998—June 1998, NUREG/CR–4667 Vol. 26, ANL–98/30 (December 1998).
July 1998—December 1998, NUREG/CR–4667 Vol. 27, ANL–99/11 (October 1999).
January 1999—June 1999, NUREG/CR–4667 Vol. 28, ANL–00/7 (July 2000).
July 1999—December 1999, NUREG/CR–4667 Vol. 29, ANL–00/23 (November 2000).
January 2000—June 2000, NUREG/CR–4667 Vol. 30, ANL–01/08 (June 2001).

Environmentally Assisted Cracking in Light Water Reactors Semiannual Report July 2000–December 2000

by

O. K. Chopra, H. M. Chung, E. E. Gruber,
W. J. Shack, W. K. Soppet, and R. V. Strain

Abstract

This report summarizes work performed by Argonne National Laboratory on fatigue and environmentally assisted cracking (EAC) in light water reactors (LWRs) from July 2000 to December 2000. Topics that have been investigated include (a) environmental effects on fatigue S–N behavior of primary pressure boundary materials, (b) irradiation–assisted stress corrosion cracking (IASCC) of austenitic stainless steels (SSs), and (c) EAC of Alloys 600 and 690.

The fatigue strain-vs.–life data are summarized for the effects of various material, loading, and environmental parameters on the fatigue lives of carbon and low–alloy steels and austenitic SSs. Effects of the reactor coolant environment on the mechanism of fatigue crack initiation are discussed. Two methods for incorporating the effects of LWR coolant environments into the ASME Code fatigue evaluations are presented.

Slow-strain-rate tensile tests and posttest fractographic analyses were conducted on several model SS alloys irradiated to $\approx 0.9 \times 10^{21}$ n·cm^{-2} (E > 1 MeV) in He at 289°C in the Halden reactor. The results were used to determine the influence of alloying and impurity elements on the susceptibility of these steels to IASCC. A fracture toughness J–R curve test was conducted on a commercial heat of Type 304 SS that was irradiated to $\approx 2.0 \times 10^{21}$ n·cm^{-2} in the Halden reactor. The results were compared with the data obtained earlier on steels irradiated to 0.3 and 0.9×10^{21} n·cm^{-2} (E > 1 MeV) (0.45 and 1.35 dpa). Neutron irradiation at 288°C was found to decrease the fracture toughness of austenitic SSs.

Tests were conducted on compact-tension specimens of Alloy 600 under cyclic loading to evaluate the enhancement of crack growth rates in LWR environments. Then, the existing fatigue crack growth data on Alloys 600 and 690 were analyzed to establish the effects of temperature, load ratio, frequency, and stress intensity range on crack growth rates in air.

Contents

Figures

Tables

Executive Summary

The ASME Boiler and Pressure Vessel Code provides rules for the construction of nuclear power plant components. Appendix I to Section III of the Code specifies fatigue design curves for structural materials. However, the effects of light water reactor (LWR) coolant environments are not explicitly addressed by the Code design curves. Test data illustrate potentially significant effects of LWR environments on the fatigue resistance of carbon and low–alloy steels and austenitic stainless steels. The existing fatigue S–N data (strain vs. fatigue life) have been evaluated to establish the effects of various material and loading variables, such as steel type, strain range, strain rate, temperature, and dissolved–oxygen level in water, on the fatigue lives of these steels. Statistical models are presented for estimating the fatigue S–N curves for carbon and low–alloy steels and austenitic stainless steels as a function of material, loading, and environmental variables. The influence of reactor environments on the mechanism of fatigue crack initiation is discussed.

Two methods have been proposed for incorporating the effects of LWR coolant environments into the ASME Code fatigue evaluations: (a) develop new design fatigue curves for LWR applications and (b) use a fatigue life correction factor to account for environmental effects. Both methods are based on statistical models for estimating fatigue lives of carbon and low–alloy steels and austenitic SSs in LWR environments. Although estimates of fatigue lives based on the two methods may differ because of differences between the ASME mean curves used to develop the current design curves and the best–fit curves to the existing data used to develop the environmentally adjusted curves, either method provides an acceptable approach to account for environmental effects.

Hot-cell tests are being conducted to determine the susceptibility to irradiation-assisted stress corrosion cracking (IASCC) of model austenitic stainless steels (SSs) that were irradiated in the Halden Boiling Heavy Water Reactor in simulation of irradiation-induced degradation of core internal components in a boiling water reactor (BWR). Slow-strain-rate tensile tests in simulated BWR-like water were conducted on 23 model austenitic stainless steel alloys that were irradiated at 288°C in helium in the Halden reactor to a fluence of $\approx 0.9 \times 10^{21}$ n·cm^{-2} (E > 1 MeV). Fractographic analysis by scanning electron microscopy was conducted to determine the susceptibility to IASCC, as manifested by the degree of intergranular (IG) and transgranular (TG) fracture on the surface. These results were compared with similar test results obtained for 16 alloys that were irradiated to a fluence of $\approx 0.3 \times 10^{21}$ n·cm^{-2} (E > 1 MeV).

As fluence was increased from $\approx 0.3 \times 10^{21}$ n·cm^{-2} to $\approx 0.9 \times 10^{21}$ n·cm^{-2}, the IG fracture surfaces emerged in many austenitic SSs, usually in the middle of, and surrounded by, TG fracture surfaces. This observation indicates that the susceptibility to TGSCC at low fluence is related to the susceptibility to IGSCC at higher fluence.

The susceptibility to TGSCC at $\approx 0.3 \times 10^{21}$ n·cm^{-2} and to IGSCC at $\approx 0.9 \times 10^{21}$ n·cm^{-2} was strongly influenced by the bulk concentration of S in steel. This finding indicates that the strength of metallic bonding in grain matrices at low fluence and the bonding strength of grain boundaries at higher fluences are strongly influenced by the local concentration of S. At $\approx 2.0 \times 10^{21}$ n·cm^{-2}, Type 304 and 304L SS heats that contain very low concentrations of S ($\leq$0.002 wt.%) were not susceptible to IASCC, whereas heats that contain higher concentrations of S were susceptible.

Type 304L and 316L SSs that contained unusually low concentrations of Si (<0.05 wt.%) and that were irradiated either in the Halden reactor or in BWRs exhibited unusually high susceptibility to IASCC, even at low fluences.

A fracture toughness (J–R curve) test has been conducted on a commercial heat of Type 304 SS that was irradiated to a fluence level of 2.0×10^{21} n·cm^{-2} (E > 1 MeV) (≈3 dpa) at ≈288°C in a helium environment in the Halden reactor. The test was performed on a 1/4–T CT specimen in air at 288°C; crack extensions were determined by both DC–potential and elastic–unloading compliance techniques. The results of the test are consistent with the data obtained earlier on steels irradiated to 0.3 and 0.9×10^{21} n·cm^{-2} (E > 1 MeV) (0.45 and 1.35 dpa). The results indicate that neutron irradiation at 288°C decreases the fracture toughness of austenitic SSs. All of the CT specimen data from commercial heats fell within the scatter band for the data obtained at higher temperatures.

The resistance of Ni–alloys to EAC is being evaluated in simulated LWR environments. Existing data for the crack growth rate (CGR) of Alloys 600 and 690 under cyclic loads were analyzed to establish the effects of alloy chemistry, material heat treatment, cold work, temperature, load ratio, stress intensity, and dissolved oxygen (DO) level. The experimental CGRs in high–temperature, high–purity water were compared with CGRs that would be expected in air under the same mechanical loading conditions. The objective was to obtain a qualitative understanding of the degree and range of conditions that are necessary for significant environmental enhancement in growth rates. Several conclusions were reached. The fatigue CGRs of Alloy 600 are enhanced in high–DO water. The environmental enhancement of growth rates does not appear to depend on either the carbon content or heat treatment of the material. Also, in high–DO water, the CGRs at 320°C are comparable to those at 289°C. In low–DO water, environmental enhancement of CGRs of Alloy 600 seems to depend on material conditions, such as yield strength and grain boundary coverage of carbides. The data also suggest that materials with high yield strength and/or low grain boundary coverage of carbides exhibit enhanced CGRs. Correlations have been developed for estimating the enhancement of CGRs for Alloy 600 in LWR environments relative to the CGRs in air under the same loading conditions.

During the current reporting period, a CGR test was completed on a mill–annealed Alloy 600 specimen in high–purity water under different environmental and loading conditions. The growth rates from this test in high–DO water show good agreement with data obtained earlier. At 289°C, decreasing the DO content in water from ≈300 to < 10 ppb decreased the growth rates. The actual reduction in CGRs depends on the loading conditions. For loading conditions that correspond to $\approx 4 \times 10^{-12}$ m/s CGR in air, CGR in low–DO water is a factor of ≈7 lower than that in high–DO water. Also, the fracture mode changes from IG to TG cracking in low–DO water. The results also indicate that in low–DO water, growth rates increase with temperature. The CGRs at 320°C in water with < 10 ppb DO are comparable to those at 289°C in water with ≈ 300 ppb DO.

Acknowledgments

The authors thank T. M. Galvin, R. W. Clark, and J. Tezak (Argonne National Laboratory) for their contributions to the experimental effort. This work is sponsored by the Office of Nuclear Regulatory Research, U.S. Nuclear Regulatory Commission, under Job Code W6610; Program Manager: Dr. M. B. McNeil; Task 1 Manager: Dr. J. Muscara.

1 Introduction

The U.S. Nuclear Regulatory Commission (NRC) and its predecessor, the U.S. Atomic Energy Commission, have conducted research programs that address the aging of reactor components. The results of the research have been used to evaluate and establish regulatory guidelines to ensure acceptable levels of reliability for light water reactor (LWR) components. The products of this program have been technical reports, methodologies for evaluating licensee submittals, and other inputs to the regulatory process. Results have led to the resolution of regulatory issues, as well as to the development, validation, and improvement of regulations and regulatory guides. The present research on the effects of simulated reactor coolant environments on cracking of reactor components was initiated to resolve the remaining critical technical issues related to cracking phenomena in LWR components. Initially, this project addressed cracking of boiling water reactor (BWR) pipes. Subsequently, in response to requests from the NRC Office of Nuclear Reactor Regulation (NRR) for assistance in dealing with developing cracking problems in aging reactors, the focus shifted to other problems in environmentally assisted cracking (EAC) of LWR components.

The overall objective of this program is to provide data and physical models to be used by the NRC staff in assessing environmentally assisted degradation of primary pressure boundary components in LWRs. The research is divided into five tasks:

(a) *Environmental effects on fatigue, crack growth, and stress corrosion cracking*
Fatigue and EAC of piping, pressure vessels, and core components in LWRs are important concerns during plant operation and extended reactor lifetimes. The degradation processes in U.S. reactors include fatigue, intergranular stress corrosion cracking (IGSCC), and propagation of fatigue or stress corrosion cracks that initiate in the weld-sensitized heat-affected zones of stainless steel (SS) components. Occurrences of failures induced by mechanical–vibration and thermal-fluctuation fatigue in LWR plants have also been documented. The objective of this task is to improve fatigue design curves and assess the additivity of fatigue damage in piping and vessel steels under load histories that are typical of LWR components. Results of this work will be used to assess industry fatigue evaluations that are related to license renewal.

(b) *Component vulnerability to irradiation-assisted stress corrosion cracking*
Irradiation–assisted stress corrosion cracking (IASCC) of in–core components in both BWRs and pressurized water reactors (PWRs) is becoming a more common problem as reactors age. The general pattern of the observed failures indicates that as nuclear plants age and neutron fluence increases, many apparently nonsensitized austenitic materials become susceptible to intergranular failure by IASCC. Some of these failures have been reported for components that are subjected to relatively low or negligible stress levels, e.g., control–blade sheaths and handles and instrument dry tubes of BWRs. Although most failed components can be replaced, it would be very difficult or impractical to replace some safety–significant structural components, such as the BWR top guide, core plate, and shroud. The objective of this task is to provide data and models that are needed to assess industry analyses of the likelihood of degradation and failure of

core internal components that are due to IASCC, and to evaluate licensee submissions related to inspection and remediation.

(c) *Cracking of nickel alloy components of LWR primary systems*
Internal components of reactor vessels are made of Ni-based alloys, e.g., Alloys 600, X750, and 182, which are susceptible to IGSCC. The causes and mechanisms of this cracking are not adequately understood, and the uncertainty is increased when licensee submissions are evaluated for factors such as damage accumulation and inspection intervals. The objective of this task is to provide technical data on the effects of cracks in Ni–alloy components on the residual life, inspection, and repair of the component. The results will be used to support NRR staff assessments of industry crack–growth models, and potential detection and mitigation measures.

(d) *Analysis of postweld heat treatment processes and validation of flaw acceptance criteria*
The objective of this task is to evaluate the effect of postweld heat treatment on long–term resistance to environmental cracking by assessing sensitization and other microstructural changes. This evaluation will provide the NRC with insights for use in reviewing licensee submittals.

(e) *Assessment of industry crack-growth models*
This task has two objectives. The first is to perform an independent evaluation of industry models that are used to establish inspection intervals and repair criteria. The second objective is to perform more detailed analyses of flaw acceptance criteria.

2 Environmental Effects on Fatigue Strain-versus-Life (S–N) Behavior of Primary Pressure Boundary Materials (O. K. Chopra)

Experience with operating nuclear power plants worldwide reveals that many failures may be attributed to fatigue; examples include piping components, nozzles, valves, and pumps.[1–3] In most cases, these failures have been associated with thermal loading due to thermal stratification and striping, or mechanical loading due to vibratory loading. Significant thermal loadings due to flow stratification were not included in the original design–basis analysis. The effect of these loadings may also have been aggravated by corrosion effects due to a high–temperature aqueous environment.

2.1 Introduction

Cyclic loadings on a structural component occur because of changes in mechanical and thermal loadings as the system goes from one load set (e.g., pressure, temperature, moment, and force loading) to another. For each load set, an individual fatigue usage factor is determined by the ratio of the number of cycles anticipated during the lifetime of the component to the allowable cycles. Figures I–9.1 through I–9.6 of Appendix I to Section III of the ASME Boiler and Pressure Vessel Code specify design fatigue curves that define the allowable number of cycles as a function of applied stress amplitude. The cumulative usage factor (CUF) is the sum of the individual usage factors, and the ASME Code Section III requires that the CUF at each location must not exceed 1.

The fatigue design curves, given in Appendix I of Section III of the ASME Code, are based on strain–controlled tests of small polished specimens at room temperature in air. The fatigue design curves were developed from the best–fit curves of the experimental data by first adjusting for the effects of mean stress on fatigue life and then reducing the fatigue life at each point on the adjusted curve by a factor of 2 on strain or 20 on cycles, whichever was more conservative. As described in the Section III criteria document, these factors were intended to account for data scatter (heat–to–heat variability), effects of mean stress or loading history, and differences in surface condition and size between the test specimens and actual components. The factors of 2 and 20 are not safety margins but rather conversion factors that must be applied to the experimental data to obtain reasonable estimates of the lives of actual reactor components. However, because the mean fatigue curve used to develop the current Code design curve for austenitic stainless steels (SSs) does not accurately represent the available experimental data,[4,5] the current Code design curve for SSs includes a reduction of only ≈1.5 and 15 from the mean curve for the SS data, not the 2 and 20 originally intended.

As explicitly noted in Subsection NB–3121 of Section III of the Code, the data used to develop the design fatigue curves (Figs. I–9.1 through I–9.6 of Appendix I to Section III) did not include tests in the presence of corrosive environments that might accelerate fatigue failure. Article B–2131 in Appendix B to Section III states that the owner's design specifications should provide information about any reduction to design fatigue curves that has been necessitated by environmental conditions. Existing fatigue–strain–vs.–life (S–N) data illustrate potentially significant effects of LWR coolant environments on the fatigue resistance of carbon steels (CSs) and low–alloy steels (LASs),[6–18] as well as of austenitic SSs[5,18–28] (Fig. 1). Under certain environmental and loading conditions, fatigue lives of CSs can be a factor of 70 lower than in air.[7,15] Therefore, the margins in the ASME Code may be less conservative than originally intended.

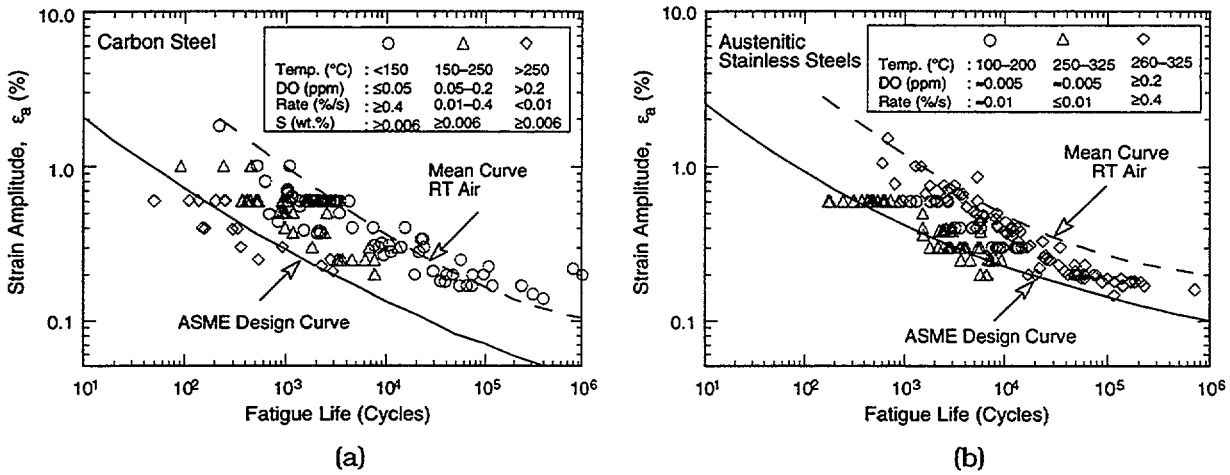

Figure 1. S–N data for (a) carbon steels and (b) austenitic stainless steels in water. RT = room temperature

A program was initiated at Argonne National Laboratory (ANL) to provide data and models for predicting environmental effects on fatigue design curves and an assessment of the validity of fatigue damage summation in piping and vessel steels under load histories typical of LWR components. The existing fatigue S–N data, both foreign and domestic, have been compiled and evaluated to establish the effects of key material, loading, and environmental parameters on the fatigue lives of carbon and low–alloy steels, wrought and cast austenitic SSs, and Alloy 600. Experimental data were obtained under conditions where information was lacking in the existing fatigue data base. As data have become available, correlations for the best–fit fatigue S–N curves have been developed and updated to include the effects of various parameters on fatigue life.

Based on the S-N data available at that time, interim fatigue design curves that address environmental effects on the fatigue life of carbon and low–alloy steels and austenitic SSs have been proposed by Majumdar et al.[29] More rigorous statistical models have been developed by Keisler et al.[30,31] based on a larger data base than that which was available when the interim design curves were developed. Results of the statistical analysis have also been used to interpret S–N curves in terms of the probability of fatigue cracking. The Idaho National Engineering Laboratory (INEL) assessed the significance of the interim fatigue design curves, developed by ANL, by performing fatigue evaluations of a sample of components in the reactor coolant pressure boundary.[32] In all, components from six locations at facilities designed by each of the four U.S. vendors of nuclear steam supply systems were evaluated. Selected components from older vintage plants designed under the B31.1 Code were also included in the evaluation. The design curves and statistical models for estimating fatigue lives in LWR environments have recently been updated for carbon and low–alloy steels[15–18] and austenitic SSs.[5,18–28]

Two approaches have been proposed for incorporating the effects of LWR environments into ASME Section III fatigue evaluations: (a) develop new fatigue design curves for LWR applications, and (b) use an environmental correction factor to account for the effects of the coolant environment. Both approaches are based on the existing fatigue S–N data in LWR environments, i.e., the best–fit curves to the experimental fatigue S–N data in LWR environments are used to obtain the design curves or environmental correction factor.

Environmentally adjusted fatigue design curves have been developed from the best fit to the experimental data in LWR environments by the same procedure that was used to develop the current fatigue design curves in the ASME Code. These curves provide allowable cycles for fatigue crack initiation in LWR coolant environments. The second approach, proposed initially by Higuchi and Iida,[7] considers the effects of reactor coolant environments on fatigue life in terms of an environmental correction factor F_{en}, which is the ratio of fatigue life in air at room temperature to that in water at reactor operating conditions. To incorporate environmental effects into the fatigue evaluations of the ASME Code, a fatigue usage for a specific load set, based on the current design curves, is multiplied by the correction factor. Specific expressions for F_{en}, based on the statistical models[5,15–18,33,34] and on the correlations developed by the Environmental Fatigue Data Committee of Thermal and Nuclear Power Engineering Society of Japan,[35] have been proposed.

This section summarizes the data available on the effects of various material, loading, and environmental parameters on the fatigue lives of ferritic steels and austenitic SSs. Effects of the reactor coolant environment on the mechanism of fatigue crack initiation are discussed. The two methods for incorporating the effects of LWR environments into the ASME Code fatigue evaluations are presented. Although estimates of fatigue lives based on the two methods may vary because of differences between the ASME mean curves used to develop the current design curves and the best–fit curves used to develop the environmentally adjusted curves, either method provides an acceptable approach to account for environmental effects. The fatigue S–N behavior of carbon and low–alloy steels in air and LWR environments has also been examined by a fracture mechanics approach and use of crack–growth–rate (CGR) data. Fatigue life is considered to be composed of the growth of microstructurally small cracks (MSCs) and mechanically small cracks. The growth of the latter has been characterized in terms of the J–integral range and CGR data in air and LWR environments.

2.2 Mechanism of Fatigue Crack Initiation

The formation of surface cracks and their growth as shear (Stage I) and tensile (Stage II) cracks to an engineering size (3 mm deep) constitute the fatigue life of a material, which is represented by the fatigue S–N curves. The curves specify, for a given stress or strain amplitude, the number of cycles needed to form an engineering crack. During fatigue loading of smooth test specimens, surface cracks 10 μm or longer form quite early in life (i.e., <10% of life) at surface irregularities or discontinuities either already in existence or produced by slip bands, grain boundaries, second–phase particles, etc.[15,36–40] Consequently, fatigue life may be considered to be composed entirely of crack propagation.[41]

Growth of these surface cracks may be divided into two regimes. The initial period (Stage I), which involves growth of MSCs, is very sensitive to microstructure and is characterized by decelerating crack growth (Region AB in Fig. 2). Next, the propagation period involves growth of mechanically small cracks, which can be predicted by fracture mechanics methodology and is characterized by accelerating crack growth (Region BC in Fig. 2). Mechanically small cracks, which correspond to Stage II, or tensile cracks, are characterized by striated crack growth and a fracture surface normal to the maximum principal stress. Conventionally, the initiation stage is considered sensitive to stress or strain amplitude, while the propagation stage is less sensitive to strain amplitude. The characterization and understanding of both crack initiation and propagation are important for obtaining accurate estimates of the fatigue lives of structural materials.

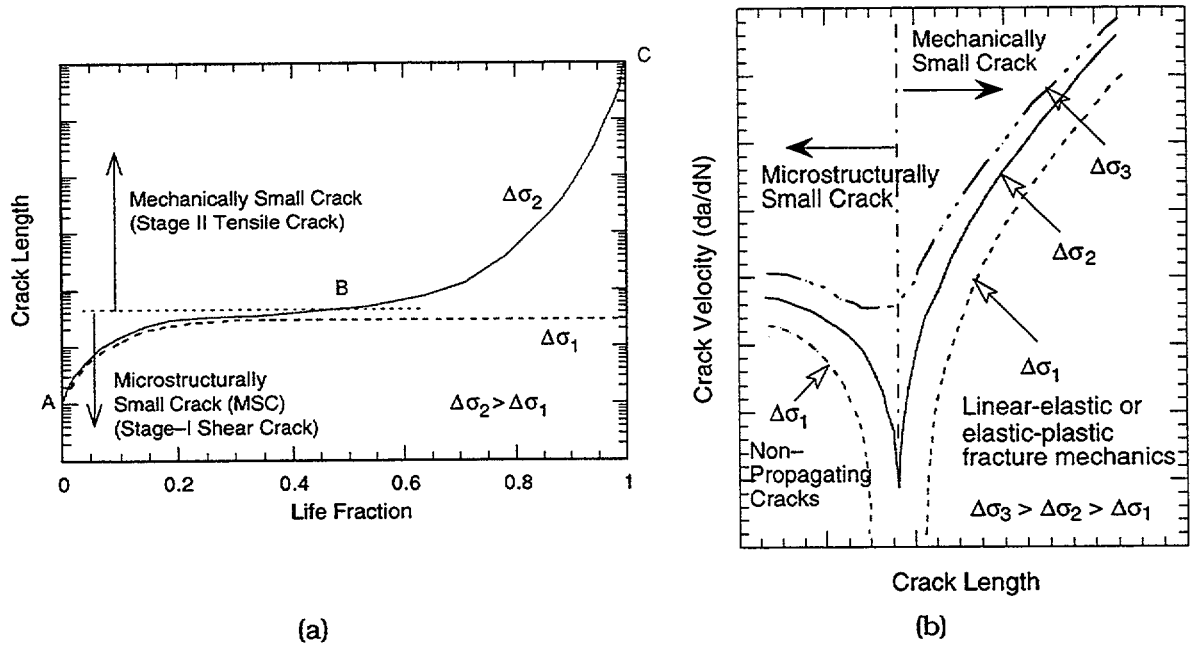

Figure 2. Schematic illustration of (a) growth of short cracks in smooth specimens as a function of fatigue life fraction and (b) crack velocity as a function of crack length

Studies on fatigue crack initiation in smooth test specimens[38,42] indicate that the decrease in fatigue life of pressure vessel and piping steels in LWR environments is caused primarily by the effects of the environment on the growth of microstructurally small cracks, i.e., cracks that are <300 μm deep. In LWR environments, the growth of these small fatigue cracks in carbon and low-alloy steels occurs by a slip oxidation/dissolution process. However, environmentally assisted reduction in the fatigue life of austenitic SSs is most likely caused by other mechanisms, such as hydrogen–enhanced crack growth.

To predict the fatigue lives of carbon and low-alloy steels in air and LWR environments, we used a fracture mechanics approach in which fatigue life is considered to consist of the growth of MSCs and mechanically small cracks. The growth of the MSCs is very sensitive to microstructure and is characterized by decelerating crack growth, that of mechanically small cracks, which can be predicted by the fracture mechanics methodology, is characterized by accelerating crack growth. It has also been characterized in terms of the J–integral range (ΔJ) and CGR data in air and LWR environments.

The growth of MSCs is expressed by a modified Hobson relationship in air and by the slip dissolution/oxidation process in water. The crack length for transition from microstructurally to mechanically small cracks was based on studies of small crack growth. Fatigue lives estimated from the present model show good agreement with the experimental data for carbon and low–alloy steels in air and LWR environments. At low strain amplitudes (i.e., fatigue lives of $>10^4$ cycles), the predicted lives in water are slightly lower than those observed experimentally, most likely because of the effects of crack closure.

2.3 Overview of Fatigue S–N Data

2.3.1 Carbon and Low–Alloy Steels

The fatigue lives of both CSs and LASs are decreased in LWR environments; the reduction depends on temperature, strain rate, DO level in water, and S content of the steel. The fatigue S–N data obtained at ANL on carbon and low–alloy steels are summarized in Appendix A, Tables A1–A4. Fatigue life is decreased significantly when four conditions are satisfied simultaneously, viz., strain amplitude, temperature, and DO in water are above a minimum level, and strain rate is below a threshold value. The S content in the steel is also important; its effect on life depends on the DO level in water. Although the microstructures and cyclic–hardening behavior of CSs and LASs differ significantly, environmental degradation of fatigue lives of these steels is very similar. For both steels, only a moderate decrease in life (by a factor of <2) is observed when any one of the threshold conditions is not satisfied. The effects of the critical parameters on fatigue life and their threshold values are summarized below.

(a) *Strain:* A minimum threshold strain is required for an environmentally assisted decrease in fatigue lives of CSs and LASs.[15–18] Limited data suggest that the threshold value is ≈20% higher than the fatigue limit for the steel. Figure 3 shows the results from fatigue tests conducted at constant strain range and from exploratory tests conducted with waveforms in which the slow strain rate is applied during only a fraction of the tensile loading cycle. Both types of test yield similar values for threshold strain.[15] The data from the exploratory tests indicate that loading histories with slow strain rate applied near maximum compressive strain produce no damage (line AD in Fig. 3) until the fraction of the strain is sufficiently large that slow strain rates are occurring for strain amplitudes greater than the threshold. The relative damage due to the slow strain rate is independent of strain amplitude once the amplitude exceeds a threshold value. However, it is not known whether the threshold strain corresponds to the rupture strain of the surface oxide film.

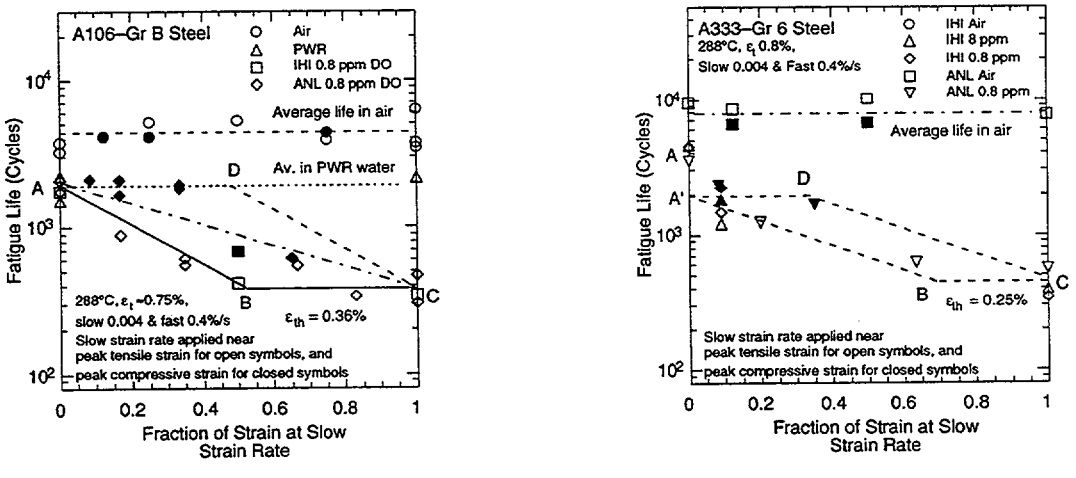

(a) (b)

Figure 3. Fatigue life of (a) A106–Gr B and (b) A333–Gr 6 carbon steels tested with loading waveforms, where a slow strain rate is applied during fraction of tensile loading cycle. IHI = Ishikawajima–Harima Heavy Industries Co., Japan.

(b) *Strain Rate*: Environmental effects on fatigue life occur primarily during the tensile-loading cycle and at strain levels greater than the threshold value. When any one of the threshold conditions is not satisfied, e.g., DO <0.05 ppm or temperature <150°C, the effects of strain rate are consistent with those in air, i.e., only the heats that are sensitive to strain rate in air show a decrease in life in water. When all other threshold conditions are satisfied, fatigue life decreases logarithmically with decreasing strain rate below 1%/s;[7,11,43] the effect of environment on life saturates at ≈0.001%/s.[15–18] The dependence of fatigue life on strain rate for A106-Gr B CS and A533-Gr B LAS is shown in Fig. 4. For A533-Gr B steel, the fatigue life at a strain rate of 0.0004%/s in high-DO water (≈0.7 ppm DO) is lower by more than a factor of 40 than it is in air.

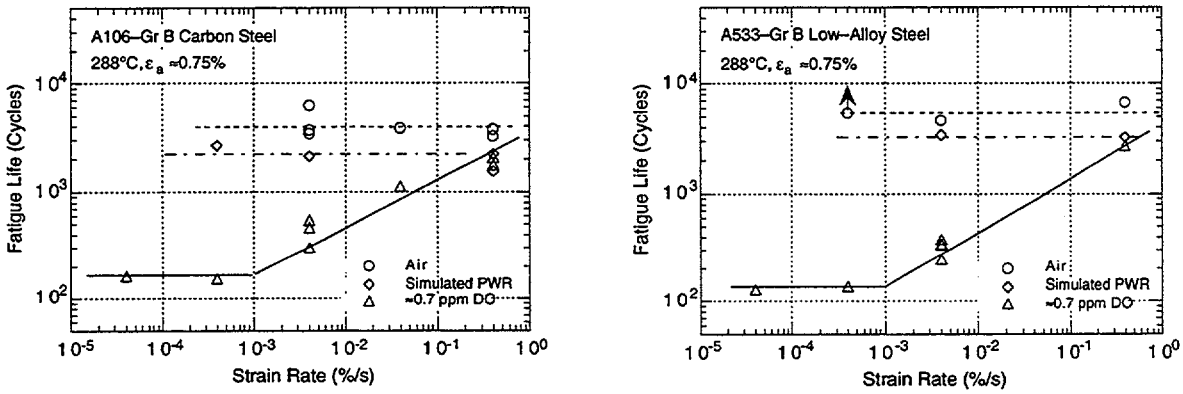

Figure 4. Dependence of fatigue lives of (a) carbon steel and (b) low-alloy steel on strain rate

(c) *Temperature*: When other threshold conditions are satisfied, fatigue life decreases linearly with temperature above 150°C and up to 320°C.[7,8,11] Fatigue life is insensitive to temperatures below 150°C or when any other threshold condition is not satisfied.

(d) *Dissolved Oxygen in Water*: When other threshold conditions are satisfied, fatigue life decreases logarithmically with DO above 0.05 ppm; the effect saturates at ≈0.5 ppm DO.[8,11] Fatigue life is insensitive to the DO level below 0.05 ppm or when any other threshold condition is not satisfied.

(e) *Sulfur Content of Steel*: The effect of the S content of steel on fatigue life depends on the DO content in water. When the threshold conditions are satisfied and DO contents are ≤1.0 ppm, the fatigue life decreases with increasing S content. Limited data suggest that the effects of environment on life saturate at a S content of ≈0.015 wt.%.[15] At high DO levels (e.g., >1.0 ppm), fatigue life seems to be insensitive to S content in the range of 0.002–0.015 wt.%.[44] When any one of the threshold conditions is not satisfied, environmental effects on life are minimal and relatively insensitive to changes in S content.

(f) *Flow Rate*: It has long been recognized that the flow rate may have a strong effect on the fatigue life of materials because it may cause differences in the local environmental conditions at the crack tip. However, information about the effects of flow rate has been very limited. Recent results indicate that under the

environmental conditions typical of operating BWRs, e.g., high-purity water at 289°C with ≈0.2 ppm DO, environmental effects on the fatigue life of CSs and LASs are a factor of ≈2 lower at high flow rates than the environmental effects under semistagnant conditions or very low flow rates. Data on A333-Gr 6 CS indicate that at 289°C, relatively slow strain rate (0.01%/s), and under all DO conditions, a high flow rate has an appreciable effect on the fatigue life of the steel.[45] In high-DO water (i.e., 0.2 ppm or higher) at 289°C, environmental effects on the fatigue life are a factor of ≈2 lower at a flow rate of 7 m/s than at 0.3 m/s. The results also indicate that flow rate has little or no effect at high strain rates (0.4%/s). Similar effects have also been observed in another study at Kraftwerk Union (KWU) laboratories on A508 carbon steel pipe; environmental effects on fatigue life were a factor of ≈2 lower at a flow rate of 0.6 m/s than those at very low flow.[46]

2.3.2 Austenitic Stainless Steels

The fatigue lives of austenitic SSs are decreased in LWR environments; the reduction depends on strain rate, level of DO in water, and temperature.[18,22,26-28] The fatigue S-N data obtained at ANL on austenitic SSs and cast austenitic SSs are summarized in Appendix A, Tables A5-A7. The effects of LWR environments on fatigue life of wrought materials are comparable for Types 304, 316, and 316NG SS. Although the fatigue lives of cast SSs are relatively insensitive to changes in ferrite content in the range of 12-28%,[22] the effects of loading and environmental parameters on the fatigue life of cast SSs differ somewhat. The significant results and threshold values of critical parameters are summarized below.

(a) *Dissolved Oxygen in Water*: For wrought austenitic SSs, environmental effects on fatigue life are more pronounced in low-DO (i.e., <0.01 ppm), than in high-DO (i.e., ≥0.1 ppm), water.[22,28] In high-DO water, environmental effects are moderate (less than a factor of 2 decrease in life) when conductivity is maintained at <0.1 μS/cm, and electrochemical potential (ECP) of the steel has reached a stable value (Fig. 5). For fatigue tests in high-DO water, the SS specimens must be soaked for 5-6 days for the ECP of the steel to stabilize. Figure 5 shows that, although fatigue life is decreased by a factor of ≈2 when the conductivity of water is increased from ≈0.07 to 0.4 μS/cm, the length of presoaking appears to have a greater effect on life than does the conductivity of water. For Type 304 SS in low-DO water, the addition of lithium and boron, low conductivity, preexposure for ≈5 days prior to the test, or dissolved hydrogen have no effect on fatigue life (Table 1).

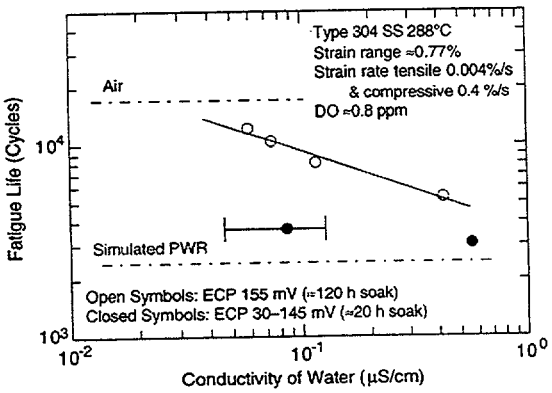

Figure 5.
Effects of conductivity of water and soak period on fatigue lives of Type 304 SS in high-DO water

Table 1. Fatigue test[a] results for Type 304 austenitic SS at 288°C

Test No.	Dis. Oxygen[b] (ppb)	Dis. Hydrogen (cc/kg)	Li (ppm)	Boron (ppm)	Pre-soak (days)	pH at RT	Conductivity[c] (μS/cm)	ECP SS[b] mV (SHE)	Ten. Rate (%/s)	Stress Range (MPa)	Strain Range (%)	Life N_{25} (Cycles)
1805	–	–	–	–	–	–	–	–	4.0E-3	467.9	0.76	14,410
1808	4	23	2	1000	1	6.4	18.87	–690	4.0E-3	468.3	0.77	2,850
1821	2	23	2	1000	1	6.5	22.22	–697	4.0E-3	474.3	0.76	2,420
1859	2	23	2	1000	1	6.5	18.69	–696	4.0E-3	471.7	0.77	2,420
1861	1	23	–	–	1	6.2	0.06	–614	4.0E-3	463.0	0.79	2,620
1862	2	23	–	–	5	6.2	0.06	–607	4.0E-3	466.1	0.78	2,450
1863	1	–	–	–	5	6.3	0.06	–540	4.0E-3	476.5	0.77	2,250
1871[d]	5	–	–	–	7	6.1	0.09	–609	4.0E-3	477.9	0.77	2,180

[a]Fully reversed axial fatigue tests at 288°C, ≈0.77% strain range, and sawtooth waveform.
[b]DO and ECPs measured in effluent.
[c]Conductivity of water measured in feedwater supply tank.
[d]Test conducted with a 2-min hold period at zero strain.

(b) *Strain:* Nearly all of the existing fatigue S–N data have been obtained under loading histories with constant strain rate, temperature, and strain amplitude. Actual loading histories encountered during service of nuclear power plants are far more complex. Exploratory fatigue tests have been conducted with waveforms in which the slow strain rate is applied during only a fraction of the tensile loading cycle.[23] The results indicate that a minimum threshold strain is required for the environmentally assisted decrease in fatigue lives of SSs to occur (Fig. 6). Limited data suggest that the threshold strain range is between 0.32 and 0.36%.[23,28]

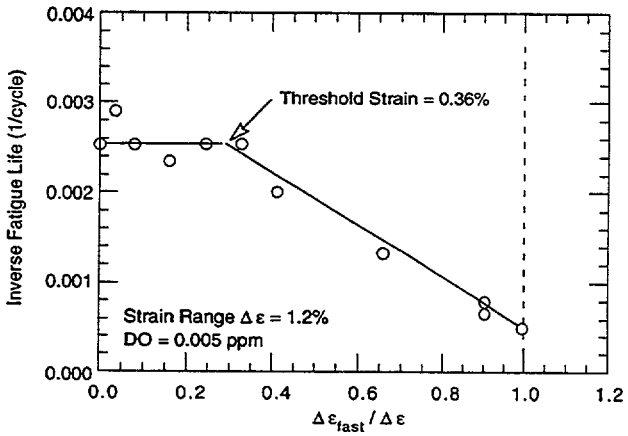

Figure 6.
Results of strain rate change tests on Type 316 SS in low–DO water at 325°C

During each fatigue cycle, relative damage due to the slow strain rate is the same once the strain amplitude exceeds a threshold value. However, data also indicate that threshold strain does not correspond to rupture strain of the surface oxide film. A fully reversed (R = –1) axial fatigue test was conducted with Type 304 SS at 288°C in high-purity water with <3 ppb DO, 0.75% strain range, sawtooth waveform with 0.004%/s tensile strain rate, and a 2–min hold period at zero strain during the tensile rise portion. The fatigue life was identical to that of tests conducted under similar loading conditions but without the hold period (Table 1). If this threshold strain corresponds to the rupture strain of the surface oxide film, a hold period at the middle of each cycle should allow repassivation of the oxide film, and environmental effects on fatigue life should diminish.

(c) *Strain Rate*: In high-DO water (conductivity <0.1 μS/cm and stable ECP of the steel), fatigue life is insensitive to changes in strain rate. In low-DO water, fatigue life decreases logarithmically with decreasing strain rate below ≈0.4%/s; the effect of environment on life saturates at ≈0.0004%/s for wrought SSs.[23,28]

(d) *Temperature*: Existing data are also too sparse to establish the effects of temperature on fatigue life over the entire range from room temperature to reactor operating temperatures. Limited data indicate that environmental effects on fatigue life are minimal below 200°C and significant above 250°C;[23] life appears to be relatively insensitive to changes in temperature in the range of 250–330°C. The Pressure Vessel Research Council (PVRC) steering committee for cyclic life and environmental effects (CLEE) has proposed a ramp function to describe temperature effects on the fatigue lives of austenitic SSs; environmental effects are moderate at temperatures below 180°C, are significant above 220°C, and increase linearly from 180 to 220°C.[47]

(e) *Flow Rate*: It is generally recognized that the flow rate most likely has a significant effect on the fatigue life of materials. However, fatigue S–N data that evaluate the effects of flow rate on the fatigue life of austenitic SSs are not available.

(f) *Cast Austenitic Stainless Steel*: The effects of loading and environmental parameters on the fatigue life of cast SSs differ somewhat from those for wrought SSs. For cast SSs, the fatigue lives are approximately the same in both high- or low-DO water and are comparable to those observed for wrought SSs in low-DO water.[28] Existing data are too sparse to define the saturation strain rate for cast SSs or to establish the dependence of temperature on the fatigue life in LWR environments; the effects of strain rate and temperature are assumed to be similar to those for wrought SSs.

2.4 Operating Experience in Nuclear Power Industry

Experience with operating nuclear power plants worldwide reveals that many failures may be attributed to fatigue; examples include piping components, nozzles, valves, and pumps.[1,2] In most cases, these failures have been associated with thermal loading due to thermal stratification and striping, or mechanical loading due to vibratory loading. Significant thermal loadings due to flow stratification were not included in the original design-basis analysis. The effect of these loadings may also have been aggravated by corrosion effects due to a high-temperature aqueous environment. Fatigue cracks have been observed in pressurizer surge lines in PWRs,[48] as well as feedwater lines connected to nozzles of pressure vessels in BWRs and steam generators in PWRs.[49,50] Significant occurrences of corrosion fatigue damage and failures in various nuclear power plant systems have been reviewed in an Electric Power Research Institute report;[51] the results are summarized below.

2.4.1 Cracking in Feedwater Nozzle and Piping

Fatigue cracks have been observed in feedwater piping and nozzles of the pressure vessel in BWRs and steam generators in PWRs.[3,49,50] The mechanism of cracking has been attributed to corrosion fatigue[52,53] or strain-induced corrosion cracking (SICC).[54] Case histories and identification of conditions that lead to SICC of LASs in LWR systems have been summarized by Hickling and Blind.[55]

In BWR nozzle cracking, initiation has been attributed to high–cycle fatigue caused by the leakage of cold water around the junction area of the thermal sleeve, and crack propagation has been attributed to low–cycle fatigue due to plant transients such as startups/shutdowns and any feedwater on/off transients. The frequency of the high–cycle fatigue phenomenon due to leakage around the sleeve is ≈0.5–1 Hz; therefore, it is not expected to be influenced by the reactor coolant environment. Estimates of strain range and strain rates for typical transients associated with low–cycle fatigue are given in Table 2.[56] Under these loading and environmental conditions, significant reduction in fatigue life has been observed for carbon and low–alloy steels.[15,17]

In PWR feedwater systems, cracking has been attributed to a combination of thermal stratification and thermal striping.[51] Environmental factors, such as high DO in the feedwater, are believed to also have played a significant role in crack initiation. The thermal stratification is caused by the injection of relatively cold feedwater at a low flow rate during plant startup, hot standby, and variations below 20% of full power, whereas thermal striping is caused by rapid, localized fluctuations at the interface between the hot and cold feedwater.

Table 2. Typical chemical and cyclic strain transients in feedwater (FW) components

Component	Operation	DO (ppb)	Temp. (°C)	Strain Range (%)	Strain Rate (%/s)
FW Nozzle	Startup	20/200	216/38	0.2-0.4	10^{-2}
FW Piping	Startup	20/200	216/38	0.2-0.5	10^{-3}–10^{-2}
FW Piping	Startup	20/200	288/38	0.07-0.1	4–8x10^{-6}
FW Piping	Turbine Roll	<200	288/80	0.4	3–6x10^{-3}
FW Piping	Hot Standby	<200	288/90	0.26	4x10^{-4}
FW Piping	Cool Down	<20	288/RT	0.2	6x10^{-4}
FW Piping	Stratification	200	250/50	0.2-0.7	10^{-4}–10^{-3}

Lenz et al.[54] showed that in feedwater lines, the strain rates are 10^{-3}–10^{-5} %/s due to thermal stratification and 10^{-1}%/s due to thermal shock, and that thermal stratification is the primary cause of crack initiation due to SICC. Also, the results from small–size specimens, medium–size components (model vessels), and full–size thermal–shock experiments suggest an influence of oxygen content in pressurized water on crack initiation.[3]

Several studies have been conducted at Electricité de France (EdF) to investigate the thermal and mechanical effects of stratification in pipes. Stephan and Masson[57] subjected a full–scale mock–up of the steam generator feedwater system to various regimes of stratification. After 4000 cycles of fatigue, destructive examination performed between two stable states of stratification revealed small cracks, 1.4–4.0 mm deep, in the weld region. The fatigue usage factors calculated with elastic and cyclic–elastic–plastic computations gave values of 1.3–1.9. However, because the average DO level in water was ≈5 ppb, which corresponds to the maximum admissible value under normal operating conditions in French PWRs, environmental effects on life are expected to be minimal, and environmental correction factors were not applied in the computations of the fatigue usage factor.

A detailed examination of cracking in a CS elbow adjacent to the steam–generator nozzle weld[58] indicates crack morphologies that are identical to those observed in smooth specimens tested in high–DO water. For example, the deepest crack was straight, nonbranching, transgranular through both the ferrite and pearlite regions without any preference, and showed significant oxidation and some pitting at the crack origin. In fatigue test specimens,

near–surface cracks grow entirely as tensile cracks normal to the stress and across both the soft ferrite and hard pearlite regions, whereas in air, cracks grow at an angle of 45° to the stress axis and only along the ferrite regions. The identical crack morphologies indicate that environment played a dominant role in crack initiation. Similar characteristics of transgranular crack propagation through both weld and base metal, without regard to microstructural features, have also been identified in German reactors.[55]

Tests have been conducted on components to validate the calculation procedures and the applicability of the test results from specimen to actual reactor component. Tests on pipes, plates, and nozzles under cyclic thermal loading in an aqueous environment[1] indicate that crack initiation in simulated LWR environments may occur earlier than indicated by the values of the fatigue design curve in ASME Section III; environmental effects are more pronounced in the ferritic steel than in the austenitic cladding. Tests performed at the reactor pressure vessel of the decommissioned HDR (Heissdampfreaktor)[59] have also shown good agreement between the fatigue lives applicable to specimens and components, e.g., first incipient crack on pipes appeared in 1200 cycles, compared with 1400 cycles for a test specimen made of the same material and tested under comparable conditions (8 ppm DO).

2.4.2 Girth Weld Cracking in Steam Generator

Another instance of thermal–fatigue–induced cracking where environmental effects are believed to have played a role in crack initiation has been observed at the weld joint between the two shells of a steam generator.[60] The feedwater temperature in this region is nominally 204–227°C (440–440°F), compared with the steam generator temperature of 288°C (550°C). The primary mechanism of cracking has been considered corrosion fatigue, with possible slow crack growth due to stress corrosion cracking. A detailed analysis of girth–weld cracking indicates that crack initiation was dominated by environmental influences, particularly under relatively high–DO content and/or oxidizing potential.[61]

2.4.3 PWR Primary System Leaks

Significant cracking has also occurred in unisolable pipe sections in the safety injection system piping connected to the PWR coolant system.[62,63] This phenomenon, which is similar to the nozzle cracking discussed above, is caused by thermal stratification. Also, regulatory evaluation has indicated that thermal stratification can occur in all PWR surge lines.[48] In PWRs, the pressurizer water is heated to ≈227°C (440°F). The hot water, flowing at a very slow rate from the pressurizer through the surge line to the hot–leg piping, rides on a cooler water layer. The thermal gradients between the upper and lower parts of the pipe can be as high as 149°C (300°F). Unisolable leaks due to thermal–stratification cycling have occurred in reactor–coolant loop drain lines and excess letdown lines at Three Mile Island, Oconee, Mihama, and Loviisa plants.[64] Thermal fatigue has caused leakage in the CVCS (chemical and volume control system) pipe of the regenerative heat exchanger at Tsuruga 2[65] and in the residual heat removal system of the Civaux 1 plant.[66]

Full–scale mock-up tests to generate thermal stratification in a pipe in a laboratory have confirmed the applicability of laboratory data to component behavior.[67] The material, loading, and environmental conditions were simulated on a 1:1 scale, taking into account only thermohydraulic effects. Under the loading conditions, i.e., strain rate and strain range typical

of thermal stratification in these piping systems, the coolant environment is known to have a significant effect on fatigue crack initiation.[17,22,23]

2.5 Incorporating Environmental Effects into Fatigue Evaluations

Two procedures have been proposed for incorporating the effects of LWR coolant environments into the ASME Section III fatigue evaluations: (a) develop a new set of environmentally adjusted design fatigue curves[5,15,17,18,28] or (b) use a fatigue life correction factor (F_{en}) to adjust the current ASME Code fatigue usage values for environmental effects.[5,17,18,33,34] For both approaches, the range and bounding values must be defined for key service parameters that influence fatigue life. Estimates of fatigue life based on the two methods may differ because of differences between the ASME mean curves used to develop the current design curves and the best-fit curves to the existing data that are used to develop the environmentally adjusted curves. However, either of these methods provides an acceptable approach to account for environmental effects.

2.5.1 Design Fatigue Curves

A set of environmentally adjusted design fatigue curves can be developed from the best-fit stress-vs.-life curves to the experimental data in LWR environments by employing the same procedure that was used to develop the current design fatigue curves in the ASME Code. The stress-vs.-life curves are obtained from the S-N curves, where stress amplitude is the product of strain amplitude and elastic modulus. The best-fit experimental curves are first adjusted for the effect of mean stress by using the modified Goodman relationship:

$$S'_a = S_a\left(\frac{\sigma_u - \sigma_y}{\sigma_u - S_a}\right) \qquad \text{for } S_a < \sigma_y, \tag{1}$$

and

$$S'_a = S_a \qquad \text{for } S_a > \sigma_y, \tag{2}$$

where S'_a is the adjusted value of the stress amplitude, and σ_y and σ_u are the yield and ultimate strengths of the material, respectively. Equations 1 and 2 assume the maximum possible mean stress and typically give a conservative adjustment for mean stress, at least when environmental effects are not significant. The design fatigue curves are then obtained by lowering the adjusted best-fit curve by a factor of 2 on stress or 20 on cycles, whichever is more conservative, to account for differences and uncertainties in fatigue life that are associated with material and loading conditions.

Statistical models based on the existing fatigue S-N data have been developed for estimating the fatigue lives of pressure vessel and piping steels in air and LWR environments.[15,17,18,28] In room-temperature air, the fatigue life (N) of CSs is represented by

$$\ln(N) = 6.564 - 1.975 \ln(\varepsilon_a - 0.113) \tag{3}$$

and of LASs by

$$\ln(N) = 6.627 - 1.808 \ln(\varepsilon_a - 0.151), \tag{4}$$

where ε_a is applied strain amplitude (%). In LWR environments, the fatigue life of CSs is represented by

$$\ln(N) = 6.010 - 1.975 \ln(\varepsilon_a - 0.113) + 0.101\, S^*\, T^*\, O^*\, \dot{\varepsilon}^* \quad (5)$$

and of LASs, by

$$\ln(N) = 5.729 - 1.808 \ln(\varepsilon_a - 0.151) + 0.101\, S^*\, T^*\, O^*\, \dot{\varepsilon}^*. \quad (6)$$

In Eqs. 5 and 6, S^*, T^*, O^*, and $\dot{\varepsilon}^*$ are transformed S content, temperature, DO, and strain rate, respectively, defined as follows:

$$\begin{aligned} S^* &= 0.015 && \text{(DO} > 1.0 \text{ ppm)} \\ S^* &= S && \text{(DO} \le 1.0 \text{ ppm and } 0 < S \le 0.015 \text{ wt.\%)} \\ S^* &= 0.015 && \text{(DO} \le 1.0 \text{ ppm and } S > 0.015 \text{ wt.\%)} \end{aligned} \quad (7)$$

$$\begin{aligned} T^* &= 0 && (T < 150°C) \\ T^* &= T - 150 && (T = 150\text{–}350°C) \end{aligned} \quad (8)$$

$$\begin{aligned} O^* &= 0 && (DO \le 0.04 \text{ ppm}) \\ O^* &= \ln(DO/0.04) && (0.04 \text{ ppm} < DO \le 0.5 \text{ ppm}) \\ O^* &= \ln(12.5) && (DO > 0.5 \text{ ppm}) \end{aligned} \quad (9)$$

$$\begin{aligned} \dot{\varepsilon}^* &= 0 && (\dot{\varepsilon} > 1\%/s) \\ \dot{\varepsilon}^* &= \ln(\dot{\varepsilon}) && (0.001 \le \dot{\varepsilon} \le 1\%/s) \\ \dot{\varepsilon}^* &= \ln(0.001) && (\dot{\varepsilon} < 0.001\%/s). \end{aligned} \quad (10)$$

In air at room temperature, the fatigue data for Types 304 and 316 SS are best represented by

$$\ln(N) = 6.703 - 2.030 \ln(\varepsilon_a - 0.126) \quad (11)$$

and for Type 316NG, by

$$\ln(N) = 7.422 - 1.671 \ln(\varepsilon_a - 0.126). \quad (12)$$

In LWR environments, fatigue data for Types 304 and 316 SS are best represented by

$$\ln(N) = 5.768 - 2.030 \ln(\varepsilon_a - 0.126) + T'\, \dot{\varepsilon}'\, O' \quad (13)$$

and for Type 316NG, by

$$\ln(N) = 6.913 - 1.671 \ln(\varepsilon_a - 0.126) + T'\, \dot{\varepsilon}'\, O', \quad (14)$$

where T', $\dot{\varepsilon}'$, and O' are transformed temperature, strain rate, and DO, respectively, defined as follows:

$$
\begin{aligned}
T' &= 0 && (T < 180°C) \\
T' &= (T - 180)/40 && (180 \le T < 220°C) \\
T' &= 1 && (T \ge 220°C) \qquad (15)
\end{aligned}
$$

$$
\begin{aligned}
\dot{\varepsilon}' &= 0 && (\dot{\varepsilon} > 0.4\%/s) \\
\dot{\varepsilon}' &= \ln(\dot{\varepsilon}/0.4) && (0.0004 \le \dot{\varepsilon} \le 0.4\%/s) \\
\dot{\varepsilon}' &= \ln(0.0004/0.4) && (\dot{\varepsilon} < 0.0004\%/s) \qquad (16)
\end{aligned}
$$

$$
\begin{aligned}
O' &= 0.260 && (DO < 0.05 \text{ ppm}) \\
O' &= 0 && (DO \ge 0.05 \text{ ppm}). \qquad (17)
\end{aligned}
$$

The models are recommended for predicted fatigue lives of $\le 10^6$ cycles. The design fatigue curves were obtained from the best–fit curves, represented by Eqs. 3–6 for CSs and LASs, and by Eqs. 11 and 13 for austenitic SSs. To be consistent with the current ASME Code philosophy, the best–fit curves were first adjusted for the effect of mean stress by using the modified Goodman relationship, and the mean–stress–adjusted curves were then decreased by a factor of 2 on stress and 20 on cycles to obtain the design fatigue curves.

The new design fatigue curves for CSs and LASs and austenitic SS in air are shown in Fig. 7, and those in various LWR coolant environments are shown in Figs. 8–11, which represent only the portions of the environmentally adjusted curves that fall below the current ASME Code curve. Because the fatigue life of Type 316NG is superior to that of Types 304 or 316 SS,

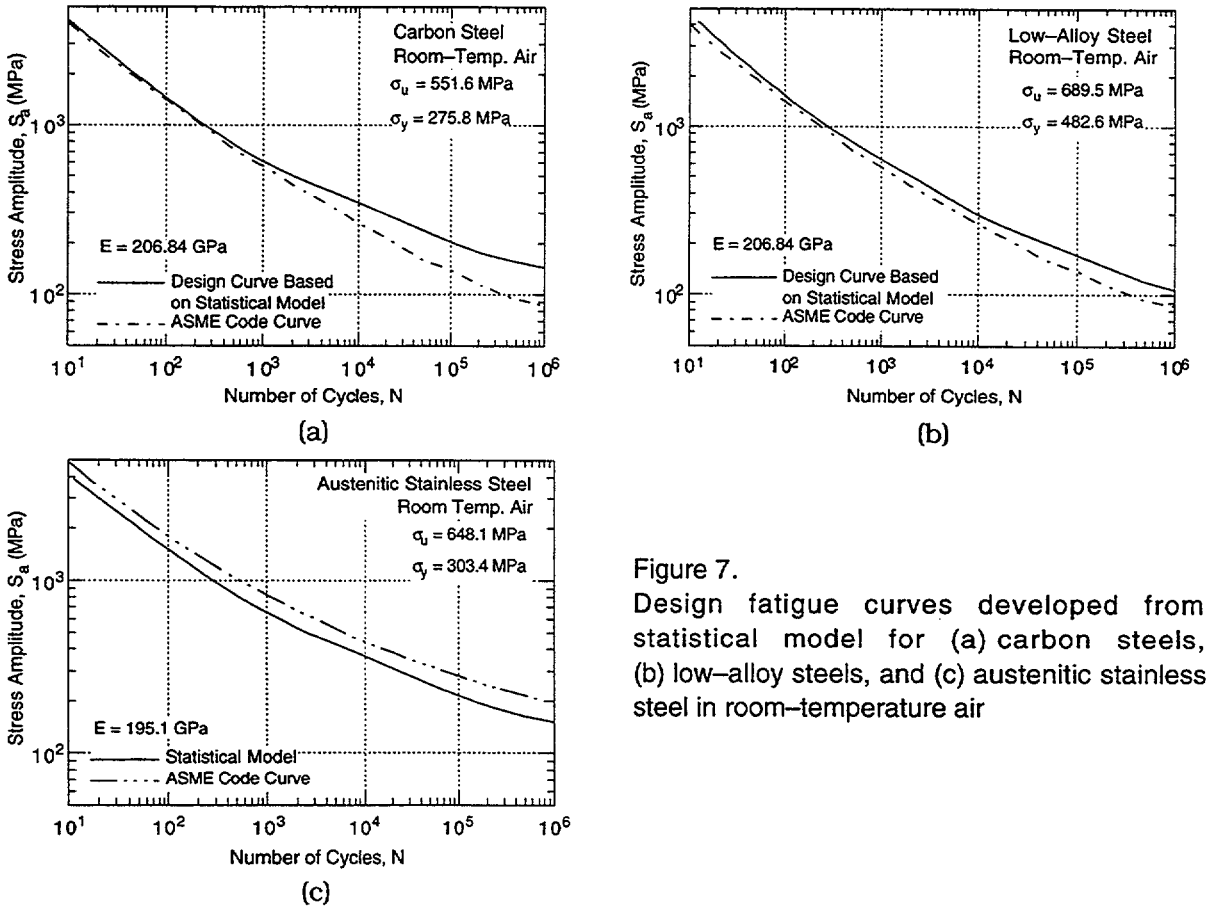

Figure 7.
Design fatigue curves developed from statistical model for (a) carbon steels, (b) low–alloy steels, and (c) austenitic stainless steel in room–temperature air

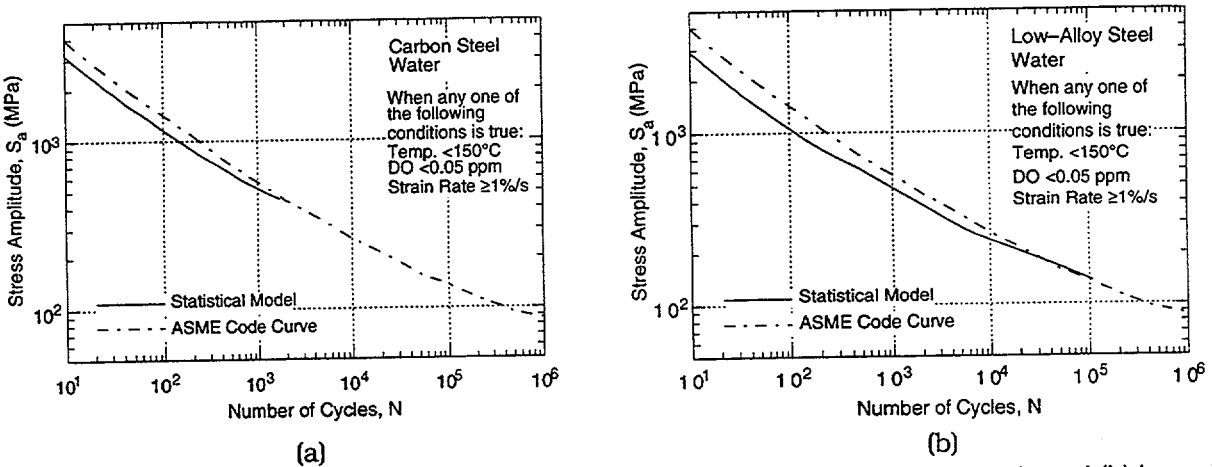

Figure 8. Design fatigue curves developed from statistical model for (a) carbon steels and (b) low–alloy steels under service conditions where one or more critical threshold values are not satisfied

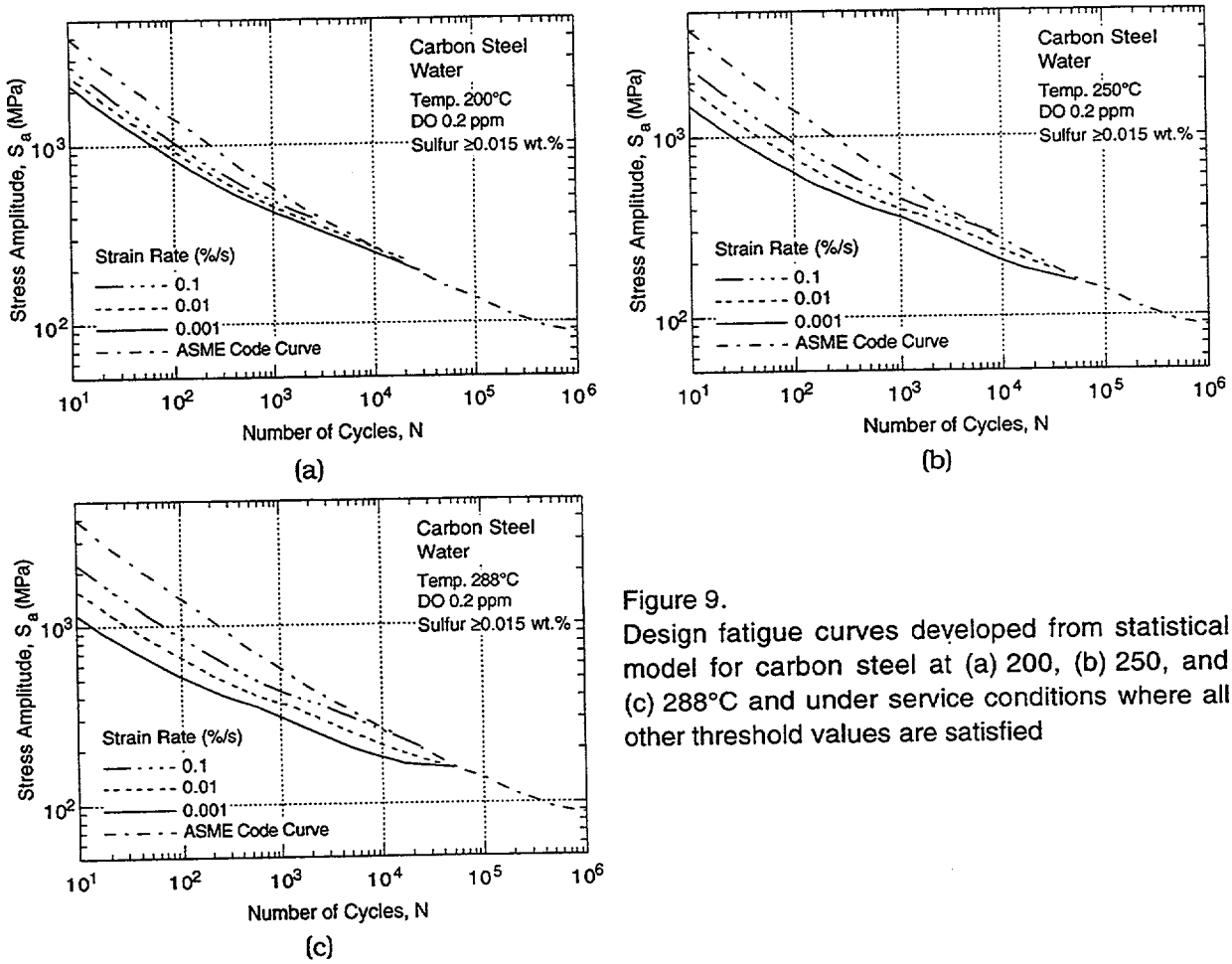

Figure 9.
Design fatigue curves developed from statistical model for carbon steel at (a) 200, (b) 250, and (c) 288°C and under service conditions where all other threshold values are satisfied

the design curves in Figs. 7 and 11 are somewhat conservative for Type 316NG SS. For CSs and LASs, a set of design curves similar to those shown in Figs. 9 and 10 can be developed for low–S steels, i.e., steels with ≤0.007 wt.% S. The results in Fig. 7 indicate that in room–temperature air, the current ASME Code design curve for CSs and LASs is somewhat

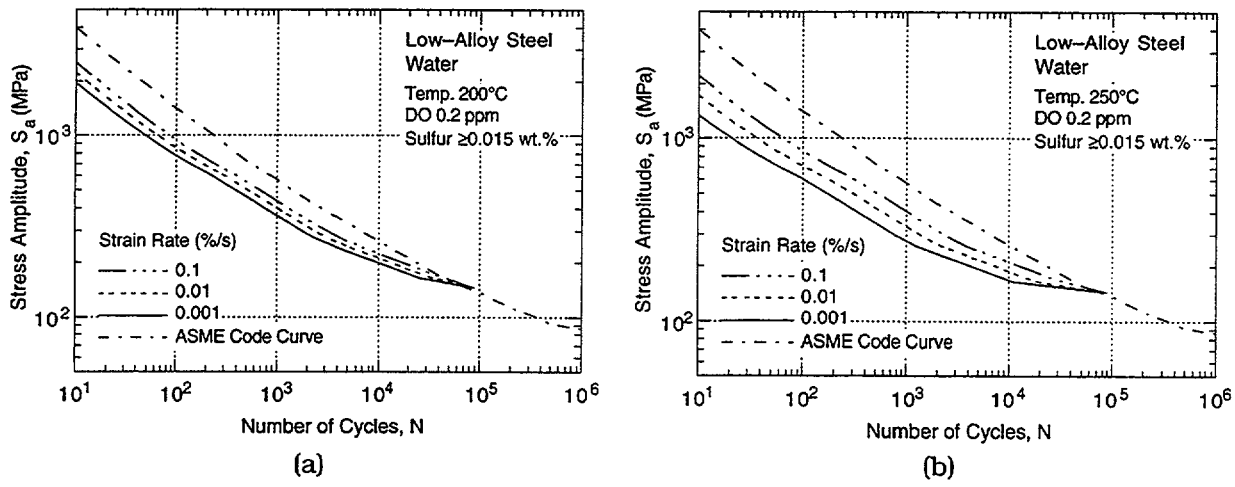

Figure 10.
Design fatigue curves developed from statistical model for low–alloy steel at (a) 200, (b) 250, and (c) 288°C and under service conditions where all other threshold values are satisfied

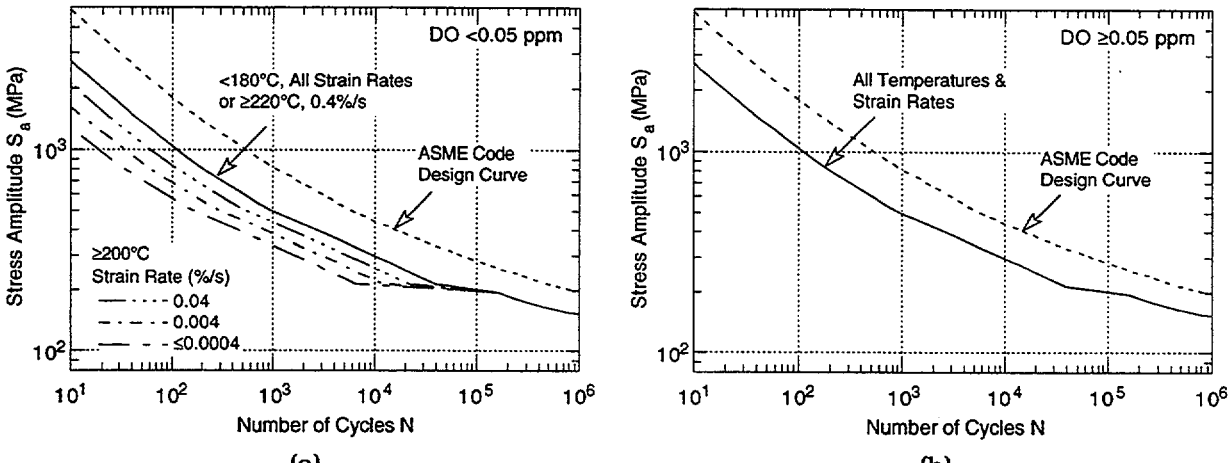

Figure 11. Design fatigue curves developed from statistical models for Types 304 and 316 SS in water with (a) <0.05 and (b) ≥0.05 ppm DO

conservative, and that for austenitic SSs is nonconservative with respect to the design curves based on the statistical models. In other words, the margins between the current Code design curve and the best fit of existing experimental data are greater than 2 on stress and 20 on

cycles for CSs and LASs, and less than 2 on stress and 20 on cycles for austenitic SSs. For SSs, actual margins are ≈1.5 on stress and 10–16 on cycles.

The environmentally adjusted design fatigue curves (Figs. 8–11) have a minimum threshold strain below which environmental effects are modest. The threshold strain for CSs and LASs appears to be ≈20% higher than the fatigue limit of the steel. This translates into strain amplitudes of 0.140 and 0.185%, respectively, for CSs and LASs. These values must be adjusted for mean stress effects and variability due to material and experimental scatter. The threshold strain amplitudes are decreased by ≈15% for CSs and ≈40% for LASs to account for the effects of mean stress, and by a factor of 1.7 on strain to provide 90% confidence for the variations in fatigue life associated with material variability and experimental scatter.[30] These values translate to a threshold strain amplitude of 0.07% (or a stress amplitude of 145 MPa) for both CSs and LASs. The existing fatigue data indicate a threshold strain range of ≈0.32% for austenitic SSs. This value is decreased by ≈10% to account for mean stress effects and by a factor of 1.5 to account for uncertainties in fatigue life that are associated with material and loading variability. These values yield a threshold strain amplitude of 0.097% (stress amplitude of 189 MPa) for austenitic SSs. The PVRC steering committee for CLEE[47] has proposed a ramp–type behavior for the threshold strain; a lower strain amplitude below which environmental effects are insignificant, a slightly higher strain amplitude above which environmental effects decrease fatigue life, and a ramp between the two values. The two strain amplitudes are 0.07 and 0.08% for carbon and low–alloy steels, and 0.10 and 0.11% for austenitic SSs (both wrought and cast SS). These threshold values were used to generate Figs. 9–11.

2.5.2 Fatigue Life Correction Factor

The effects of reactor coolant environments on fatigue life have also been expressed in terms of a fatigue life correction factor F_{en}, which is the ratio of life in air at room temperature to that in water at the service temperature.[7] The fatigue life correction factor can be obtained from the statistical model (Eqs. 3–17), where

$$\ln(F_{en}) = \ln(N_{RTair}) - \ln(N_{water}). \quad (18)$$

The fatigue life correction factor for CSs is given by

$$F_{en} = \exp(0.554 - 0.101\, S^*\, T^*\, O^*\, \dot{\varepsilon}^*); \quad (19)$$

for LASs, by

$$F_{en} = \exp(0.898 - 0.101\, S^*\, T^*\, O^*\, \dot{\varepsilon}^*); \quad (20)$$

and for austenitic SSs, by

$$F_{en} = \exp(0.935 - T'\, \dot{\varepsilon}'\, O'), \quad (21)$$

where the constants S^*, T^*, $\dot{\varepsilon}^*$, and O^* are defined in Eqs. 7–10, and T', $\dot{\varepsilon}'$, and O' are defined in Eqs. 15–17. A strain threshold is also defined, below which environmental effects are modest. The strain threshold is represented by a ramp, i.e., a lower strain amplitude below which environmental effects are insignificant, a slightly higher strain amplitude above which

environmental effects are significant, and a ramp between the two values. Thus, the negative terms in Eqs. 19–21 are scaled from zero to their actual values between the two strain thresholds. The two strain amplitudes are 0.07 and 0.08% for CSs and LASs, and 0.10 and 0.11% for austenitic SSs (both wrought and cast SS). To incorporate environmental effects into the Section III fatigue evaluation, a fatigue usage for a specific stress cycle, based on the current Code design fatigue curve, is multiplied by the correction factor. The experimental data adjusted for environmental effects, i.e., the product of experimentally observed fatigue life in LWR environments and F_{en}, are presented with the best–fit S–N curves for room–temperature air in Fig. 12.

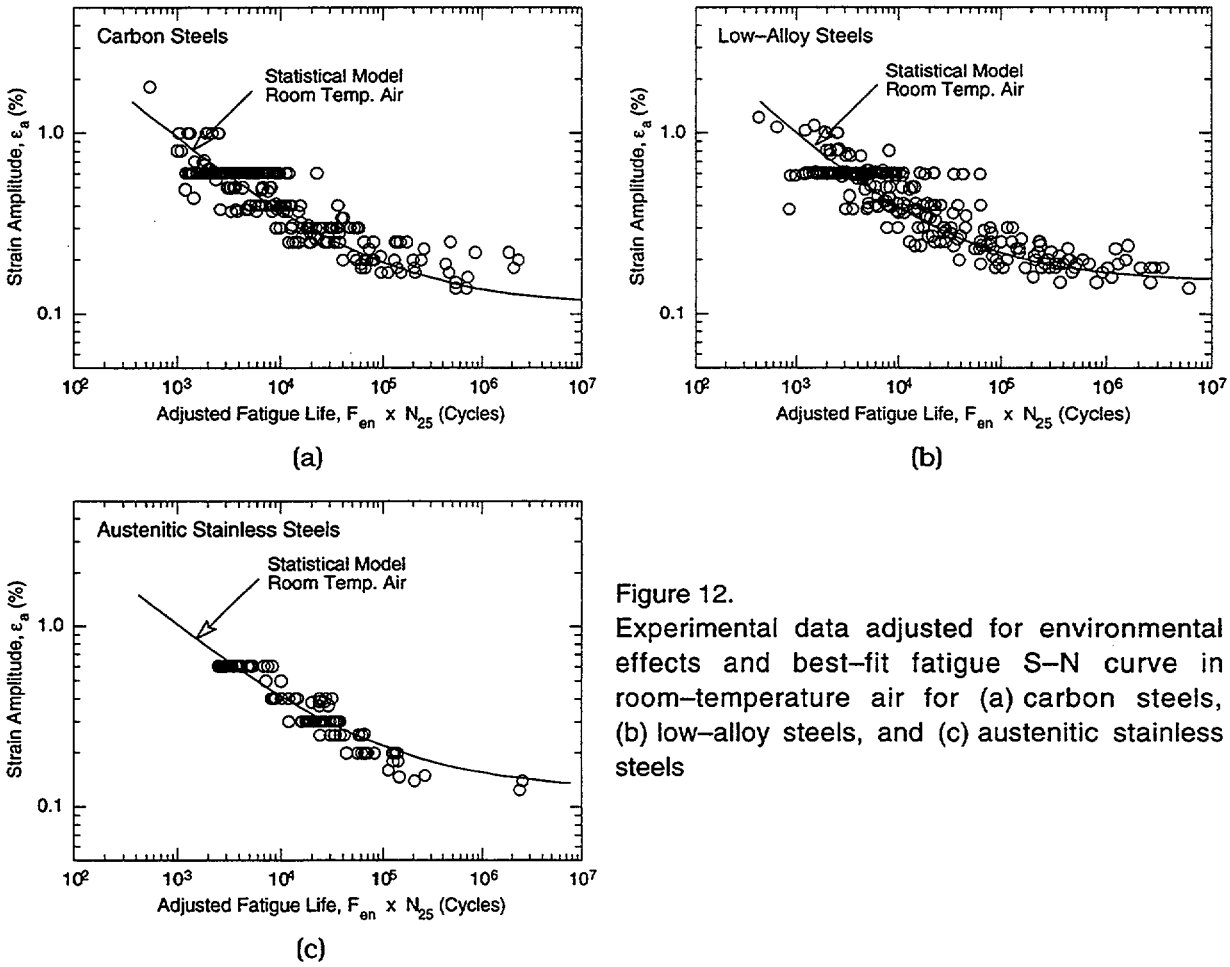

Figure 12.
Experimental data adjusted for environmental effects and best–fit fatigue S–N curve in room–temperature air for (a) carbon steels, (b) low–alloy steels, and (c) austenitic stainless steels

The F_{en} approach has been proposed by Mehta and Gosselin;[33,34] however, they defined F_{en} as the ratio of the life in air to that in water, both at service temperature. The F_{en} approach, also known as the EPRI/GE approach, has recently been updated to include the revised statistical models and the PVRC discussions on evaluating environmental fatigue.[68] The "effective" fatigue life correction factor can be expressed as $F_{en,eff} = F_{en}/Z$, where Z is a factor that represents the perceived conservatism in the ASME Code design curves. The $F_{en,eff}$ approach presumes that all uncertainties have been anticipated and accounted for.

3 Irradiation–Assisted Stress Corrosion Cracking of Austenitic SS

3.1 Introduction

Failures of some core internal components have been observed after accumulation of fast neutron fluences higher than $\approx 0.5 \times 10^{21}$ n·cm^{-2} (E >1 MeV) (≈0.7 dpa) in BWRs and at fluences approximately an order of magnitude higher in PWRs. The general pattern of the observed failures indicates that as nuclear plants age and fluence increases, various nonsensitized austenitic SSs become susceptible to intergranular (IG) failure. Welded components (such as core shrouds fabricated from Type 304 or 304L SS) have also failed in many BWRs, usually at fluence levels significantly lower than the threshold fluence for the solution-annealed base-metal components.

Although most failed components can be replaced, some structural components of importance to reactor safety (e.g., the BWR top guide, core shroud, and core plate) would be very difficult or costly to replace. Therefore, the structural integrity of these components has been a subject of concern, and extensive research has been conducted to provide an understanding of this type of degradation, which is commonly known as irradiation-assisted stress corrosion cracking (IASCC).[69–90]

Irradiation produces profound effects on local coolant water chemistry and component microstructure. Neutron irradiation causes alteration of microchemistry, microstructure, and mechanical properties of the core internal components, which are usually fabricated from ASTM Types 304, 304L, 316, or 348 SS. Irradiation produces defects, defect clusters, and defect-impurity complexes in grain matrices and alters the dislocation and dislocation loop structures, leading to radiation-induced hardening and, in many cases, flow localization via dislocation channeling. Irradiation also leads to changes in the stability of second–phase precipitates and the local alloy chemistry near grain boundaries, precipitates, and defect clusters. Grain–boundary microchemistry significantly different from bulk composition can be produced in association with not only radiation–induced segregation but also thermally driven equilibrium and nonequilibrium segregation of alloying and impurity elements.

Irradiation–induced grain–boundary depletion of Cr has been considered for many years to be the primary metallurgical process that leads to IASCC in BWRs. One of the most important factors that seems to support the Cr–depletion mechanism is that the IGSCC of nonirradiated thermally sensitized material and of BWR–irradiated solution–annealed material depend similarly on water chemistry (i.e., oxidizing potential).[69–71] Many investigators have also implicated the involvement of radiation–induced segregation of ASTM–specified impurities, such as Si and P and other minor impurities not specified in the ASTM specifications.[74–87] However, the exact mechanism of IASCC still remains unknown.

In general, IASCC is characterized by strong heat-to-heat variation in susceptibility, in addition to strong effects of irradiation condition, material type, and grade, even among materials of virtually identical chemical compositions. This indicates that the traditional interpretation based on the role of grain-boundary Cr depletion alone cannot completely explain the IASCC mechanism. In view of this background, an irradiation testing program is being conducted to investigate systematically the effects of alloying and impurity elements (Cr, Ni, Si, P, S, Mn, C, N, and O) on the susceptibility of austenitic SSs to IASCC at several fluence

levels. In previous studies, slow-strain-rate-tensile (SSRT) tests and fractographic analysis were conducted on model austenitic SS alloys irradiated at 289°C in helium in the Halden reactor to a "low-fluence" level of ≈0.3 x 10^{21} n·cm^{-2} (E > 1 MeV), or ≈0.43 dpa, and to a "medium-fluence" level of ≈0.9 x 10^{21} n·cm^{-2} (E > 1 MeV), or ≈1.3 dpa.[91–93] This report describes results of further analysis of SSRT data and posttest fractographs that were obtained for the specimens irradiated to ≈0.9 x 10^{21} n·cm^{-2} (E > 1 MeV). Initial test results obtained for "high-fluence" specimens irradiated to ≈2.0 x 10^{21} n·cm^{-2} (E > 1 MeV) are also reported.

3.2 Slow-Strain-Rate-Tensile Test of Model Austenitic Stainless Steels Irradiated in the Halden Reactor (H. M. Chung, R. V. Strain, and R. W. Clark)

3.2.1 Approach

The irradiation test matrix consists of 27 model austenitic SS alloys, listed in Table 3. Of these 27 alloys, 8 are commercially fabricated heats of Types 304, 304L, and 316 SS. The prefix "C" is added to the identification number of these 8 commercial heats. The remaining 19 heats were fabricated in the laboratory; all are designated with identification numbers that begin with "L".

Table 3. Elemental composition of 27 commercial and laboratory model austenitic SS alloys irradiated in the Halden Reactor

ANL	Source	Composition (wt.%)										
ID[a]	Heat ID	Ni	Si	P	S	Mn	C	N	Cr	O	B	Mo or Nb
C1	DAN-70378	8.12	0.50	0.038	0.002	1.00	0.060	0.060	18.11	-	<0.001	-
L2	BPC-4-111	10.50	0.82	0.080	0.034	1.58	0.074	0.102	17.02	0.0065	<0.001	-
C3	PNL-C-1	8.91	0.46	0.019	0.004	1.81	0.016	0.083	18.55	-	<0.001	-
L4	BPC-4-88	10.20	0.94	0.031	0.010	1.75	0.110	0.002	15.80	-	<0.001	-
L5	BPC-4-104	9.66	0.90	0.113	0.028	0.47	0.006	0.033	21.00	-	<0.001	-
L6	BPC-4-127	10.00	1.90	0.020	0.005	1.13	0.096	0.087	17.10	0.0058	<0.001	-
L7	BPC-4-112	10.60	0.18	0.040	0.038	1.02	0.007	0.111	15.40	0.0274	<0.001	-
L8	BPC-4-91	10.20	0.15	0.093	0.010	1.85	0.041	0.001	18.30	-	<0.001	-
C9	PNL-C-6	8.75	0.39	0.013	0.013	1.72	0.062	0.065	18.48	-	<0.001	-
C10	DAN-23381	8.13	0.55	0.033	0.002	1.00	0.060	0.086	18.19	-	<0.001	-
L11	BPC-4-93	8.15	0.47	0.097	0.009	1.02	0.014	0.004	17.40	-	<0.001	-
C12	DAN-23805	8.23	0.47	0.018	0.002	1.00	0.060	0.070	18.43	-	<0.001	-
L13	BPC-4-96	8.18	1.18	0.027	0.022	0.36	0.026	0.001	17.40	-	<0.001	-
L14	BPC-4-129	7.93	1.49	0.080	0.002	1.76	0.107	0.028	15.00	0.0045	<0.001	-
L15	BPC-4-126	8.00	1.82	0.010	0.013	1.07	0.020	0.085	17.80	0.0110	<0.001	-
C16	PNL-SS-14	12.90	0.38	0.014	0.002	1.66	0.020	0.011	16.92	0.0157	<0.001	-
L17	BPC-4-128	8.00	0.66	0.090	0.009	0.48	0.061	0.078	15.30	0.0090	<0.001	-
L18	BPC-4-98	8.13	0.14	0.016	0.033	1.13	0.080	0.001	18.00	-	<0.001	-
C19	DAN-74827	8.08	0.45	0.031	0.003	0.99	0.060	0.070	18.21	0.0200	<0.001	-
L20	BPC-4-101	8.91	0.017	0.010	0.004	0.41	0.002	0.002	18.10	0.0940	<0.001	-
C21	DAN-12455	10.24	0.51	0.034	0.001	1.19	0.060	0.020	16.28	-	<0.001	Mo 2.08
L22	BPC-4-100	13.30	0.024	0.015	0.004	0.40	0.003	0.001	16.10	-	<0.001	Mo 2.04
L23	BPC-4-114	12.04	0.68	0.030	0.047	0.96	0.043	0.092	17.30	0.0093	<0.001	Nb 1.06
L24	BPC-4-105	12.30	0.03	0.007	0.005	0.48	0.031	0.002	16.90	0.0129	<0.001	Nb 1.72
L25C3	BPC-4-133	8.93	0.92	0.020	0.008	1.54	0.019	0.095	17.20	0.0085	0.010	-
L26C19	BPC-4-131	8.09	0.79	0.004	0.002	0.91	0.070	0.089	17.20	0.0080	<0.001	-
L27C21	BPC-4-132	10.30	0.96	0.040	0.002	0.97	0.057	0.019	15.30	0.0058	0.030	Mo 2.01

[a]The first letters "C" or "L" denotes, respectively, a commercial or a laboratory heat.

The SSRT specimens were irradiated in the Halden heavy-water boiling reactor in six helium-filled capsules maintained at 289°C. All SSRT tests were conducted in a low-activity-level hot cell in simulated BWR-like water at 289°C. Dissolved oxygen (DO) in the water was maintained at ≈8 ppm. Conductivity and pH of the water were kept at ≈0.07-0.10 and 6.3-6.8, respectively. The strain rate was held constant at 1.65×10^{-7} s^{-1}. The electrochemical potential (ECP) was measured on the effluent side at regular intervals. After completion of SSRT testing, the fracture tip of each specimen was cut and examined in a shielded scanning electron microscope (SEM) to determine the morphology of the fracture surface, i.e., percent transgranular stress corrosion cracking and percent intergranular stress corrosion cracking (%TGSCC and %IGSCC).

3.2.2 Tabulation of Test Results

Tables 4-9 summarize the results of SSRT tests and fractographic analysis, completed for unirradiated specimens and the specimens that were irradiated to fluence levels of $\approx 0.3 \times 10^{21}$ and $\approx 0.9 \times 10^{21}$ n·cm^{-2} (E > 1 MeV). Test conditions, results of SSRT, and fractographic characteristics (percent IGSCC, percent TGSCC, and combined percent IGSCC+TGSCC) are listed. These results are correlated with compositional characteristics of the alloys in Tables 5, 7, and 9.

Table 4. Stress corrosion test conditions, results of SSRT[a] tests, and SEM fractography for unirradiated model austenitic SS alloys

Alloy & Spec. Ident. No.	SSRT No.	Feedwater Chemistry: Oxygen Conc. (ppm)	Feedwater Chemistry: Average ECP (mV SHE)	Feedwater Chemistry: Cond. at 25°C (μS·cm^{-1})	Feedwater Chemistry: pH at 25°C	SSRT Parameters: Yield Stress (MPa)	SSRT Parameters: Max. Stress (MPa)	SSRT Parameters: Uniform Elong. (%)	SSRT Parameters: Total Elong. (%)	Fracture Behavior: TGSCC[b] (%)	Fracture Behavior: IGSCC (%)	Fracture Behavior: TGSCC + IGSCC (%)
L23-4	CHR-1	8.6	+228	0.07	6.65	332	480	15.6	17.0	15	0	15
L7-4	CHR-2	8.0	+217	0.07	7.37	195	370	2.5	5.2	20	0	20
L7-B1	CHR-7		Tested in Air			282	676	42.3	43.9	0	0	0
L14-4	CHR-3	8.6	+208	0.07	7.37	240	474	41.8	44.2	0	0	0
L17-4	CHR-4	7.5	+262	0.06	7.09	189	412	11.6	13.3	60	0	60
L6-4	CHR-5	7.9	+256	0.08	6.85	227	545	43.0	44.5	0	0	0
L27-4	CHR-6	9.3	+247	0.08	6.96	298	483	20.6	22.9	0	0	0
L26-4	CHR-8	9.4	+223	0.07	6.65	184	596	38.2	40.2	0	0	0
L2-4	CHR-9	8.6	+292	0.06	6.55	193	348	6.6	7.8	57	0	57
L25-4	CHR-10	8.2	+239	0.06	6.42	184	458	25.5	27.0	0	0	0
L15-4	CHR-11	8.2	+195	0.06	6.32	218	512	36.7	37.9	10	0	10
L24-4	CHR-12	8.4	+200	0.07	6.20	352	461	10.4	12.3	10	0	10
C1-15	CHR-13	8.1	+187	0.07	6.33	179	498	49.4	51.7	0	0	0
C19-B1	CHR-14	8.8	+179	0.08	6.29	178	501	47.4	49.2	0	0	0
C9-B1	CHR-15	8.5	+166	0.07	6.83	178	408	17.4	19.4	32	0	32
C12-B1	CHR-16	8.5	+124	0.07	6.18	182	511	46.0	47.6	0	0	0
C10-B1	CHR-17	9.2	+145	0.07	6.26	174	478	30.6	35.1	0	0	0
C21-9	CHR-18	9.2	+187	0.07	6.41	277	455	48.9	59.5	0	0	0

[a]Test at 289°C and a strain rate of 1.65×10^{-7} s^{-1} in simulated BWR-like water; DO ≈8 ppm.

Table 5. Compositional characteristics (composition in wt.%) of unirradiated model austenitic SS alloys correlated with results of SSRT[a] tests and SEM fractography.

Alloy ID	Ni	Si	P	S	Mn	C	N	Cr	Mo/Nb	O (wppm)	Remark[b]	YS (MPa)	UTS (MPa)	UE (%)	TE (%)	TG (%)	IG (%)	TG+IG SCC (%)
L23	12.04	0.68	0.030	0.047	0.96	0.043	0.092	17.30	Nb 1.06	93	CP 348	332	480	15.6	17.0	15	0	15
L7	10.60	0.18	0.040	0.038	1.02	0.007	0.111	15.40	-	274	High N, O; Low Si, C	195	370	2.5	5.2	20	0	20
L14	7.93	1.49	0.080	0.002	1.76	0.107	0.028	15.00	-	45	High Si, P, C; Low S	240	474	41.8	44.2	0	0	0
L17	8.00	0.66	0.090	0.009	0.48	0.061	0.078	15.30	-	90	High P; Low Cr, Mn, S	189	412	11.6	13.3	60	0	60
L6	10.00	1.90	0.020	0.005	1.13	0.096	0.087	17.10	-	58	High Si, C, Cr; Low S	227	515	43.0	44.5	0	0	0
L27	10.30	0.96	0.040	0.002	0.97	0.057	0.019	15.30	Mo 2.01	-	CP 316 ; high B (0.030)	298	483	20.6	22.9	0	0	0
L26	8.09	0.79	0.004	0.002	0.91	0.070	0.089	17.20	-	80	Low P, S	184	506	38.2	40.2	0	0	0
L2	10.50	0.82	0.080	0.034	1.58	0.074	0.102	17.02	-	66	High P, S, Mn, N	193	348	6.6	7.8	57	0	57
L25	8.93	0.92	0.020	0.008	1.54	0.019	0.095	17.20	-	85	high B (0.010)	184	458	25.5	27.0	0	0	0
L15	8.00	1.82	0.010	0.013	1.07	0.020	0.085	17.80	-	110	High N; Low C	218	512	36.7	37.9	10	0	10
L24	12.30	0.03	0.007	0.005	0.48	0.031	0.002	16.90	Nb 1.72	-	HP 348; Low Si, N	352	461	10.4	12.3	10	0	10
C1	8.12	0.50	0.038	0.002	1.00	0.060	0.060	18.11	-	-	Low S, CP 304	179	498	49.4	51.7	0	0	0
C19	8.08	0.45	0.031	0.003	0.99	0.060	0.070	18.21	-	-	Low Si, S, CP 304	178	501	47.4	49.2	0	0	0
C9	8.75	0.39	0.013	0.013	1.72	0.062	0.065	18.48	-	-	Low Si, High Mn	178	408	17.4	19.4	32	0	32
C12	8.23	0.47	0.018	0.002	1.00	0.060	0.070	18.43	-	-	Low Si, S, P	182	511	46.0	47.6	0	0	0
C10	8.13	0.55	0.033	0.002	1.00	0.060	0.086	18.19	-	-	Low S, high N	174	478	30.6	35.1	0	0	0
C21	10.24	0.51	0.034	0.001	1.19	0.060	0.020	16.28	Mo 2.08	-	CP 316; low B (0.001)	277	455	48.9	59.5	0	0	0

[a]Test at 289°C and a strain rate of 1.65×10^{-7} s^{-1} in simulated BWR-like water; DO ≈8 ppm.
[b]HP = high purity, CP = commercial purity.

Table 6. Stress corrosion test conditions, results of SSRT[a] tests, and SEM fractography for model austenitic SS alloys irradiated to 0.3×10^{21} n·cm^{-2} (E > 1 MeV)

Alloy & Spec. Ident. No.	SSRT No.	Feedwater Chemistry: Oxygen Conc. (ppm)	Feedwater Chemistry: Average ECP (mV SHE)	Feedwater Chemistry: Cond. at 25°C (μS·cm^{-1})	Feedwater Chemistry: pH at 25°C	SSRT Parameters: Yield Stress (MPa)	SSRT Parameters: Max. Stress (MPa)	SSRT Parameters: Uniform Elongation (%)	SSRT Parameters: Total Elongation (%)	Fracture Behavior: TGSCC (%)	Fracture Behavior: IGSCC (%)	Fracture Behavior: TGSCC IGSCC (%)
C1-1	HR-1	8.3	+184	0.07	7.03	490	680	13.4	16.6	4	0	4
L5-1	HR-2	9.7	+208	0.07	6.89	413	539	29.5	32.7	2	2	4
L22-1	HR-3	8.0	+236	0.07	6.80	360	596	6.6	9.4	50	15	65
C3-1	HR-4	8.7	+161	0.07	6.68	338	491	27.7	31.6	5	0	5
C16-1	HR-5	8.3	+204	0.08	6.74	370	527	17.6	20.6	2	0	2
L4-1	HR-6	9.0	+202	0.08	6.70	367	542	19.7	22.3	46	0	46
L18-1	HR-7	9.0	+203	0.08	6.33	503	572	6.3	8.8	54	0	54
C10-1	HR-8	8.2	+174	0.07	6.35	523	640	17.4	18.9	6	0	6
C21-1	HR-9	8.1	+149	0.08	6.49	480	620	15.9	19.4	4	0	4
L11-1	HR-10	9.0	+157	0.08	6.17	487	599	2.3	3.8	62	0	62
L13-1	HR-11	8.7	+164	0.08	6.17	248	461	22.1	24.8	18	0	18
L20-1	HR-12	8.4	+174	0.07	6.20	454	552	2.9	5.1	Dendritic strucrure		
C19-1	HR-13	9.5	+132	0.12	6.36	554	682	10.5	14.7	7	0	7
C9-1	HR-14	8.0	+192	0.11	6.30	522	607	13.4	14.6	24	0	24
C12-1	HR-15	9.0	+195	0.08	6.40	404	589	20.4	24.2	5	0	5
L8-1	HR-16	9.0	+215	0.08	6.60	411	571	15.6	17.9	54	0	54

[a]Test at 289°C and a strain rate of 1.65×10^{-7} s^{-1} in simulated BWR-like water; DO ≈8 ppm.

Table 7. Compositional characteristics (wt.%) of model austenitic SS alloys irradiated to 0.3 x 10^{21} n·cm^{-2} (E > 1 MeV) correlated with results of SSRT[a] tests and SEM fractography

Alloy ID	Ni	Si	P	S	Mn	C	N	Cr	Mo/Nb	Remark[b]	YS (MPa)	UTS (MPa)	UE (%)	TE (%)	TG (%)	IG (%)	TG+IG SCC (%)
C1	8.12	0.50	0.038	0.002	1.00	0.060	0.060	18.11	-	Low S, CP 304	490	680	13.4	16.6	4	0	4
L5	9.66	0.90	0.113	0.028	0.47	0.006	0.033	21.00	-	High P, Cr; Low C	413	539	29.5	32.7	2	2	4
L22	13.30	0.024	0.015	0.004	0.40	0.003	0.001	16.10	Mo 2.04	HP 316L, low Si, N	360	596	6.6	9.4	50	15	65
C3	8.91	0.46	0.019	0.004	1.81	0.016	0.083	18.55	-	CP 304L, Low Si	338	491	27.7	31.6	5	0	5
C16	12.90	0.38	0.014	0.002	1.66	0.020	0.011	16.92	-	High Ni; Low Si, S	370	527	17.6	20.6	2	0	2
L4	10.20	0.94	0.031	0.010	1.75	0.110	0.002	15.80	-	High Ni, Mn, C; Low N	367	542	19.7	22.3	46	0	46
L18	8.13	0.14	0.016	0.033	1.13	0.080	0.001	18.00	-	Low Si, N	503	572	6.3	8.8	54	0	54
C10	8.13	0.55	0.033	0.002	1.00	0.060	0.086	18.19	-	Low S, CP 304	523	640	17.4	18.9	6	0	6
C21	10.24	0.51	0.034	0.001	1.19	0.060	0.020	16.28	Mo 2.08	CP 316	480	620	15.9	19.4	4	0	4
L11	8.15	0.47	0.097	0.009	1.02	0.014	0.004	17.40	-	High P; Low Si, C, S, N	487	599	2.3	3.8	62	0	62
L13	8.18	1.18	0.027	0.022	0.36	0.026	0.001	17.40	-	High Si; Low Mn, C, N	248	461	22.1	24.8	18	0	18
L20	8.91	0.017	0.010	0.004	0.41	0.002	0.002	18.10	O 0.0940	highO; low Si, N; HP 304L	454	552	2.9	5.1	Dendritic structure		
C19	8.08	0.45	0.031	0.003	0.99	0.060	0.070	18.21	-	Low Si, S	554	682	10.5	14.7	7	0	7
C9	8.75	0.39	0.013	0.013	1.72	0.062	0.065	18.48	-	Low Si; High Mn	522	607	13.4	14.6	24	0	24
C12	8.23	0.47	0.018	0.002	1.00	0.060	0.070	18.43	-	Low Si, P, S	404	589	20.4	24.2	5	0	5
L8	10.20	0.15	0.093	0.010	1.85	0.041	0.001	18.30	-	High Ni, P, Mn; Low Si, N	411	571	15.6	17.8	64	0	64

[a]Test at 289°C and a strain rate of 1.65 x 10^{-7} s^{-1} in simulated BWR-like water; DO ≈8 ppm.
[b]HP = high purity, CP = commercial purity.

Table 8. Stress corrosion test conditions, results of SSRT[a] tests, and SEM fractography for model austenitic SS alloys irradiated to 0.9 x 10^{21} n·cm^{-2} (E > 1 MeV)

Alloy & Spec. Ident. No.	SSRT No.	Feedwater Chemistry: Oxygen Conc. (ppm)	Average ECP (mV SHE)	Cond. at 25°C (μS·cm^{-1})	pH at 25°C	SSRT Parameters: Yield Stress (MPa)	Max. Stress (MPa)	Uniform Elongation (%)	Total Elongation (%)	Fracture Behavior: TGSCC (%)	IGSCC (%)	TGSCC IGSCC (%)
L22-02	HR-17	8.0	+181	0.08	6.77	475	549	4.20	5.82	30	35	65
L11-02	HR-18	8.0	+191	0.08	6.55	820	856	0.43	1.65	50	14	64
L18-02	HR-19	8.0	+193	0.10	6.07	710	755	3.98	5.05	38	14	52
L20-02	HR-28	Test in 289°C Air				826	845	0.31	2.09	Dendritic structure		
L20-05	HR-26	9.0	+182	0.09	6.32	670	743	0.37	1.03	Dendritic structure		
L20-06	HR-27	8.0	+274	0.07	6.05	632	697	0.85	2.72	0	0	0
C9-02	HR-21	8.0	+240	0.07	6.47	651	679	1.42	2.50	62	22	84
L17-02	HR-22	8.0	+198	0.07	6.42	574	654	2.02	3.08	44	41	85
L7-02	HR-23	8.0	+215	0.07	6.03	553	561	0.24	2.44	38	54	92
C10-02	HR-24	7.0	+221	0.07	5.26	651	706	6.35	9.25	14	0	14
C3-02	HR-25	8.0	+240	0.07	6.34	632	668	16.72	19.74	9	4	13
C19-02	HR-30	Test in 289°C Air				888	894	6.41	10.21	1	0	1
C19-04	HR-31	8.0	+252	0.07	6.18	750	769	6.06	8.79	1	0	1
L6-02	HR-32	8.0	+250	0.07	6.40	493	546	2.45	3.77	8	27	35
L14-02	HR-33	8.0	+246	0.08	6.07	649	684	1.90	4.67	84	2	86
L13-02	HR-34	7.0	+222	0.09	6.85	602	624	1.67	4.95	55	12	67
L04-02	HR-35	7.0	+259	0.08	6.54	634	680	1.07	2.02	58	12	70
L05-02	HR-36	7.0	+243	0.07	6.85	665	725	3.07	4.57	3	5	8
C16-02	HR-37	7.0	+230	0.07	6.62	562	618	11.99	15.80	7	1	8
L8-02	HR-38	8.0	+242	0.07	6.57	838	838	0.12	3.12	15	22	37
C21-02	HR-39	8.0	+231	0.08	6.21	643	716	15.38	18.30	1	2	3
L2-02	HR-40	7.0	+239	0.07	7.11	839	849	0.88	1.56	31	11	42
L24-02	HR-41	8.0	+239	0.06	6.40	725	725	0.15	2.45	2	1	3
L23-02	HR-42	7.0	+237	0.08	6.60	787	818	0.38	1.24	3	24	27
C12-02	HR-43	7.0	+227	0.07	6.19	747	756	14.96	18.57	4	0	4
C1-02	HR-44	8.0	+229	0.07	6.30	707	763	13.36	17.04	2	0	2

[a]Test at 289°C and a strain rate of 1.65 x 10^{-7} s^{-1} in simulated BWR-like water; DO ≈8 ppm.

Table 9. Compositional characteristics (wt.%) of model austenitic SS alloys irradiated to 0.9 x 10^{21} n·cm^{-2} (E > 1 MeV) correlated with results of SSRT[a] tests and SEM fractography

Alloy ID	Ni	Si	P	S	Mn	C	N	Cr	Mo, Nb, or O	Remark[b]	YS (MPa)	UTS (MPa)	UE (%)	TE (%)	TG (%)	IG (%)	TG+IG (%)
L22-02	13.30	0.024	0.015	0.004	0.40	0.003	0.001	16.10	Mo 2.04	HP 316L; low Si, N, S	475	549	4.20	5.82	30	35	65
L11-02	8.15	0.47	0.097	0.009	1.02	0.014	0.004	17.40	-	high P; low Si, C, S, N	820	856	0.43	1.65	50	14	64
L18-02	8.13	0.14	0.016	0.033	1.13	0.080	0.001	18.00	-	low Si, N	710	755	3.98	5.05	38	14	52
L20-05	8.91	0.017	0.010	0.004	0.41	0.002	0.002	18.10	O 0.0940	high O; low Si, N; HP 304L	670	743	0.37	1.03	Dendritic structure		
L20-06	8.91	0.017	0.010	0.004	0.41	0.002	0.002	18.10	O 0.0940	highO; low Si, N; HP 304L	632	697	0.85	2.72	Dendritic structure		
C9-02	8.75	0.39	0.013	0.013	1.72	0.062	0.065	18.48	-	low Si; high Mn	651	679	1.42	2.50	62	22	84
L17-02	8.00	0.66	0.090	0.009	0.48	0.061	0.078	15.30	O 0.0090	high P; low Cr, Mn, S	574	654	2.02	3.08	44	41	85
L7-02	10.60	0.18	0.040	0.038	1.02	0.007	0.111	15.40	O 0.0274	high S, N, O; low Si, C	553	561	0.24	2.44	38	54	92
C10-02	8.13	0.55	0.033	0.002	1.00	0.060	0.086	18.19	-	CP 304; low S; high N	651	706	6.35	9.25	14	0	14
C3-02	8.91	0.46	0.019	0.004	1.81	0.016	0.083	18.55	-	CP 304L; high Mn, N; low S	632	668	16.7	19.7	9	4	13
C19-04	8.08	0.45	0.031	0.003	0.99	0.060	0.070	18.21	O 0.0200	CP 304; low S	750	769	6.06	8.79	1	0	1
L6-02	10.00	1.90	0.020	0.005	1.13	0.096	0.087	17.10	O 0.0058	high Si; low S	493	546	2.45	3.77	8	27	35
L14-02	7.93	1.49	0.080	0.002	1.76	0.107	0.028	15.00	O 0.0045	high Si, P, Mn; low Cr, S	649	684	1.90	4.67	84	2	86
L13-02	8.18	1.18	0.027	0.022	0.36	0.026	0.001	17.40	-	high Si, S; Low Mn, C, N	602	624	1.67	4.95	55	12	67
L4-02	10.20	0.94	0.031	0.010	1.75	0.110	0.002	15.80	-	high Si, C; low N, Cr	634	680	1.07	2.02	58	12	70
L5-02	9.66	0.90	0.113	0.028	0.47	0.006	0.033	21.00	3% ferrite	high Si, P, Cr; Low Mn, C	665	725	3.07	4.57	3	5	8
C16-02	12.90	0.38	0.014	0.002	1.66	0.020	0.011	16.92	0.0157	high Ni; low P, S, C	562	618	12.0	15.8	7	1	8
L8-02	10.20	0.15	0.093	0.010	1.85	0.041	0.001	18.30	-	high P, Mn; low Si, N	838	838	0.12	3.12	15	22	37
C21-02	10.24	0.51	0.034	0.001	1.19	0.060	0.020	16.28	Mo 2.08	CP 316, low S	643	716	15.4	18.3	1	2	3
L2-02	10.50	0.82	0.080	0.034	1.58	0.074	0.102	17.02	O 0.0066	high O, P, S, N	839	849	0.88	1.56	31	11	42
L24-02	12.30	0.03	0.007	0.005	0.48	0.031	0.002	16.90	Nb 1.72 O 0.0129	HP 348L; low Si, P, S, C, N	725	725	0.15	2.45	2	1	3
L23-02	12.04	0.68	0.030	0.047	0.96	0.043	0.092	17.30	Nb 1.06 O 0.0093	CP 348, high S	787	818	0.38	1.24	3	24	27
C12-02	8.23	0.47	0.018	0.002	1.00	0.060	0.070	18.43	-	304, low S, low P	747	756	15.0	18.6	4	0	4
C1-02	8.12	0.50	0.038	0.002	1.00	0.060	0.060	18.11	-	304, low S	707	763	13.4	17.0	2	0	2

[a]Test at 289°C and a strain rate of 1.65 x 10^{-7} s^{-1} in simulated BWR-like water; DO ≈8 ppm.
[b]HP = high purity, CP = commercial purity.

3.2.3 Effect of Fluence on Yield Strength

Figure 13 shows the effect of fluence on 0.2% yield strength of specimens fabricated from commercial heats of Types 304 and 304L SS and irradiated in the Halden reactor. Results from laboratory-fabricated alloys are not included in the figure. As shown in Fig. 13, the data obtained from the Halden-irradiated specimens are consistent with those from BWR-irradiated tensile specimens or BWR components that have been reported in the literature.[74,76,82] The yield strength of Types 304 and 304L SS, irradiated under BWR conditions, appears to saturate at ≈840 MPa and fluence levels higher than ≈2.0 x 10^{21} n·cm^{-2} (E > 1 MeV). There was no systematic dependence of yield strength vs. fluence on carbon content (i.e., Type 304 vs. 304L SS), indicating that the effect of carbon is secondary or insignificant in comparison with the effect of irradiation-induced damage.

3.2.4 Effect of Silicon

Yield strength of the model alloys, measured in BWR-like water at 289°C, was nearly constant at ≈200 MPa in the unirradiated state and was more or less independent of Si concentration (see Fig. 14). However, as fluence was increased to ≈0.3 x 10^{21} n·cm^{-2} and ≈0.9 x 10^{21} n·cm^{-2}, the degree of increase in the yield strength was significantly lower for alloys that contain >0.9 wt.% Si. This finding indicates that irradiation-induced hardening centers and the degree of irradiation hardening are significantly influenced by alloy Si content. Because Si

atoms in austenitic SSs occupy substitutional sites, they are likely to interact preferentially with irradiation-induced vacancy sites in the steel. This effect is likely to inhibit the formation of vacancy clusters or vacancy-impurity complexes and is, therefore, conducive to a less significant irradiation-induced hardening. An effect similar to that of Si was, however, not observed for C and N.

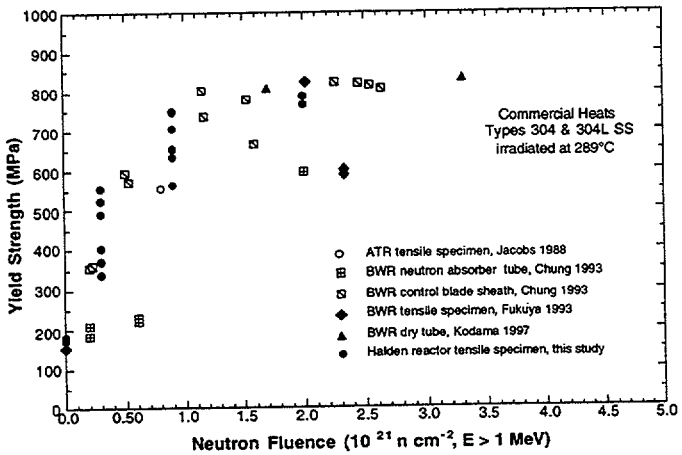

Figure 13.
Effect of fast neutron fluence on yield strength of Types 304 and 304L SS irradiated in BWR or test reactors at 289°C

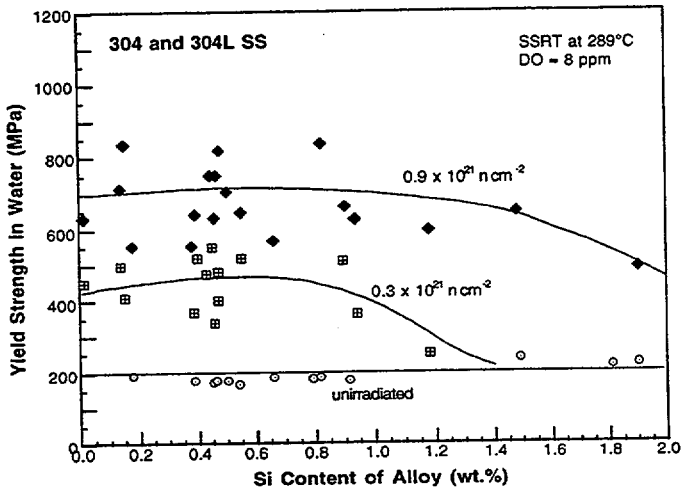

Figure 14.
Effect of Si concentration on yield strength of Types 304 and 304L SS measured in 289°C water before and after irradiation.

Under the present SSRT test condition, most alloys did not exhibit susceptibility to IASCC (i.e., percent IGSCC negligible) at ≈0.3 x 10^{21} n·cm^{-2}, whereas at ≈2.0 x 10^{21} n·cm^{-2} the percent IGSCC of most alloys was close to 100%. The influence of impurities on the susceptibility to IASCC appears to be strongly manifested at ≈0.9 x 10^{21} n·cm^{-2}.

At ≈0.3 x 10^{21} n·cm^{-2} (E > 1 MeV), only one laboratory heat (Heat L22, a Type 316L SS) that contains an unusually low concentration of Si (≈0.024 wt.% Si) exhibited appreciable susceptibility to IASCC (see Fig. 15). By the time the fluence reached ≈0.9 x 10^{21} n·cm^{-2} (E > 1 MeV), many alloys exhibited significant susceptibility to IASCC (i.e., significant level of percent IGSCC). At this fluence, Types 304 and 304L SS that contain <0.67 wt.% Si exhibited relatively higher susceptibility to IASCC, whereas heats with 0.8-1.5 wt.% Si exhibited insignificant susceptibility to IASCC. This behavior is shown in Fig. 16.

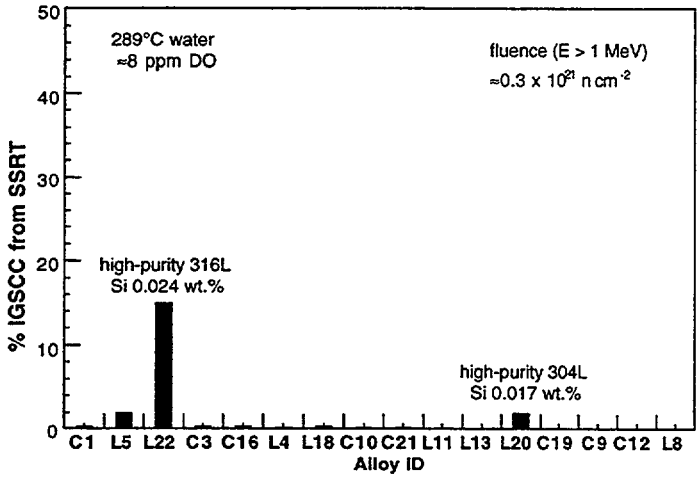

Figure 15.
Susceptibility to IGSCC after irradiation to ≈0.3 x 10^{21} n·cm^{-2} (E > 1 MeV). Only laboratory heats that contain very low Si concentrations of <0.025 wt.% exhibited some susceptibility at this low fluence.

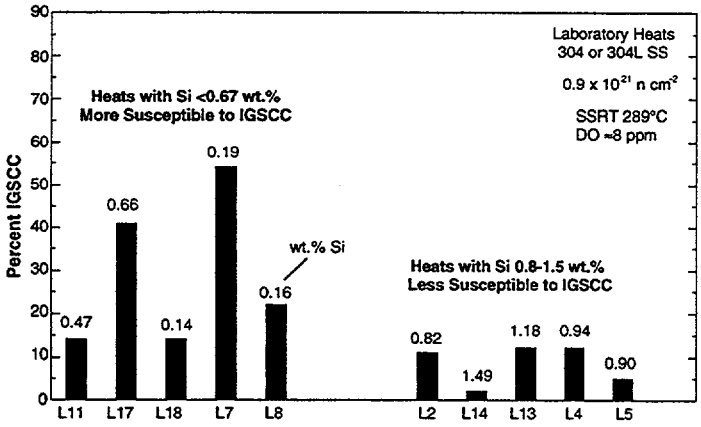

Figure 16.
Effect of Si on susceptibility to IGSCC of laboratory heats of Types 304 and 304L SS measured after irradiation to ≈0.9 x 10^{21} n·cm^{-2} (E > 1 MeV). Heats containing low concentrations of Si (<0.67 wt.%) were more susceptible to IGSCC; heats containing 0.8-1.5 wt.% Si were less susceptible to IGSCC.

A behavior similar to that of Heat L22 (Fig. 15) was observed for BWR neutron absorber tubes that were fabricated from high-purity heats of Type 304L SS with only 0.02-0.05 wt.% Si (see Fig. 17 and Table 10). The observations summarized in Figs. 15–17 appear to be consistent with each other and indicate that unusually low concentrations of Si exacerbate the susceptibility to IASCC.

3.2.5 Effect of Sulfur

In the unirradiated state or at ≈0.3 x 10^{21} n·cm^{-2} (E > 1 MeV), commercial and laboratory heats of Types 304 and 304L SS that contain relatively high concentrations of S (>0.009 wt.% S, 15.0-18.5 wt.% Cr) exhibited significant susceptibility to TGSCC, whereas alloys that contain a relatively low concentration of S (<0.008 wt.% S) exhibited good resistance to TGSCC. These relationships are shown in Fig. 18.

At ≈0.9 x 10^{21} n·cm^{-2} (E > 1 MeV), commercial and laboratory heats of Types 304 and 316 SS that contain low concentrations of S (<0.004 wt.% S) exhibited negligible susceptibility to IGSCC, whereas heats that contain relatively high concentrations of S (>0.005 wt.%) exhibited significant susceptibility to IGSCC (see Fig. 19). The same commercial and laboratory heats that contain low concentrations of S (<0.004 wt.% S) also exhibited high ductility (i.e., large uniform and total elongations), whereas the heats that contain relatively

high concentrations of S (>0.005 wt.%) exhibited relatively low ductility (small uniform and total elongations) (Fig. 20).

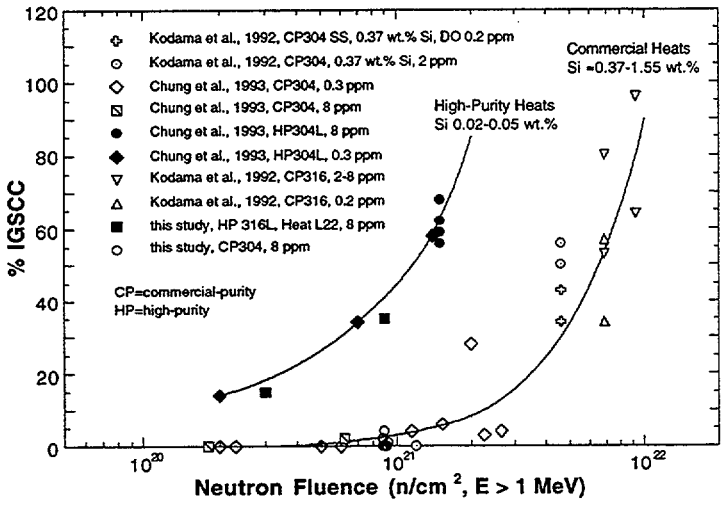

Figure 17.
Susceptibility of irradiated Types 304 and 316 SS to IGSCC as function of fluence, from SSRT tests in BWR-like water that contains 0.2 to 8 ppm DO; Note that high-purity heats that contain very low concentrations of Si (0.02-0.05 wt.%) are more susceptible to IGSCC than commercial-purity heats that contain 0.37-1.55 wt.%.

Table 10. Elemental composition (in wt.%) and susceptibility to IGSCC of high-purity heats of Types 304 and 316 SS that contain very low concentrations of Si (<0.05 wt.%). Composition of some commercial heats are given for comparison.

Heat ID	Cr	Ni	Mn	C	N	B	Si	P	S	Mo	Reactor	Fluence (10^{21} n/cm^2)	Percent IGSCC
HP304-A[a]	18.50	9.45	1.53	0.018	0.100	<0.001	0.03	0.005	0.003	-	BWR-B	0.2, 1.4	14, 58
HP304-B[a]	18.30	9.75	1.32	0.015	0.080	<0.001	0.05	0.005	0.005	-	BWR-B	0.2-1.4	-
HP304-CD[a]	18.58	9.44	1.22	0.017	0.037	0.001	0.02	0.002	0.003	-	BWR-B	0.7	34
HP304-CD[a]	18.58	9.44	1.22	0.017	0.037	0.001	0.02	0.002	0.003	-	BWR-QC	2.0	56, 59, 62, 68
L22	16.10	13.30	0.40	0.003	0.001	0.001	0.02	0.015	0.004	2.04	Halden	0.3, 0.9	15, 35
CP304-A[b]	16.80	8.77	1.65	-	0.052	-	1.55	0.045[c]	0.030[c]	-	BWR-Y	0.2, 0.6, 2.0	0, 0, 28
CP304-B[c]	18-20	8-10	2.00	0.080	-	-	1.00	0.045	0.030	-	BWR-L	0.23-2.64	0-6

[a]High-purity 304L SS, BWR neutron absorber tubes.
[b]Commercial-purity 304 SS, BWR neutron absorber tubes, high Si content.
[c]Commercial-purity 304 SS, BWR control blade sheath, ASTM specification, actual composition not measured.

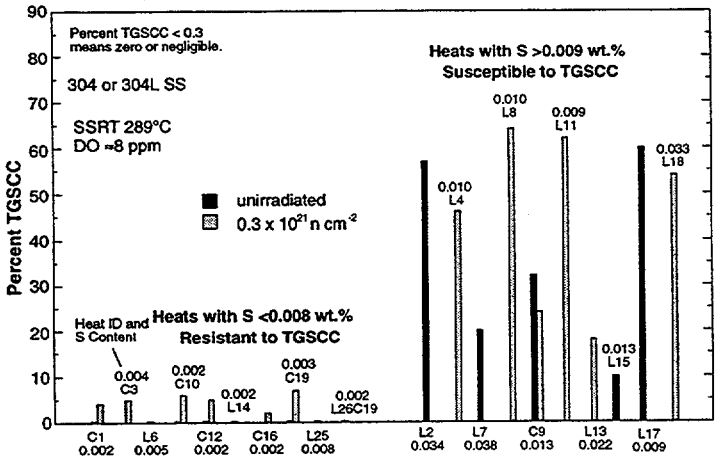

Figure 18.
Effect of S on susceptibility to TGSCC in unirradiated state or after irradiation to ≈0.3 x 10^{21} n·cm^{-2} (E > 1 MeV). Alloys containing low concentrations of S (<0.008 wt.%) are resistant to TGSCC, but alloys containing relatively high concentrations of S (>0.009 wt.%) are susceptible.

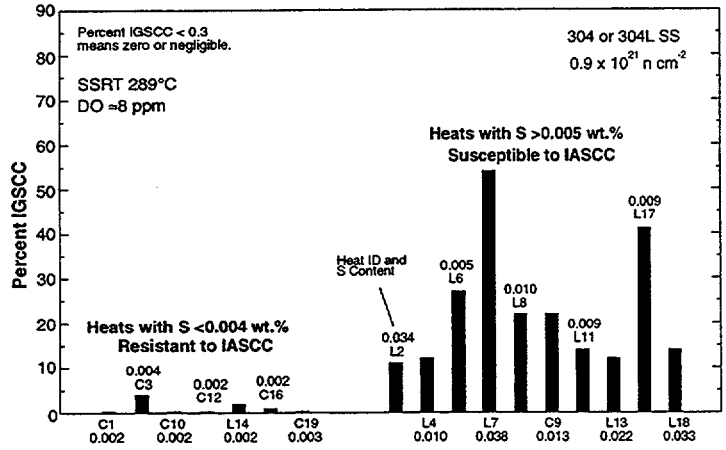

Figure 19.
Effect of S on susceptibility to IGSCC after irradiation to ≈0.9 x 10^{21} n·cm^{-2} (E > 1 MeV). Alloys containing low concentrations of S (<0.004 wt.%) are resistant to IGSCC, but alloys containing relatively high concentrations of S (>0.005 wt.%) are susceptible.

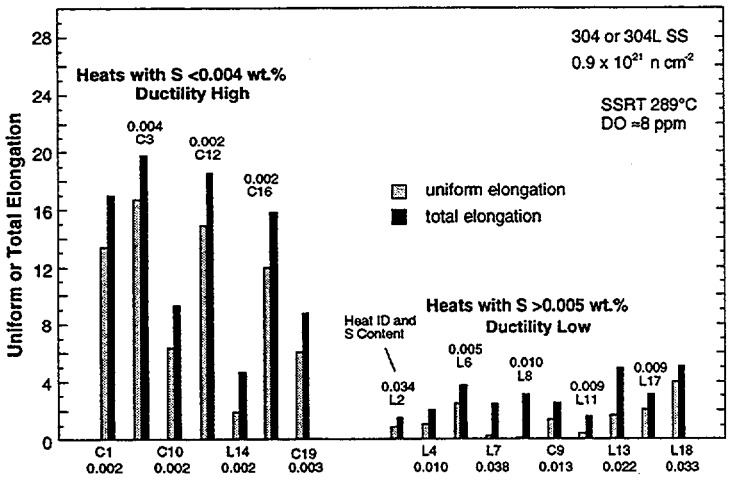

Figure 20.
Effect of S on ductility after irradiation to ≈0.9 x 10^{21} n·cm^{-2} (E > 1 MeV). Alloys containing low concentrations of S (<0.004 wt.%) retain high ductility, but ductility of alloys containing relatively high concentrations of S (>0.005 wt.%) is low.

Initial results obtained for specimens irradiated to ≈2.0 x 10^{21} n·cm^{-2} (E > 1 MeV) indicate a similar effect of S. As shown in Fig. 21, Types 304 and 304L SS that contain ≤0.002 wt.% S exhibited negligible susceptibility to IASCC, whereas heats with ≥0.003 wt.% S exhibited high susceptibility to IASCC. The observations summarized in Figs. 19 and 21 are consistent and strongly indicate that for Types 304 and 304L SS, a high concentration of S exacerbates the susceptibility to IASCC, while a sufficiently low concentration of S (≤0.002 wt.%) provides a better resistance to IASCC.

The uncertainty limit of the measured S concentration is probably significantly large in the extremely low concentration range of 0.002-0.004 wt.% (20-40 wppm). Therefore, it is difficult to predict the limit of bulk S concentration that is required to ensure a good resistance to IASCC for fluences higher than ≈2.0 x 10^{21} n·cm^{-2} (E > 1 MeV). Nevertheless, sensitivity of the susceptibility to IASCC to the bulk concentration of S appears to be more pronounced at ≈2.0 x 10^{21} n·cm^{-2} (E > 1 MeV) than at ≈0.9 x 10^{21} n·cm^{-2} (E > 1 MeV) (compare Fig. 21 and Fig. 19). This finding indicates that irradiation-induced grain-boundary segregation of S plays a major role in IASCC.

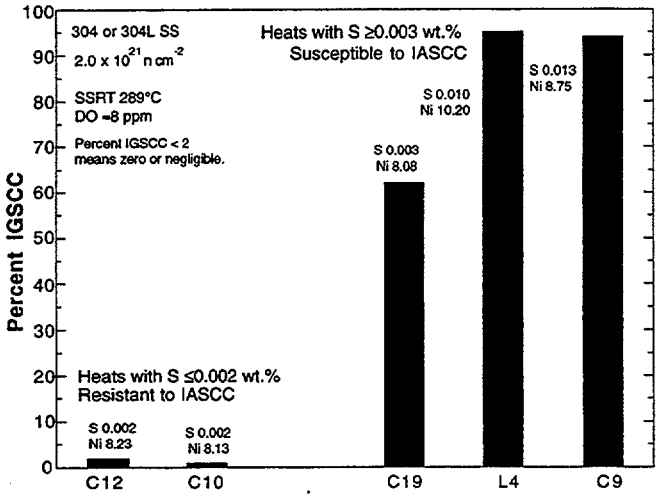

Figure 21.
Effect of S on susceptibility to IGSCC after irradiation to ≈2.0 x 10^{21} n·cm^{-2}. Alloys containing low concentrations of S (<0.002 wt.%) are resistant to IGSCC, but alloys containing higher concentrations of S are susceptible.

In a recent investigation, Kasahara et al.[84] measured the susceptibility of irradiated steel tubes (fluence ≈2.5 x 10^{21} n·cm^{-2}, E > 1 MeV) to IASCC on the basis of the density of crack lines observed on the outer-diameter (OD) surface of the tube, which failed under the tangential stress produced by swelling alumina pellets. They reported that susceptibility to IASCC was significant for one heat of Type 316L SS that contained 0.035 wt.% S, whereas for a similar heat of Type 316L SS that contained 0.001 wt.% S, the susceptibility to IASCC was insignificant. In contrast, one heat of Type 304L SS that contained 0.035 wt.% S exhibited somewhat higher susceptibility index than a similar heat that contained 0.001 wt.% S. In other studies on steels irradiated to ≈0.67 x 10^{21} n·cm^{-2} (E > 1 MeV), Tsukada and his coauthors reported deleterious effects of high concentrations of S for one heat of Type 304L SS (0.032 wt.% S)[80] and a Ti-doped heat of Type 316 SS (0.037 wt.% S).[87] These results appear to be consistent with the present observation that S, even at very low concentrations, strongly exacerbates the susceptibility to IASCC.

3.2.6 Role of Sulfur in IASCC

Elucidating the role of S in IASCC requires an understanding of the behavior of S segregation to grain boundaries via nonequilibrium or irradiation-induced processes. For unirradiated steels, Andresen and Briant[90] have measured the thermally induced grain-boundary segregation of S by Auger electron spectroscopy (AES) for one heat of Type 304L and one heat of Type 316NG SS that contained 0.030-0.037 wt.% S. Both heats were annealed at 400-700°C. Susceptibility of both materials to IGSCC was significant. The Type 304L material did not contain any Mn; therefore, IGSCC in that material was attributed to grain-boundary segregation of S. The lower percent IGSCC observed for the Type 316NG material, which contained 1.1 wt.% Mn and 0.067 wt.% P, was attributed to lower grain-boundary segregation of S, which may have occurred in the material because P and S must compete for grain-boundary sites for segregation.

A similar AES investigation has been performed to determine the grain-boundary concentrations of S in BWR neutron absorber tubes and control blade sheath fabricated from several high- and commercial-purity heats of Types 304 and 304L SS that had been irradiated to ≈2.6 x 10^{21} n·cm^{-2} (E > 1 MeV).[82] The elemental composition of these components is given in Table 10. The irradiated specimens were cathodically charged with hydrogen for ≈48 h at

≈50°C in a solution that contains 100 mg/L $NaAsO_2$ dissolved in 0.1 N H_2SO_4 at a current density of ≈500 mA/cm^2. This procedure is commonly used to produce an IG fracture surface before the grain-boundary composition of an irradiated steel is determined by AES. Then, the hydrogen-charged specimen was fractured by repeated bending at ≈23°C in the ultrahigh vacuum of a shielded scanning Auger microprobe (SAM). However, because of a concern regarding possible S contamination from the hydrogen-charging solution, only limited analysis of grain-boundary segregation of S was performed for the BWR components. Partly because of the experimental difficulty, radiation-induced segregation (RIS) and the role of S on IASCC have been only poorly understood up to now. In the present investigation, however, the effect of S could be determined unambiguously because SSRT tests were performed on a large number of heats that contain S over a sufficiently wide range of concentrations.

The exact mechanism is not clear of how such low concentrations of S exacerbate the susceptibility to TGSCC at zero or very low fluences and the susceptibility to IGSCC at higher fluences, as shown in Figs. 18-21. The effect of S promoting the susceptibility to TGSCC at zero or low fluences is, however, an indication that S solutes significantly decrease the strength of metallic bonding of the grain matrices. For a field-cracked core internal component, IG separation is the predominant fracture surface morphology, and the degree of TGSCC is insignificant. Because of this observation, TGSCC is regarded as an artifact of SSRT tests, and susceptibility to IGSCC from SSRT tests has been commonly used as a measure of the susceptibility to IASCC. However, the results in Figs. 18 and 19 suggest that TGSCC susceptibility at zero and low fluences is related to IGSCC susceptibility at high fluences. Results of the SSRT tests at ≈0.3 x 10^{21} n·cm^{-2} and ≈0.9 x 10^{21} n·cm^{-2} provide useful information on the transition of material state from TGSCC to IGSCC susceptibility. In this "transitional" range, IGSCC fracture surface was often observed in the middle of, and surrounded by, TGSCC fracture surface (Fig. 22). This observation indicates that the strength of metallic bonding in grain matrices at low fluence and the bonding strength of grain boundaries at higher fluences are both strongly influenced by the local S concentration.

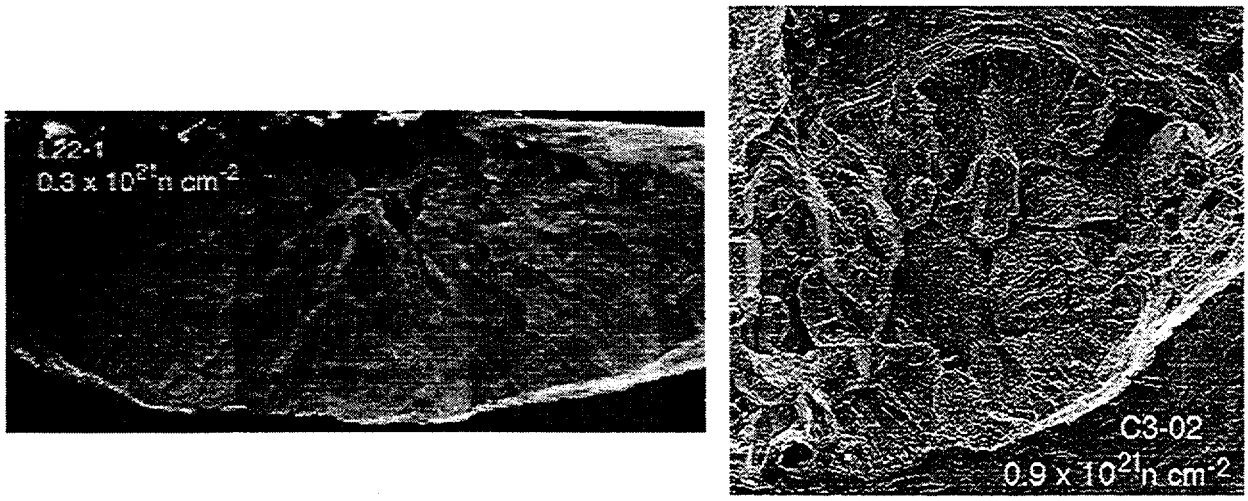

(a) (b)

Figure 22. Examples of IG fracture surface surrounded by TG fracture surface: (a) Type 316L SS Heat L22, fluence ≈0.9 x 10^{21} n·cm^{-2} and (b) Type 304 SS Heat C3, fluence ≈0.9 x 10^{21} n·cm^{-2}

3.3 Fracture Toughness of Austenitic Stainless Steels Irradiated in the Halden Reactor (E. E. Gruber and O. K. Chopra)

3.3.1 Introduction

Austenitic SSs are used extensively as structural alloys in reactor-pressure-vessel internal components because of their high strength, ductility, and fracture toughness. Fracture of these steels occurs by stable tearing at stresses well above the yield stress, and tearing instabilities require extensive plastic deformation. However, exposure to neutron irradiation for extended periods changes the microstructure and degrades the fracture properties of these steels. Irradiation leads to a significant increase in yield strength and reduction in ductility and fracture resistance of austenitic SSs.[94-96]

Neutron irradiation of austenitic SSs at temperatures below 400°C leads to a substructure with very fine defects that consist of small (<5 nm) vacancy and interstitial loops or "black spots" and larger (>5 nm) faulted interstitial loops.[97-99] The latter are obstacles to dislocation motion and lead to matrix strengthening and an increase in tensile strength. Also, irradiation-induced defects cause loss of ductility and reduced strain-hardening capacity of the material. The effects of radiation on various austenitic SSs vary significantly and appear to be related to minor differences in the chemical composition of the steels;[94] the chemical composition can influence the stacking fault energy and/or irradiation-induced microstructure. As the yield strength approaches ultimate strength, planar slip or dislocation channeling is promoted and leads to pronounced degradation in the fracture resistance of these steels.[96] In general, higher stacking-fault energy enhances and cold working inhibits dislocation channeling.[94]

The effect of neutron exposure on the fracture toughness (J_{IC}) of austenitic SSs irradiated at 350–450°C is shown in Fig. 23.[100-108] The effects of irradiation may be divided into three regimes: little or no loss of toughness below a threshold exposure of ≈1 dpa, substantial decrease in toughness at exposures of 1–10 dpa, and no further reduction in toughness above a saturation exposure of 10 dpa. The effect is largest in high-toughness steels. The degradation in fracture properties saturates at J_{IC} ≈30 kJ/m^2 (or equivalent critical stress intensity factor, Kjc, of 70 MPa·m$^{0.5}$). Also, the failure mode changes from dimple fracture to channel fracture.

Most of the existing fracture-toughness test data have been obtained at temperatures above 350°C; fracture toughness results that are relevant to LWRs are very limited.[95,109,110] Fracture toughness J-R curve tests have been conducted at ANL on four heats of Type 304 stainless steel that were irradiated to fluence levels of ≈0.3 and 0.9 x 10^{21} n·cm^{-2} (E > 1 MeV) (≈0.45 and 1.35 dpa) at ≈288°C in a helium environment in the Halden boiling heavy water reactor.[109,110] The tests were performed on 1/4-T compact tension (CT) specimens in air at 288°C; crack extensions were determined by both DC potential and elastic unloading compliance techniques. The composition of the various heats of Type 304 SS is presented in Table 11. Figure 24 shows the configuration of the CT specimens.

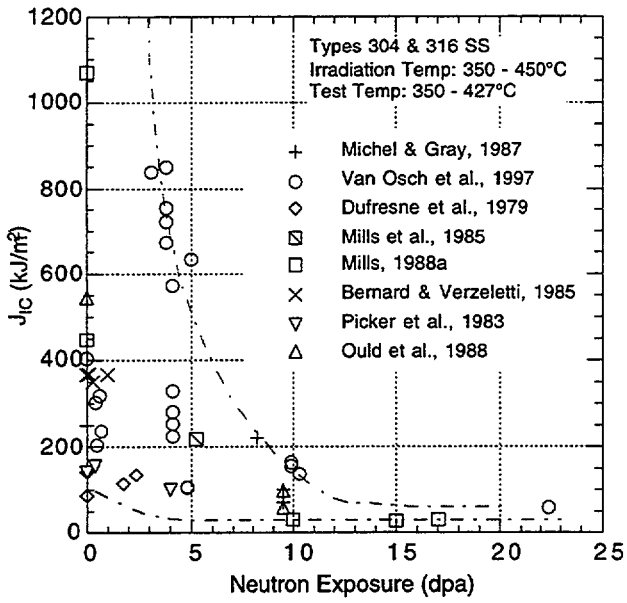

Figure 23.
Fracture toughness J_{IC} as a function of neutron exposure for austenitic Types 304 and 316 SS

Table 11. Composition (wt.%) of model Type 304 SS alloys irradiated in the Halden reactor

Alloy ID[a]	Vendor Heat ID	Analysis	Ni	Si	P	S	Mn	C	N	Cr	O[b]
L2	BPC-4-111	Vendor	10.50	0.82	0.080	0.034	1.58	0.074	0.102	17.02	66
		ANL	–	–	–	–	–	–	–	–	–
C16	PNL-SS-14	Vendor	12.90	0.38	0.014	0.002	1.66	0.020	0.011	16.92	–
		ANL	12.32	0.42	0.026	0.003	1.65	0.029	0.011	16.91	157
C19	DAN-74827	Vendor	8.08	0.45	0.031	0.003	0.99	0.060	0.070	18.21	–
		ANL	8.13	0.51	0.028	0.008	1.00	0.060	0.068	18.05	200
L20	BPC-4-101	Vendor	8.91	0.17	0.010	0.004	0.41	0.002	0.002	18.10	–
		ANL	8.88	0.10	0.020	0.005	0.47	0.009	0.036	18.06	940

[a]First letters "C" and "L" denote commercial and laboratory heats, respectively.
[b]In wppm.

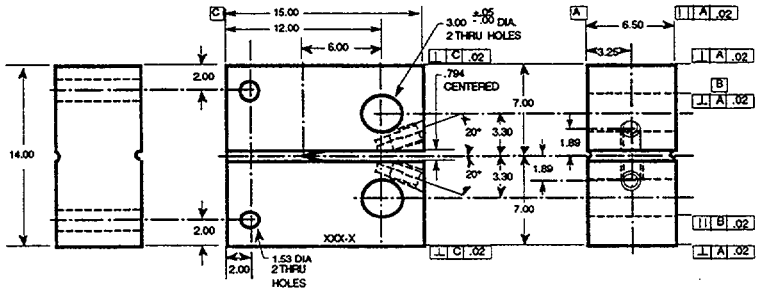

Figure 24. Configuration of compact–tension specimen for this study (dimensions in mm)

Neutron irradiation at 288°C to 0.9 x 10^{21} n·cm^{-2} (E > 1 MeV) (1.35 dpa) decreased the fracture toughness of all the steels. Minor differences in the chemical composition of these steels, e.g., the Ni content for Heats C16 and C19 or the Si content for heats L2 and L20, have little or no effect on their fracture toughness after irradiation. The commercial Heats C16 and C19 exhibited fracture toughness that is superior to that of laboratory Heats L20 and L2. The

poor fracture toughness of Heats L2 and L20 may be attributed to their microstructure.[109] Heat L2 contains relatively high S and P contents and many clusters of MnS inclusions. Failure occurs primarily by grain boundary separation, which is accompanied by some plastic deformation and loss of cohesion along the MnS clusters. Heat L20 contains a relatively high O and many oxide particle inclusions. Failure occurs by nucleation and growth of microvoids and rupture of remaining ligaments. In contrast, commercial heats exhibit ductile failure with some dimple fracture.

For steels irradiated to 0.9 x 10^{21} n·cm^{-2} (E > 1 MeV) (1.35 dpa), the J_{IC} values are 299 and 304 kJ/m^2, respectively, for Heats C16 and C19, and 38 and 39 kJ/m^2, respectively, for Heats L2 and L20. The data from commercial heats fall within the scatter band for the data obtained at temperatures higher than 288°C.

During the current reporting period a fracture toughness J–R curve test was conducted on commercial Heat C19 of Type 304 SS, which was irradiated to a fluence of 2 x 10^{21} n·cm^{-2} (E > 1 MeV) (≈3 dpa) at 289°C in the Halden reactor. The results are compared with the data obtained earlier on heats irradiated to 0.9 x 10^{21} n·cm^{-2} (E > 1 MeV) (1.35 dpa).

3.3.2 Experimental

Fracture toughness J–R curve tests were performed on 1/4–T CT specimens in air at 288°C according to the requirements of ASTM Specification E 1737 for "J–Integral Characterization of Fracture Toughness." Crack extensions were determined by both DC potential and elastic unloading compliance techniques. The crack length and J–integral were calculated with the correlations recommended for disk–shaped compact tension DC(T) specimens in ASTM Specification E 1737.

The fracture toughness test facility is designed for in–cell testing, with the hydraulic actuator, test train, furnace, and other required equipment mounted on a portable, wheeled cart that can be easily rolled into the cell. Detailed descriptions of the test facility and procedures are given in Refs. 111 and 112.

Before testing, the specimens underwent fatigue–precracking at room temperature. The precracked specimens were then tested at 288°C at a constant extension rate; tests were interrupted periodically to determine the crack length. Specimens were held at constant extension to measure the crack length by both the DC potential drop and elastic unloading compliance techniques. For most steels, load relaxation occurs during the hold period or unloading, which causes a time-dependent nonlinearity in the unloading curve. Consequently, before unloading, the specimen was held for ≈1 min to allow for load relaxation. The final crack size was marked by heat tinting and/or by fatigue cycling at room temperature. The specimens were then fractured, and the initial (i.e., fatigue precrack) and final (test) crack lengths were measured optically for both halves of the fractured specimen. The crack lengths were determined by the 9/8 averaging technique, i.e., the two near–surface measurements were averaged, and the resultant value was averaged with the remaining seven measurements.

The crack length measurements obtained by the elastic unloading compliance method were adjusted only with the measured initial crack length, whereas those obtained by the DC potential–drop technique were adjusted with both the initial and final crack lengths. The two-point pinning method was used to correct the measured potentials. The DC potential data were

also corrected for the effects of plasticity on the measured potential, i.e., large crack-tip plasticity can increase measured potentials without crack extension because of resistivity increases. As per ASTM E 1737, the change in potential before crack initiation was ignored, and the remainder of the potential change was used to establish the J–R curve. Plots of normalized potential vs. loadline displacement generally remain linear until the onset of crack extension. For all data within the linear portion of the curve, crack extension was calculated from the blunting line relationship $\Delta a = J/(4\sigma_f)$. For high–strain–hardening materials, e.g., austenitic SSs, a slope that is four times the flow stress ($4\sigma_f$) represents the blunting line better than a slope of $2\sigma_f$, as defined in ASTM E 1737.[96]

3.3.3 Results

Fracture toughness J–R curve tests were conducted at 288°C on Heat C19 of Type 304 SS irradiated in helium at 288°C to 2.0 x 10^{21} n·cm^{-2} (E > 1 MeV) (3 dpa) in the Halden reactor. The load-versus-loadline displacement curve for the test is given in Fig. 25, and the fracture toughness J–R curve determined by the unloading compliance method is shown in Fig. 26.

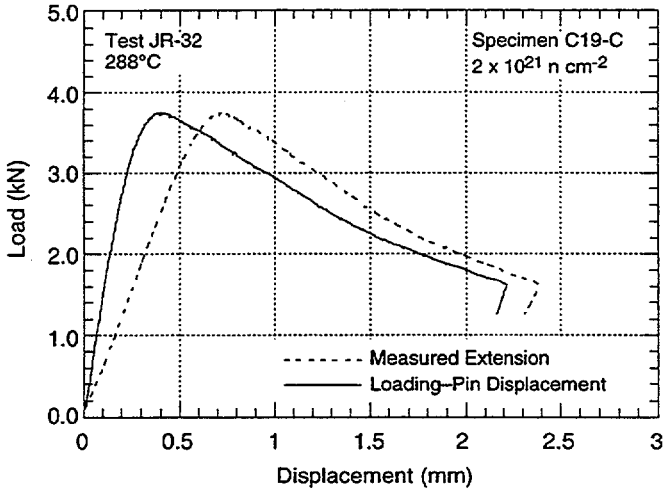

Figure 25.
Load-versus-loadline displacement curves for Heat C19 of Type 304 stainless steel irradiated to 2 x 10^{21} n·cm^{-2} (E > 1 Me) (≈3 dpa) at 289°C.

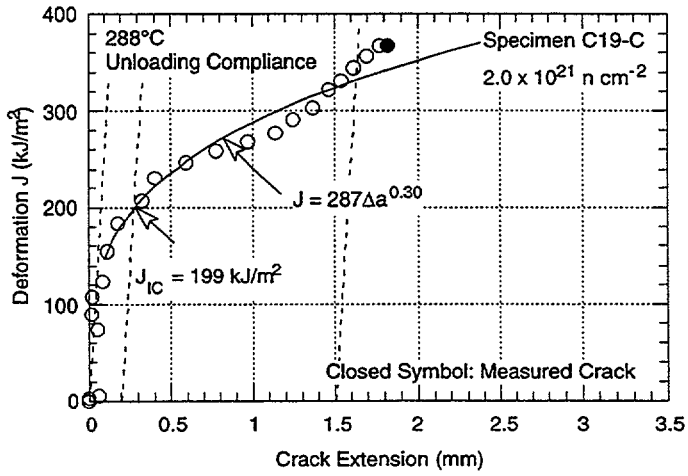

Figure 26.
Fracture toughness J–R curve determined by unloading compliance method at 288°C for Heat C19 of Type 304 stainless steel irradiated to 2 x 10^{21} n·cm^{-2} (E > 1 Me) (≈3 dpa) at 289°C. Dashed lines represent the blunting line and 0.2– and 1.5–offset lines.

The results from this test are consistent with data obtained earlier on specimens irradiated to fluence levels up to 0.9 x 10^{21} n·cm^{-2} (1.35 dpa). Neutron irradiation at 288°C decreases the fracture toughness of all steels. The values of fracture toughness J_{IC} for Heat C19 irradiated to 0.3, 0.9, and 2.0 x 10^{21} n·cm^{-2} (0.45, 1.35, and 3.00 dpa) are 496, 304, and 199 kJ/m^2, respectively. The experimental J_{IC} values for the four heats of Type 304 SS irradiated in the Halden reactor are plotted as a function of neutron exposure in Fig. 27. Results from tests on Type 304 SS reactor internal materials from operating BWRs[95] are also included in the figure. All of the CT specimen data from commercial heats fall within the scatter band for the data obtained at temperatures higher than 288°C.

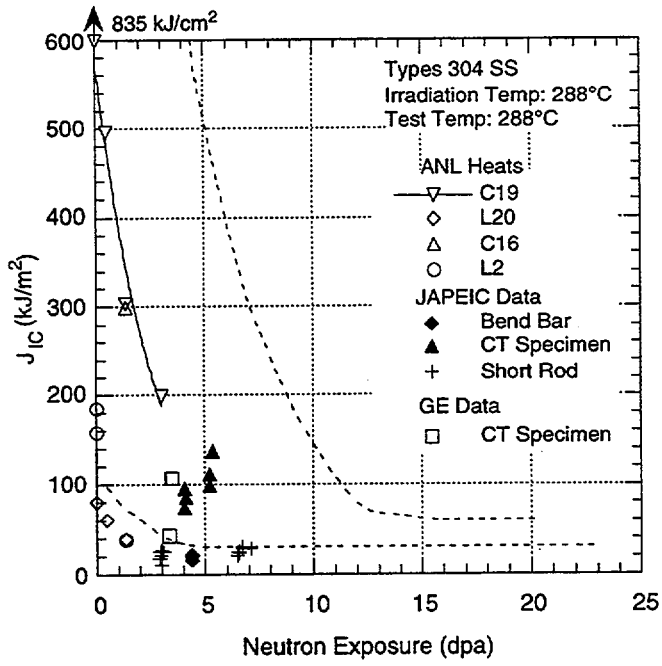

Figure 27.
Fracture toughness J_{IC} of austenitic stainless steels as a function of neutron exposure at 288°C. Dashed lines represent upper and lower bounds for change in J_{IC} for austenitic SSs irradiated at 350–450°C.
JAPEIC = Japan Power Engineering and Inspection Corporation, GE = General Electric Nuclear Energy

4 Environmentally Assisted Cracking of Alloys 600 and 690 in LWR Water (W. K. Soppet, O. K. Chopra, and W. J. Shack)

4.1 Introduction

The objective of this work is to evaluate the resistance of Alloys 600 and 690 to EAC in simulated LWR coolant environments. High–Ni alloys have experienced general corrosion (tube wall thinning), localized intergranular attack (IGA), and SCC in LWRs. Secondary–side IGA* and axial and circumferential SCC** have occurred in Alloy 600 tubes at tube support plates in many steam generators. Primary–water SCC of Alloy 600 steam generator tubes in PWRs at roll transitions and U–bends and in tube plugs*** is a widespread problem that has been studied intensively. Cracking has also occurred in Alloy 600 and other high–Ni alloys (e.g., Inconel–82 and –182 and Alloy X750) that are used in applications such as instrument nozzles and heater thermal sleeves in the pressurizer† and the penetrations for control–rod drive mechanisms in reactor vessel closure heads in the primary system of PWRs,†† in dissimilar–metal welds between SS piping and LAS nozzles, in jet pump hold–down beams,††† and in shroud–support–access–hole covers§ in BWRs. Alloy 690, which has a higher Cr content and greater resistance to SCC, has been proposed as an alternative to Alloy 600.

Alloys 600 and 690, in general, undergo different thermomechanical processing for applications other than steam generator tubes. Because environmental degradation of the alloys in many cases is very sensitive to processing, further evaluation of SCC is needed. In addition, experience strongly suggests that materials that are susceptible to SCC are also susceptible to environmental degradation of fatigue life and fatigue–crack growth properties. A program is being conducted at ANL to evaluate the resistance of Alloys 600 and 690 and their welds to EAC in simulated LWR coolant environments. Fracture–mechanics CGR tests are being conducted on CT specimens of Alloys 600 and 690 in oxygenated and deaerated water that contains B, Li, and low concentrations of dissolved H at 289–380°C; the results have been presented elsewhere.[113–117]

Also, the existing CGR data obtained at ANL and elsewhere for Alloys 600 and 690 under cyclic loading conditions have been compiled and evaluated to establish the effects of alloy type, temperature, load ratio R, stress intensity K, and DO level. The experimental CGRs have

---

*USNRC Information Notice No. 91–67, "Problems with the Reliable Detection of Intergranular Attack (IGA) of Steam Generator Tubing," Oct. 1991.

**USNRC Information Notice No. 90–49, "Stress Corrosion Cracking in PWR Steam Generator Tubes," Aug. 1990; Notice No. 91–43, "Recent Incidents Involving Rapid Increases in Primary–to–Secondary Leak Rate," July 1991; Notice No. 92–80, "Operation with Steam Generator Tubes Seriously Degraded," Dec. 1992; Notice No. 94–05, "Potential Failure of Steam Generator Tubes with Kinetically Welded Sleeves," Jan. 1994.

***USNRC Information Notice No. 89–33, "Potential Failure of Westinghouse Steam Generator Tube Mechanical Plugs," March 1989; Notice No. 89–65, "Potential for Stress Corrosion Cracking in Steam Generator Tube Plugs Supplied by Babcock and Wilcox," Sept. 1989; Notice No. 94–87, "Unanticipated Crack in a Particular Heat of Alloy 600 Used for Westinghouse Mechanical Plugs for Steam Generator Tubes," Dec. 1994.

†USNRC Information Notice No. 90–10, "Primary Water Stress Corrosion Cracking (PWSCC) of Inconel 600," Feb. 1990.

††USNRC Generic Letter 97-01: "Degradation of Control Rod Drive Mechanism and Other Vessel Closure Head Penetrations," Apr. 1, 1997; USNRC Information Notice No. 96–11, "Ingress of Demineralizer Resins Increases Potential for Stress Corrosion Cracking of Control Rod Drive Mechanism Penetrations," Feb. 1996; INPO Document SER 20–93, "Intergranular Stress Corrosion Cracking of Control Rod Drive Mechanism Penetrations," Sept. 1993.

†††USNRC Information Notice 93–101, "Jet Pump Hold–Down Beam Failure," Dec. 1993.

§USNRC Information Notice 92–57, "Radial Cracking of Shroud Support Access Hole Cover Welds," Aug. 1992.

been compared with those expected in air under the same mechanical loading conditions. The purpose was to obtain a qualitative understanding of the degree and range of conditions that are necessary for significant environmental enhancement in growth rates.

Fatigue CGRs are generally represented by

$$da/dN = C(T)\ F(f)\ S(R)\ (\Delta K)^n, \quad (22)$$

where the functions C, F, and S express the dependence of temperature, frequency, and stress ratio, and n is the exponent for the power-law dependence of growth rates on the stress intensity factor range ΔK. The existing fatigue CGR data on Alloys 600 and 690 were analyzed by using Eq. 1 to establish the effects of temperature, stress ratio R, cyclic frequency, and ΔK on the CGRs in air.[117] The CGR (m/cycle) of Alloy 600 in air is expressed as

$$da/dN = C_{A600}\ (1 - 0.82\ R)^{-2.2}\ (\Delta K)^{4.1}, \quad (23)$$

where ΔK is in MPa·$m^{1/2}$, and the constant C_{A600} is given by a third-order polynomial of temperature T (°C) expressed as

$$C_{A600} = 4.835 \times 10^{-14} + (1.622 \times 10^{-16})T - (1.490 \times 10^{-18})T^2 + (4.355 \times 10^{-21})T^3. \quad (24)$$

The CGR (m/cycle) of Alloy 690 in air is expressed as

$$da/dN = C_{A690}\ (1 - 0.82\ R)^{-2.2}\ (\Delta K)^{4.1}, \quad (25)$$

where ΔK is in MPa·$m^{1/2}$, and the constant C_{A690} is given by a third-order polynomial of temperature T (°C) expressed as

$$C_{A690} = 5.423 \times 10^{-14} + (1.83 \times 10^{-16})T - (1.725 \times 10^{-18})T^2 + (5.490 \times 10^{-21})T^3. \quad (26)$$

For both alloys, the estimated values show good agreement with the experimental results. Under similar loading conditions, the CGRs of Alloy 690 appear to be slightly higher than those of Alloy 600. This difference most likely is an artifact of a smaller database for Alloy 690.

During the current reporting period, a CGR test has been completed with a mill-annealed (MA) Alloy 600 (Heat NX131031) specimen in high-purity water under different environmental and loading conditions. The results are compared with data obtained earlier on several heats and heat treatment conditions of Alloy 600 tested in high- and low-DO water.

4.2 Experimental

The facility for conducting corrosion-fatigue tests in water at elevated temperature and pressure consists of an MTS closed-loop electro-hydraulic material test system equipped with an extra-high-load frame rated at 89 kN (20,000 lb) maximum and MTS 810 (or equivalent) control console; hydraulic pump; a commercial autoclave with a recirculating or once-through water system; temperature control unit; DC potential control console; two computers for elastic unloading compliance and DC potential measurements; and a strip chart recorder. The autoclave, mounted within the load frame, has been modified to permit a ≈19-mm (0.75-in.) shaft to load the test specimen through a "Bal-Seal" gland in the top of the autoclave cover. Up

to three 25.4–mm (1–in.) thick (1–T) CT specimens can be tested in series inside the autoclave. Figure 28 shows a photograph of the MTS load frame with the autoclave, temperature control unit and strip chart recorder (on the right), MTS 810 control console (on the left), and DC potential control console (above the MTS 810 system).

The test facility is designed for easy access to the specimens during assembly of the test train. The MTS load frame stands ≈3.7 m (12 ft) high. The actuator assembly, consisting of the hydraulic actuator, load cell , autoclave plug, and the internal specimen load train, may be raised and lowered hydraulically to position the specimens at a convenient height. A photograph of the specimen load train is shown in Fig. 29. A 1–T CT specimen may be substituted for any or all of the three central in-line blocks.

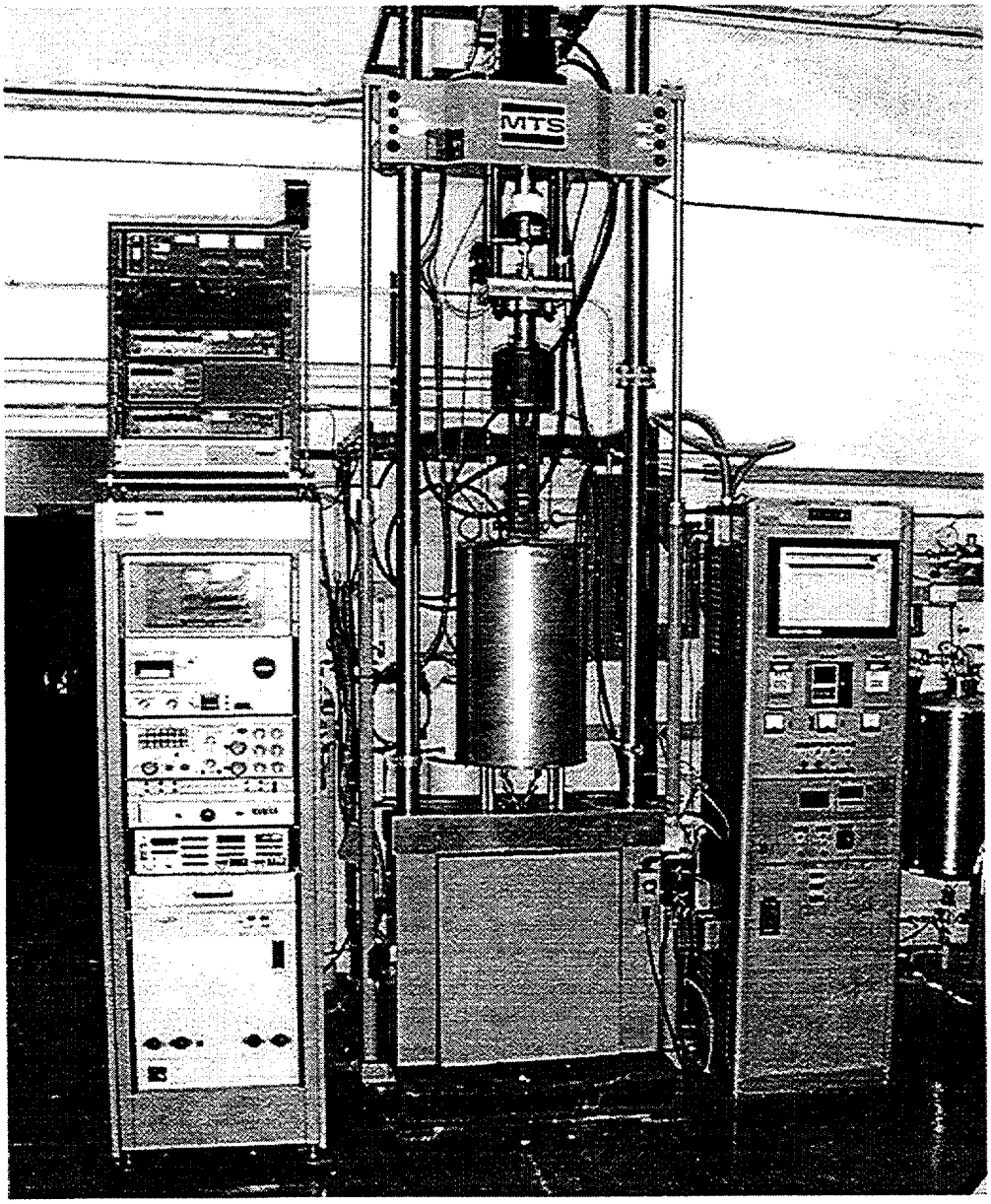

Figure 28. A photograph of the facility for conducting crack growth tests in simulated LWR environments

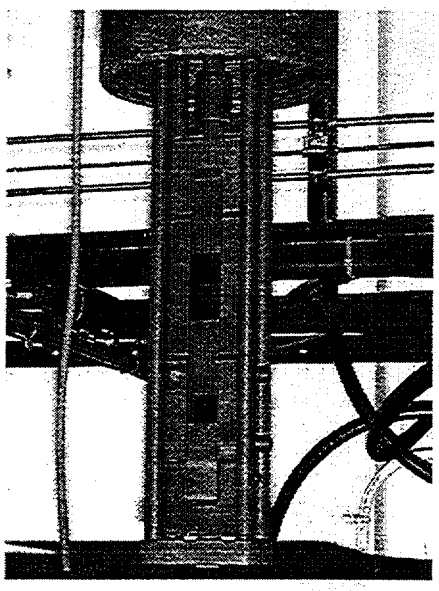

Figure 29.
A photograph of the specimen load train

Figure 30 shows a schematic diagram of the recirculating water system. The system consists of a closed feedwater storage tank, 0.2–micron filter, high pressure pump, regenerative heat exchanger, autoclave preheater, test autoclave, electrochemical potential (ECP) cell, regenerative heat exchanger, back-pressure regulator, a 0.2–micron filter, an ion exchange bed, another 0.2 micron filter, and return line to the tank. The 5.7–liter Type 316 stainless steel autoclave has a 175 mm (6–7/8 in.) OD and is rated for a working pressure of 5050 psig (35 MPa) at 343°C (650°F). The system uses Types 316 or 304 SS tubing. For tests in simulated BWR environments, water quality is maintained by recirculating the supply tank feedwater through a cleanup system consisting of a recirculating pump (item 33), ion exchange bed (item 34), and 0.2-micron filter (item 15). For tests in simulated PWR environments, the feedwater cleanup system is omitted; also, to avoid contamination, the ECP cell in the return line from the autoclave to the water supply tank is by passed during recirculation. Water from the back pressure regulator is released in the once–through water system to the drain, and in the recirculating system to the ion–exchange cleanup system. A conductivity meter and a dissolved oxygen meter (items 31 and 32) are included down stream from the back-pressure regulator to monitor the effluent water chemistry.

Water is circulated at relatively low flow rates, e.g., 5–15 mL/min. The autoclave is maintained at temperatures of 200–320°C and pressures of 1200–1800 psig (8–12 MPa). The high pressure portion of the system extends from Item 16 (high–pressure pump) through Item 30 (back–pressure regulator); over-pressurization in the high-pressure portion of the system, including the autoclave due to temperature excursions, is prevented by a rupture disk (item 20) installed upstream from the high–pressure pump; the rupture disk is set at 1500–1900 psig (10–13 MPa). Also, over-pressure due to accidentally closing the valve downstream from the Mity Mite^{TM} (V18) is prevented by a low-pressure relief valve (item 31) that vents at 9–12 psig (62–83 kPa).

The feedwater storage tank, manufactured by Filpaco Industries, is 130–L capacity and constructed of either Type 304 or 316 SS. The tank is designed for vacuum and over–pressure to 60 psig (414 kPa). The storage tank has either a nitrogen/oxygen or hydrogen cover gas to maintain a desired dissolved oxygen (DO) or hydrogen concentration in the water.

The BWR environment consists of high-purity deionized water that typically contains ≈300 ppb DO. The simulated PWR feedwater contains less than 10 ppb DO but has small additions of lithium and boron. The DO level in water is established by bubbling nitrogen that contains 1-2% oxygen through deionized water in the supply tank in concert with an adjustable over pressure of 1-10 psig. The deionized water is prepared by passing building deionized water through a local filtration system that includes a carbon filter, an Organex-Q filter, two ion exchangers, and a 0.2-mm capsule filter. Either a portable cart-mounted filtration system or the stationary wall-mounted filtration system may be used for feedwater preparation. Water samples are taken periodically to measure pH, resistivity, and DO concentration upstream or downstream from the autoclave.

Simulated PWR water is prepared by dissolving boric acid and lithium hydroxide in 20 L of deionized water before adding the solution to the supply tank. The DO in the deionized water is reduced to less than 10 ppb by bubbling/sparging nitrogen through the water. A vacuum may be applied to the feedwater tank at the vent port (item 9), to speed deoxygenation.

1. COVER GAS SUPPLY TANK
2. TWO STAGE HIGH-PRESSURE REGULATOR
3. FLASH ARRESTOR (WITH HYDROGEN CYLINDERS ONLY)
4. LOW-PRESSURE REGULATOR
5. FLOW METER
6. GAS PURIFIER
7. COMPOUND VACUUM & PRESSURE GAUGE
8. PRESSURE RELIEF VALVE
9. VENT TO AIR WITH FLASH ARRESTOR
10. FEEDWATER STORAGE TANK
11. SPARGE TUBE
12. FEEDWATER FILL PORT
13. WATER SAMPLE PORT
14. SOLENOID VALVE
15. 0.2-MICRON FILTER
16. HIGH-PRESSURE PUMP
17. CHECK VALVE
18. AIR INJECTION PORT
19. SYSTEM BLEED PORT
20. RUPTURE DISK
21. PRESSURE TRANSDUCER
22. HIGH-PRESSURE GAUGE
23. HEAT EXCHANGER
24. AUTOCLAVE PREHEATER
25. COMMERCIAL AUTOCLAVE
26. THERMOWELL
27. "BAL SEAL" RETAINER
28. ECP CELL
29. ECP CELL BYPASS LINE
30. BACK PRESSURE REGULATOR
31. PRESSURE RELIEF VALVE
32. CONDUCTIVITY METER
33. DISSOLVED OXYGEN METER
34. RECIRCULATING PUMP
35. ION EXCHANGE BED
36. ION EXCHANGE BED BYPASS LINE

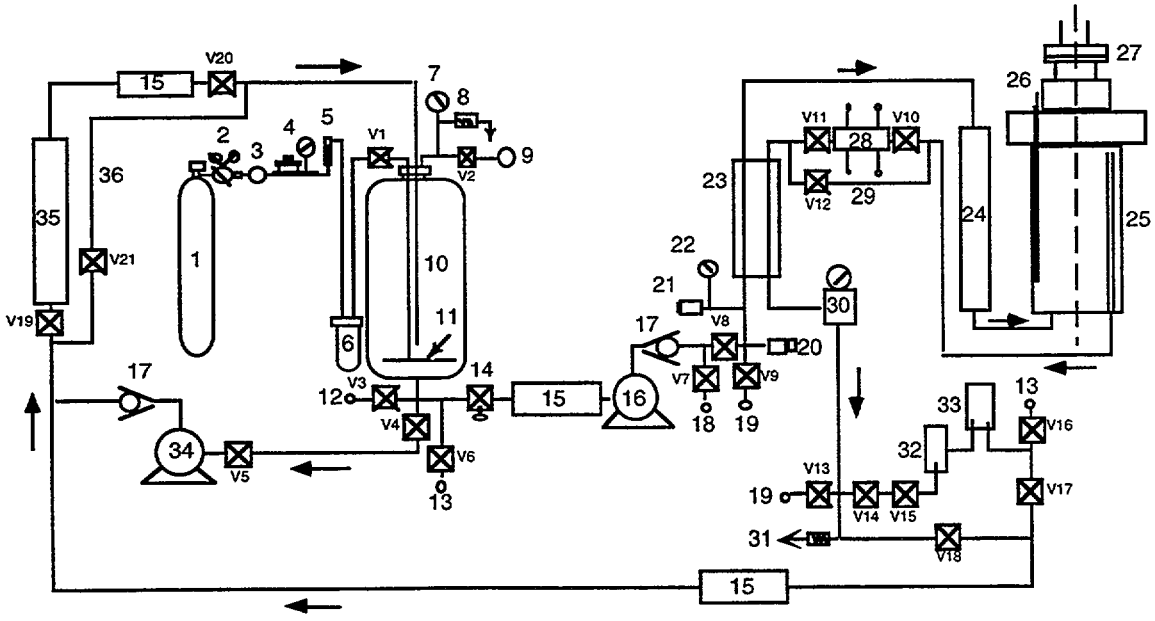

Figure 30. Schematic diagram of the recirculating autoclave system used for crack growth rate tests on 1-T compact tension specimens

The corrosion fatigue tests are being conducted according to ASTM Designation E 647 "Standard Test Method for Measurement of Fatigue Crack Growth Rates." The crack length of each specimen is monitored by DC potential measurements. The chemical composition of Alloy 600 (Heat NX131031) used for the present CGR tests is given in Table 12. Metallographic evaluation of the alloy (Fig. 31) shows a semicontinuous coverage of grain boundary carbides. The material is expected to be susceptible to environmental enhancement of CGRs in both low– and high–DO water. The existing data indicate increased growth rates for (a) nearly all material conditions that have been investigated in high–DO water and (b) materials in low–DO water with either high yield strength and/or poor coverage of grain boundary carbides.

Table 12. Chemical composition (wt.%) of Alloy 600 base metal

Alloy ID (Heat)	Analysis	C	Mn	Fe	S	P	Si	Cu	Ni	Cr	Ti	Nb	Co
Alloy 600													
NX131031	Vendor	0.07	0.22	7.39	0.002	0.006	0.12	0.05	76.00	15.55	0.24	0.07	0.058
	ANL	0.07	0.22	7.73	0.001	–	0.18	0.06	75.34	–	–	–	–

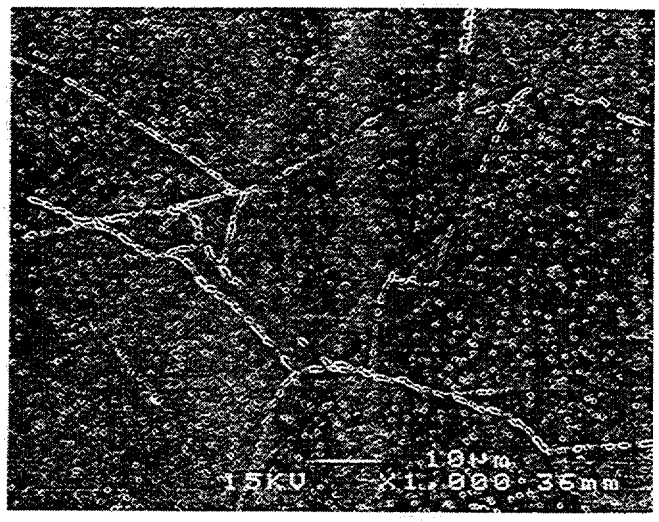

Figure 31.
Microstructure of mill–annealed Alloy 600, Heat NX131031, that shows semicontinuous intergranular and intragranular carbides

4.3 Results

The CGRs for various conditions are given in Table 13. The test was started at 289°C in high–purity water with ≈300 ppb DO. Beginning at test period 10 (≈ 1540 h), the DO content was decreased from ≈300 to < 10 ppb, and the cover gas in the feedwater tank was changed initially to pure nitrogen and then to pure hydrogen at ≈ 15 psig (103 kPa) which corresponds to ≈ 3 ppm dissolved hydrogen in the feedwater. After test period 12 (≈ 3000 h), the test temperature was increased to 320°C. The Pt and steel ECP and crack length for test periods 10 and 11 are shown in Fig. 32. The ECP values in the effluent decreased when the DO content was decreased to <10 ppb and when the cover gas was changed from nitrogen to hydrogen; the response of the Pt electrode is rapid, whereas that of the steel electrode is slow. The results also show a decrease in measured crack length when the cover gas is changed from pure nitrogen to pure hydrogen; this behavior arises because of the shift in the Ni/NiO stability line in the presence of dissolved hydrogen.

Table 13. Crack growth results for Alloy 600[a] in high–purity water

Test Period	Test Time (h)	O_2[b] Conc. (ppb)	Electrode Potential[b] [mV(SHE) at 289°C] SS	Pt	Load Ratio	Rise Time s	K_{max}[c] (MPa·m$^{1/2}$)	ΔK (MPa·m$^{1/2}$)	Growth Rate[d] (m/s) DC Pot.	Fracture Mode[e]
Test Temperature 289°C										
Pre-crack	222	262	74	220	0.2	12	25.35	20.28	4.47E-09	TG
1	552	277	–	–	0.7	1000	28.25	8.47	1.46E-10	TG
2	624	260	–	–	0.7	300	28.31	8.49	2.08E-10	TG
3	674	263	–	–	0.7	60	28.44	8.53	4.72E-10	TG
4	729	290	–	–	0.7	12	28.69	8.61	6.71E-10	TG
5	794	294	–	–	0.7	300	28.77	8.63	1.29E-10	TG
6	1037	305	–	–	0.7	3000	28.86	8.66	6.30E-11	IG
7	1226	308	–	–	0.9	75	28.95	2.89	5.46E-11	IG
8	1394	308	96	220	0.2	10000	29.14	23.31	2.13E-10	IG
9	1537	301	97	221	0.7	1000	29.29	8.79	2.16E-10 (2.40E-10)	IG
10	2043	≤5	-190	-395	0.7	1000	29.42	8.83	2.45E-11	TG
11	2689	≤5	-575	-595	0.7	1000	29.45	8.84	2.45E-11	TG
12	3008	≤5	-584	-598	0.7	60	29.58	8.87	1.17E-11[f]	TG
Test Temperature 320°C										
13	3143	≤5	–	–	0.7	60	29.80	8.94	3.41E-10[g]	TG
14	3289	≤5	–	–	0.7	300	29.86	8.96	2.18E-10[g]	IG
15	3457	≤5	–	–	0.7	1000	29.90	8.97	1.94E-10[g] (2.53E-10)	IG
16	3845	≤5	–	–	0.7	5000	29.96	8.99	8.67E-11[g]	IG

[a]Compact tension specimen (1T CT) of Alloy 600 (Heat NX131031), mill annealed.
[b]Effluent dissolved oxygen concentration and ECP. Feedwater conductivity at 25°C, 0.06 μS/cm, and pH at 25°C, 6.25.
[c]Stress intensity, K_{max}, values at the end of the time period.
[d]CGRs determined from striation measurements are given in parentheses.
[e]Fracture mode, TG = predominantly transgranular and IG = predominantly intergranular.
[f]Growth rate estimated from the value measured during period 3 with similar loading conditions but higher DO.
[g]Growth rates adjusted using the optically measured crack lengths.

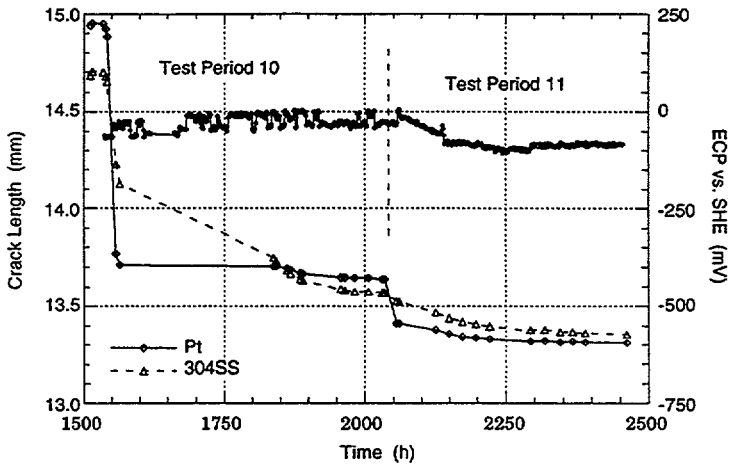

Figure 32.
The change in ECP and crack length with time for Alloy 600 in high–purity water at 289°C.

A metallographic evaluation of the fracture surface of the test specimen was performed to verify crack lengths estimated from the DC potential method. A composite micrograph of the fracture surface of the specimen is shown in Fig. 33. The fracture surface shows two distinct regions of predominantly IG cracking, e.g., during test periods 6–9 in high–DO environment at 289°C and periods 14–16 in low–DO environment at 320°C. The fracture mode, i.e., IG or TG, for the various test periods is identified in Table 13. The measured crack lengths for the test at 289°C in high–purity water with ≈300 ppb DO show good agreement with the values estimated

from the DC potential method. However, the measured lengths for the test in low-DO water with ≈3 ppm dissolved H_2 at either 289 or 320°C had to be adjusted using the optically measured values of crack length. For example, measured CGRs during test periods 13–16 were scaled by a constant factor such that the computed crack length using the adjusted CGRs matched the measured crack lengths. These adjusted CGRs are given in Table 13.

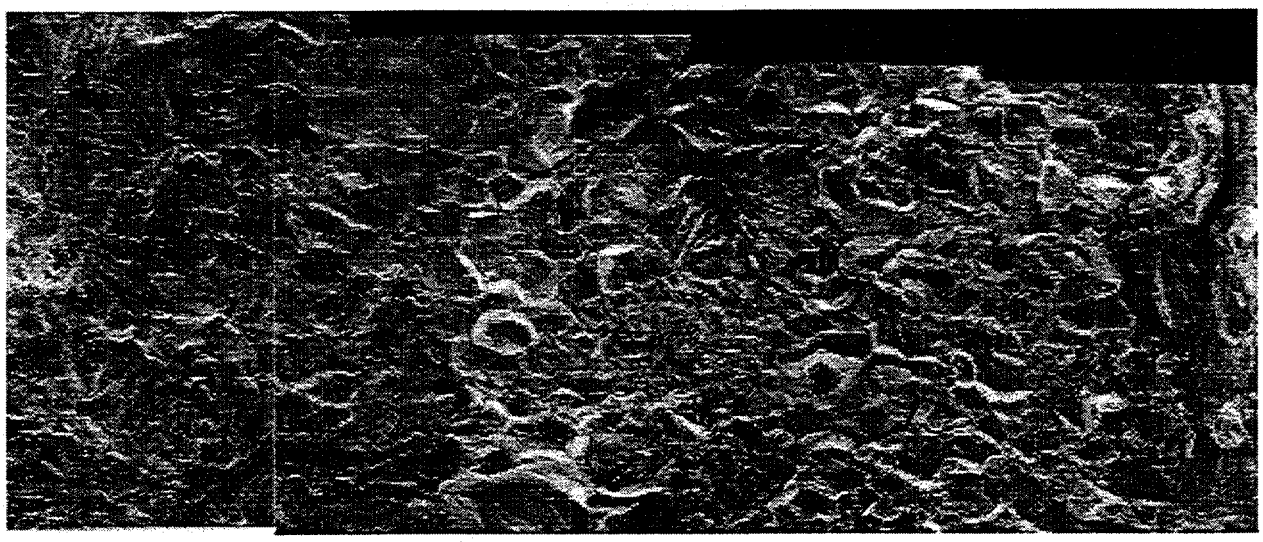

Figure 33. Micrographs of the fracture surface of Alloy 600 specimen tested in high–purity water with different environmental and loading conditions

The adjusted CGRs were further validated by measurements of fatigue striations that were observed in the regions of TG fracture. The specimen was cleaned chemically using a two step process to remove the surface oxide film and surface deposits. The specimen was first exposed to a chemical solution of 20 wt.% NaOH and 30 wt.% $KMnO_4$ for 2 h at ≈70°C and then to a solution of 20 wt.% dibasic ammonium citrate for 2 h at ≈70°C. Examples of fatigue striations observed on the fracture surface during test periods 9 and 15 are shown in Fig. 34; the CGRs determined from striation measurements are given in Table 13. The CGRs from striation measurements show good agreement with the values obtained from the DC potential method.

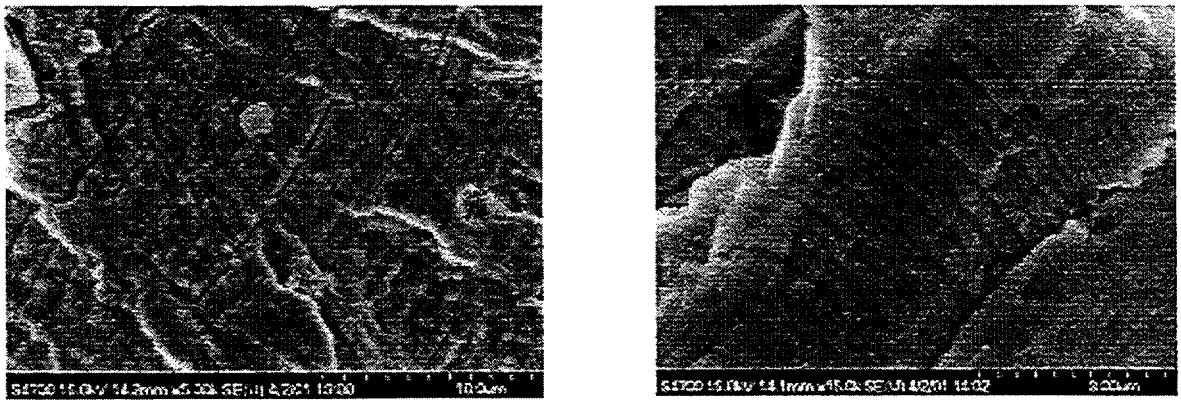

(a) (b)

Figure 34. Fatigue striations observed on the fracture surface of Alloy 600 tested in high–purity water containing (a) ≈300 ppb DO at 289°C and (b) < 5 ppb DO at 320°C

The measured and adjusted CGRs in water and those predicted in air for Alloy 600 at the same loading conditions are plotted in Fig. 35. The results obtained earlier on several other heats of Alloy 600 in ≈ 0.3 or 6 ppm and < 5 ppb DO are also included in the figure. The CGRs (m/s) in air were determined from Eqs. 23 and 24. Figure 35a shows that in high–DO water, nearly all of the heats and heat treatment conditions that have been investigated have enhanced growth rates. The best–fit curve for Alloy 600, either in the solution annealed (SA) condition or SA plus thermally treated (TT) condition, in ≈0.3 ppm DO water is given by the expression

$$CGR_{env} = CGR_{air} + 4.4x10^{-7}(CGR_{air})^{0.33}. \quad (27)$$

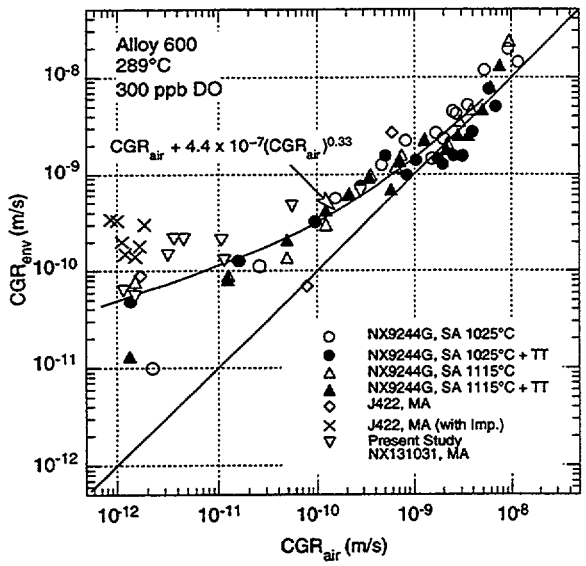

(a)

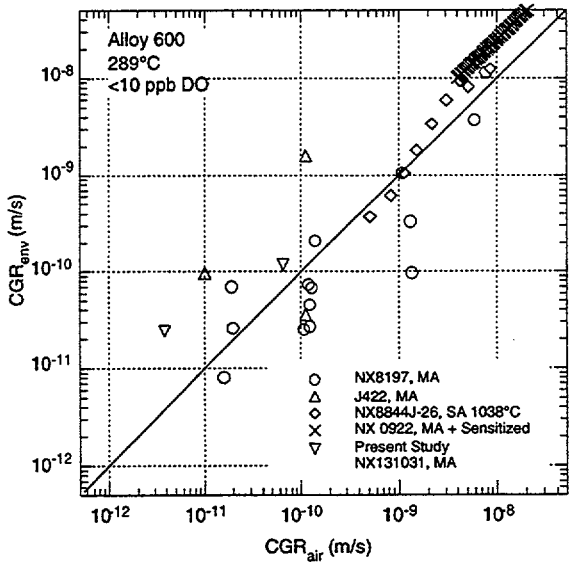

(b)

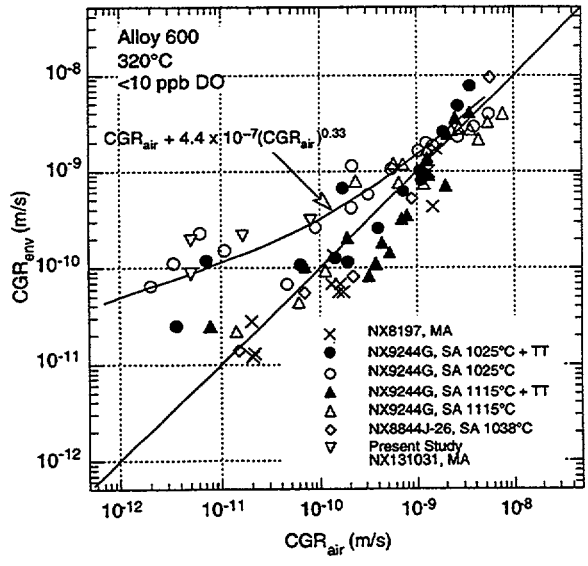

(c)

Figure 35.
Crack growth data for Alloy 600 in high–purity water at (a) 289°C with ≈300 ppb DO, (b) 289°C with < 10 ppb DO, and (c) 320°C with < 10 ppb DO

The CGRs for MA Heat NX131031 are slightly higher than this best–fit curve. The results also indicate that the plots, shown in Fig. 35, between the CGRs in LWR environments and those expected in air under the same mechanical loading conditions, can be used to obtain a qualitative understanding of the degree and range of conditions that are necessary for significant environmental enhancement in growth rates. For example, although the load ratio and rise time during test periods 6 and 7 are significantly different, the loading conditions for both periods yield the same CGR in air ($\approx 1.3 \times 10^{-12}$ m/s) and high–DO water ($\approx 5.9 \times 10^{-11}$ m/s). Similarly, the combination of load ratio and rise time during test periods 8 and 9 yield comparable CGRs in air and water environments.

At 289°C, decreasing the DO content in water from ≈300 to < 10 ppb decreased the growth rates (compare Figs. 35a and b). The actual reduction in CGRs depends on the loading conditions. For example, for loading conditions that correspond to $\approx 4 \times 10^{-12}$ m/s CGR in air, i.e., test periods 1 and 9–11, the CGR in low–DO water is a factor of ≈7 lower than that in high–DO water. Also, the fracture mode changed from IG to TG cracking in low–DO water.

In low–DO water, the growth rates increase with temperature. The CGRs at 320°C in water with < 10 ppb DO are comparable to those at 289°C in water with ≈ 300 ppb DO. Figure 35c shows that environmental enhancement of CGRs in low–DO water seems to be more sensitive to material conditions such as yield strength and grain boundary coverage of carbides. In general, materials with high yield strength and/or low grain boundary coverage of carbides exhibit enhanced CGRs. Because Heat NX131031 contains a semicontinuous coverage of grain boundary carbides, it is expected to be susceptible to environmental enhancement of CGRs in low–DO water.

Figure 33 shows a predominantly IG fracture in high–DO water at 289°C during test periods 6–9 and in low–DO water at 320°C during test periods 14–16; a TG fracture is observed during other test periods. Micrographs of the region with primarily IG fracture are shown in Fig. 36. Most of the grain boundaries, even the ones that are perpendicular to the fracture surface, appear to be separated. Also, the grain boundary surface has a very rough appearance. Not all grain boundaries show pure IG fracture; in some regions, fracture modes seem to change from IG to TG in the middle of the grain (Figs. 36a and b).

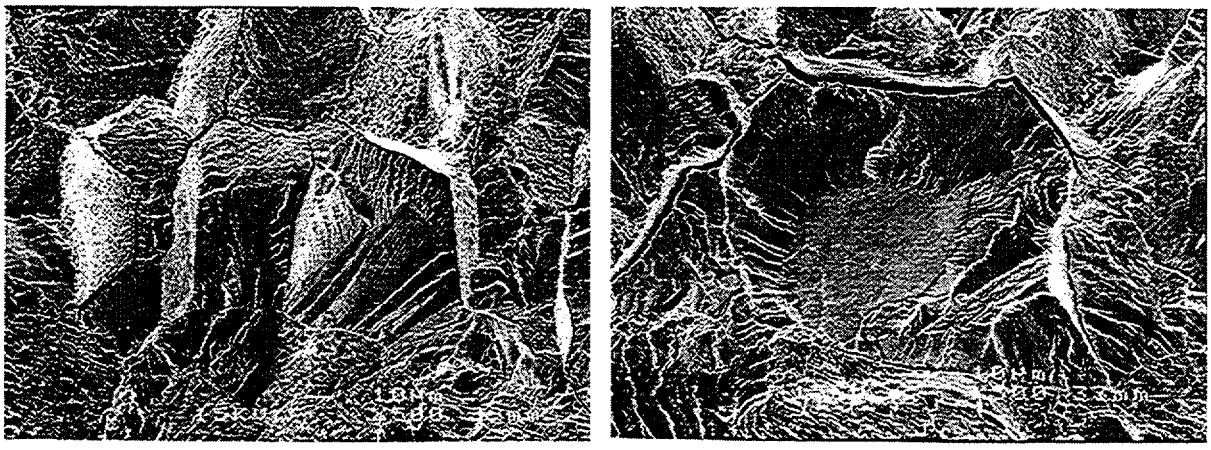

Figure 36. Examples of predominantly intergranular fracture in Alloy 600 in high–purity water

5 Summary

5.1 Environmental Effects on Fatigue S–N Behavior

This report summarizes the work performed at Argonne National Laboratory on fatigue of carbon and low–alloy steels and austenitic SSs in LWR environments. The existing fatigue S–N data have been evaluated to establish the effects of various material and loading variables, such as steel type, strain range, strain rate, temperature, S content in carbon and low–alloy steels, orientation, and DO level in water on the fatigue life of these steels. Statistical models are presented for estimating the fatigue S–N curves as a function of material, loading, and environmental variables. Case studies of fatigue failures in nuclear power plants are presented, and the contribution of environmental effects on crack initiation is discussed.

Several conclusions were reached from studying the influence of reactor environments on the mechanism of fatigue crack initiation. Decreased fatigue lives of carbon and low–alloy steels in high–DO water are caused primarily by the effects of the reactor coolant environment on the growth of small cracks, <100 μm deep. In LWR environments, the growth of these small fatigue cracks in carbon and low–alloy steels occurs by a slip oxidation/dissolution process. The reduction in fatigue life of austenitic SSs in LWR environments is most likely caused by other mechanisms, such as hydrogen–enhanced crack growth.

Also presented are the current two methods for incorporating the effects of LWR coolant environments into the ASME Code fatigue evaluations, i.e., the design fatigue curve method and the fatigue life correction factor method. Both methods are based on statistical models for estimating fatigue lives of carbon and low–alloy steels and austenitic SSs in LWR environments. The environmentally adjusted design fatigue curves provide the allowable cycles for fatigue crack initiation in LWR coolant environments. The new design curves maintain the margins of 2 on stress and 20 on life from the best–fit curves of the experimental data.

In the F_{en} method, environmental effects on life are estimated from the statistical models, but the correction is applied to fatigue lives estimated from the current design curves in the ASME Code. Therefore, fatigue lives estimated by the two methods may differ because of differences in the ASME mean curve and the best–fit curve to existing fatigue data. The current Code design curve for CSs is comparable to the statistical–model curve for LASs, whereas it is somewhat conservative at stress levels <500 MPa when compared with the statistical–model curve for CSs. Consequently, usage factors based on the F_{en} method would be comparable to those based on the environmentally adjusted design fatigue curves for LASs and would be somewhat higher for CSs.

For austenitic SSs, the current Code design fatigue curve is nonconservative when compared with the statistical–model curve, i.e., it predicts longer fatigue lives than the best–fit curve to the existing S–N data. Therefore, usage factors that are based on the F_{en} method would be lower than those determined from the environmentally corrected design fatigue curves. The environmentally adjusted design curves account for the effects of both LWR environment and the difference between the mean fatigue curve used to develop the current Code design curve and the best-fit curve of available experimental data.

5.2 Irradiation–Assisted Stress Corrosion Cracking of Austenitic SS

As fluence was increased from ≈0.3 x 10^{21} n·cm^{-2} (E > 1 MeV) to ≈0.9 x 10^{21} n·cm^{-2}, IG fracture surfaces emerged in many austenitic SSs, usually in the middle of and surrounded by TGSCC fracture surfaces. This observation indicates that the susceptibility to TGSCC at low fluence is related to the susceptibility to IGSCC at higher fluence.

The susceptibility to TGSCC at ≈0.3 x 10^{21} n·cm^{-2} (E > 1 MeV) and to IGSCC at ≈0.9 x 10^{21} n·cm^{-2} was strongly influenced by the bulk concentration of S in steel. This finding suggests that the strength of metallic bonding in grain matrices at low fluence and the bonding strength of grain boundaries at higher fluences are strongly influenced by the local concentration of S. At ≈2.0 x 10^{21} n·cm^{-2}, Type 304 and 304L SS heats that contain very low concentrations of S (≤0.002 wt.%) were not susceptible to IASCC, whereas heats that contain higher concentrations of S were susceptible.

Type 304L and 316L SSs that contained unusually low concentrations of Si (<0.05 wt.%) and that were irradiated either in the Halden reactor or in BWRs exhibited unusually high susceptibility to IASCC, even at low fluences.

A fracture toughness J–R curve test has been conducted on a commercial heat of Type 304 SS that was irradiated to a fluence level of 2.0 x 10^{21} n·cm^{-2} (E > 1 MeV) (≈3 dpa) at ≈288°C in a helium environment in the Halden boiling heavy water reactor. The test was performed on a 1/4–T CT specimen in air at 288°C; crack extensions were determined by both DC potential and elastic unloading compliance techniques. The results of the test are consistent with the data obtained earlier on steels irradiated to 0.3 and 0.9 x 10^{21} n·cm^{-2} (E > 1 MeV) (0.45 and 1.35 dpa). Neutron irradiation at 288°C decreases the fracture toughness of austenitic SSs. All of the CT specimen data from commercial heats fall within the scatter band for the data obtained at higher temperatures.

5.3 Environmentally Assisted Cracking of Alloys 600 and 690 in LWR Water

The resistance of Ni alloys to EAC in simulated LWR environments is being evaluated. Existing CGR data for Alloys 600 and 690 under cyclic loads have been analyzed to establish the effects of alloy chemistry, material heat treatment, cold work, temperature, load ratio R, stress intensity K, and DO level. The experimental CGRs in high–temperature, high–purity water are compared with CGRs that would be expected in air under the same mechanical loading conditions to obtain a qualitative understanding of the degree and range of conditions that are necessary for significant environmental enhancement in growth rates.

During the current reporting period, a CGR test has been completed on mill–annealed Alloy 600 specimen in high–purity water with different environmental and loading conditions. The growth rates from this test in high–DO water show good agreement with the data obtained earlier. At 289°C, decreasing the DO content in water from ≈300 to < 10 ppb decreased the growth rates. The actual reduction in CGRs depends on the loading conditions. For the loading conditions that correspond to ≈ 4 x 10^{-12} m/s CGR in air, CGR in low–DO water is a factor of ≈7 lower than that in high–DO water. Also, the fracture mode changed from IG to TG cracking in low–DO water. The results also indicate that in low–DO water, growth rates increase with temperature. The CGRs at 320°C in water with < 10 ppb DO are comparable to those at 289°C in water with ≈ 300 ppb DO.

References

1. K. Kussmaul, R. Rintamaa, J. Jansky, M. Kemppainen, and K. Törrönen, *On the Mechanism of Environmental Cracking Introduced by Cyclic Thermal Loading*, in IAEA Specialists Meeting Corrosion and Stress Corrosion of Steel Pressure Boundary Components and Steam Turbines, VTT Symp. 43, Espoo, Finland, pp. 195–243 (1983).

2. K. Iida, *A Review of Fatigue Failures in LWR Plants in Japan*, Nucl. Eng. Des. **138**, 297–312 (1992).

3. K. Kussmaul, D. Blind, and J. Jansky, *Formation and Growth of Cracking in Feed Water Pipes and RPV Nozzles*, Nucl. Eng. Des. **81**, 105–119 (1984).

4. C. E. Jaske and W. J. O'Donnell, *Fatigue Design Criteria for Pressure Vessel Alloys*, Trans. ASME J. Pressure Vessel Technol. **99**, 584–592 (1977).

5. O. K. Chopra, *Effects of LWR Coolant Environments on Fatigue Design Curves of Austenitic Stainless Steels*, NUREG/CR-5704, ANL-98/31 (1999).

6. S. Ranganath, J. N. Kass, and J. D. Heald, *Fatigue Behavior of Carbon Steel Components in High-Temperature Water Environments*, BWR Environmental Cracking Margins for Carbon Steel Piping, EPRI NP-2406, Electric Power Research Institute, Palo Alto, CA, Appendix 3 (1982).

7. M. Higuchi and K. Iida, *Fatigue Strength Correction Factors for Carbon and Low-Alloy Steels in Oxygen-Containing High-Temperature Water*, Nucl. Eng. Des. **129**, 293–306 (1991).

8. N. Nagata, S. Sato, and Y. Katada, *Low-Cycle Fatigue Behavior of Pressure Vessel Steels in High-Temperature Pressurized Water*, ISIJ Intl. **31** (1), 106–114 (1991).

9. W. A. Van Der Sluys, *Evaluation of the Available Data on the Effect of the Environment on the Low-Cycle Fatigue Properties in Light Water Reactor Environments*, in Proc. 6th Intl. Symp. on Environmental Degradation of Materials in Nuclear Power Systems – Water Reactors, R. E. Gold and E. P. Simonen, eds., Metallurgical Society, Warrendale, PA, pp. 1–4 (1993).

10. H. Kanasaki, M. Hayashi, K. Iida, and Y. Asada, *Effects of Temperature Change on Fatigue Life of Carbon Steel in High-Temperature Water*, in Fatigue and Crack Growth: Environmental Effects, Modeling Studies, and Design Considerations, PVP Vol. 306, S. Yukawa, ed., American Society of Mechanical Engineers, New York, pp. 117–122 (1995).

11. G. Nakao, H. Kanasaki, M. Higuchi, K. Iida, and Y. Asada, *Effects of Temperature and Dissolved Oxygen Content on Fatigue Life of Carbon and Low-Alloy Steels in LWR Water Environment*, in Fatigue and Crack Growth: Environmental Effects, Modeling Studies, and Design Considerations, PVP Vol. 306, S. Yukawa, ed., American Society of Mechanical Engineers, New York, pp. 123–128 (1995).

12. M. Higuchi, K. Iida, and Y. Asada, *Effects of Strain Rate Change on Fatigue Life of Carbon Steel in High-Temperature Water*, in Effects of the Environment on the Initiation of Crack Growth, ASTM STP 1298, W. A. Van Der Sluys, R. S. Piascik, and R. Zawierucha, eds., American Society for Testing and Materials, Philadelphia, pp. 216–231 (1997).

13. O. K. Chopra and W. J. Shack, *Evaluation of Effects of LWR Coolant Environments on Fatigue Life of Carbon and Low-Alloy Steels*, in Effects of the Environment on the Initiation of Crack Growth, ASTM STP 1298, W. A. Van Der Sluys, R. S. Piascik, and R. Zawierucha, eds., American Society for Testing and Materials, Philadelphia, pp. 247–266 (1997).

14. O. K. Chopra and W. J. Shack, *Low-Cycle Fatigue of Piping and Pressure Vessel Steels in LWR Environments*, Nucl. Eng. Des. **184**, 49–76 (1998).

15. O. K. Chopra and W. J. Shack, *Effects of LWR Coolant Environments on Fatigue Design Curves of Carbon and Low-Alloy Steels*, NUREG/CR-6583, ANL-97/18 (March 1998).

16. O. K. Chopra and W. J. Shack, *Fatigue Crack Initiation in Carbon and Low-Alloy Steels in Light Water Reactor Environments – Mechanism and Prediction*, in Fatigue, Environmental Factors, and New Materials, PVP Vol. 374, H. S. Mehta, R. W. Swindeman, J. A. Todd, S. Yukawa, M. Zako, W. H. Bamford, M. Higuchi, E. Jones, H. Nickel, and S. Rahman, eds., American Society of Mechanical Engineers, New York, pp. 155–168 (1998).

17. O. K. Chopra and W. J. Shack, *Overview of Fatigue Crack Initiation in Carbon and Low-Alloy Steels in Light Water Reactor Environments*, J. Pressure Vessel Technol. **121**, 49–60 (1999).

18. O. K. Chopra and J. Muscara, *Effects of Light Water Reactor Coolant Environments on Fatigue Crack Initiation in Piping and Pressure Vessel Steels*, in Proc. 8th Intl. Conference on Nuclear Engineering, 2.08 LWR Materials Issue, Paper 8300, American Society of Mechanical Engineers, New York (2000).

19. M. Fujiwara, T. Endo, and H. Kanasaki, *Strain Rate Effects on the Low-Cycle Fatigue Strength of 304 Stainless Steel in High-Temperature Water Environment*, in Fatigue Life: Analysis and Prediction, Proc. Intl. Conf. and Exposition on Fatigue, Corrosion Cracking, Fracture Mechanics, and Failure Analysis, ASM, Metals Park, OH, pp. 309–313 (1986).

20. H. Mimaki, H. Kanasaki, I. Suzuki, M. Koyama, M. Akiyama, T. Okubo, and Y. Mishima, *Material Aging Research Program for PWR Plants*, in Aging Management Through Maintenance Management, PVP Vol. 332, I. T. Kisisel, ed., American Society of Mechanical Engineers, New York, pp. 97–105 (1996).

21. M. Higuchi and K. Iida, *Reduction in Low-Cycle Fatigue Life of Austenitic Stainless Steels in High-Temperature Water*, in Pressure Vessel and Piping Codes and Standards, PVP Vol. 353, D. P. Jones, B. R. Newton, W. J. O'Donnell, R. Vecchio, G. A. Antaki, D. Bhavani, N. G. Cofie, and G. L. Hollinger, eds., American Society of Mechanical Engineers, New York, pp. 79–86 (1997).

22. H. Kanasaki, R. Umehara, H. Mizuta, and T. Suyama, *Fatigue Lives of Stainless Steels in PWR Primary Water*, Trans. 14th Intl. Conf. on Structural Mechanics in Reactor Technology (SMiRT 14), Lyon, France, pp. 473–483 (1997).

23. H. Kanasaki, R. Umehara, H. Mizuta, and T. Suyama, *Effects of Strain Rate and Temperature Change on the Fatigue Life of Stainless Steel in PWR Primary Water*, Trans. 14th Intl. Conf. on Structural Mechanics in Reactor Technology (SMiRT 14), Lyon, France, pp. 485–493 (1997).

24. M. Hayashi, *Thermal Fatigue Strength of Type 304 Stainless Steel in Simulated BWR Environment*, Nucl. Eng. Des. **184**, 135–144 (1998).

25. M. Hayashi, K. Enomoto, T. Saito, and T. Miyagawa, *Development of Thermal Fatigue Testing with BWR Water Environment and Thermal Fatigue Strength of Austenitic Stainless Steels*, Nucl. Eng. Des. **184**, 113–122 (1998).

26. O. K. Chopra and D. J. Gavenda, *Effects of LWR Coolant Environments on Fatigue Lives of Austenitic Stainless Steels*, in Pressure Vessel and Piping Codes and Standards, PVP Vol. 353, D. P. Jones, B. R. Newton, W. J. O'Donnell, R. Vecchio, G. A. Antaki, D. Bhavani, N. G. Cofie, and G. L. Hollinger, eds., American Society of Mechanical Engineers, New York, pp. 87–97 (1997).

27. O. K. Chopra and D. J. Gavenda, *Effects of LWR Coolant Environments on Fatigue Lives of Austenitic Stainless Steels*, J. Pressure Vessel Technol. **120**, 116–121 (1998).

28. O. K. Chopra and J. L. Smith, *Estimation of Fatigue Strain–Life Curves for Austenitic Stainless Steels in Light Water Reactor Environments*, in Fatigue, Environmental Factors, and New Materials, PVP Vol. 374, H. S. Mehta, R. W. Swindeman, J. A. Todd, S. Yukawa, M. Zako, W. H. Bamford, M. Higuchi, E. Jones, H. Nickel, and S. Rahman, eds., American Society of Mechanical Engineers, New York, pp. 249–259 (1998).

29. S. Majumdar, O. K. Chopra, and W. J. Shack, *Interim Fatigue Design Curves for Carbon, Low–Alloy, and Austenitic Stainless Steels in LWR Environments*, NUREG/CR–5999, ANL–93/3 (1993).

30. J. Keisler, O. K. Chopra, and W. J. Shack, *Fatigue Strain–Life Behavior of Carbon and Low–Alloy Steels, Austenitic Stainless Steels, and Alloy 600 in LWR Environments*, NUREG/CR–6335, ANL–95/15 (1995).

31. J. Keisler, O. K. Chopra, and W. J. Shack, *Fatigue Strain–Life Behavior of Carbon and Low–Alloy Steels, Austenitic Stainless Steels, and Alloy 600 in LWR Environments*, Nucl. Eng. Des. **167**, 129–154 (1996).

32. A. G. Ware, D. K. Morton, and M. E. Nitzel, *Application of NUREG/CR–5999 Interim Design Curves to Selected Nuclear Power Plant Components*, NUREG/CR–6260, INEL–95/0045 (1995).

33. H. S. Mehta and S. R. Gosselin, *An Environmental Factor Approach to Account for Reactor Water Effects in Light Water Reactor Pressure Vessel and Piping Fatigue Evaluations: Fatigue and Fracture, Volume 1*, PVP Vol. 323, H. S. Mehta, ed., American Society of Mechanical Engineers, New York, pp. 171–185 (1996).

34. H. S. Mehta and S. R. Gosselin, *Environmental Factor Approach to Account for Water Effects in Pressure Vessel and Piping Fatigue Evaluations*, Nucl. Eng. Des. **181**, 175–197 (1998).

35. M. Higuchi, *Difference of Environment Effects Between Japanese EFD and ANL Approaches*, presented at Working Group Meeting on S–N Data Analysis, the Pressure Vessel Research Council, Orlando, FL (May 1996).

36. K. J Miller, *Initiation and Growth Rates of Short Fatigue Cracks*, Fundamentals of Deformation and Fracture, Eshelby Memorial Symposium, Cambridge University Press, Cambridge, UK, pp. 477–500 (1985).

37. K. Tokaji, T. Ogawa, and S. Osaka, *The Growth of Microstructurally Small Fatigue Cracks in a Ferrite–Pearlite Steel*, Fatigue Fract. Eng. Mater. Struct. **11**, 311–342 (1988).

38. D. J. Gavenda, P. R. Luebbers, and O. K. Chopra, *Crack Initiation and Crack Growth Behavior of Carbon and Low–Alloy Steels*, Fatigue and Fracture 1, Vol. 350, S. Rahman, K. K. Yoon, S. Bhandari, R. Warke, and J. M. Bloom, eds., American Society of Mechanical Engineers, New York, pp. 243–255 (1997).

39. K. Obrtlik, J. Polák, M. Hájek, and A. Vasek, *Short Fatigue Crack Behaviour in 316L Stainless Steel*, Intl. J. Fatigue **19**, 471–475 (1997).

40. S. G. Sundara Raman, D. Argence, and A. Pineau, *High Temperature Short Fatigue Crack Behaviour in a Stainless Steel*, Fatigue Fract. Eng. Mater. Struct. **20**, 1015–1031 (1997).

41. K. J. Miller, *Damage in Fatigue: A New Outlook*, International Pressure Vessels and Piping Codes and Standards: Volume 1 – Current Applications, PVP Vol. 313–1, K. R. Rao and Y. Asada, eds., American Society of Mechanical Engineers, New York, pp. 191–192 (1995).

42. J. L. Smith, and O. K. Chopra, *Crack Initiation in Smooth Fatigue Specimens of Austenitic Stainless Steel in Light Water Reactor Environments*, Operations, Applications, and Components – 1999, PVP Vol. 395, I. T. Kisisel, ed., American Society of Mechanical Engineers, New York, pp. 235–242 (1999).

43. Y. Katada, N. Nagata, and S. Sato, *Effect of Dissolved Oxygen Concentration on Fatigue Crack Growth Behavior of A533 B Steel in High–Temperature Water*, ISIJ Intl. **33** (8), 877–883 (1993).

44. M. Higuchi, *Fatigue Properties of Carbon Steel Weldments in Oxygenated High–Temperature Water – Evaluation of Effects of Tensile Strength and Sulfur Content*, presented at Working Group Meeting on S–N Data Analysis, the Pressure Vessel Research Council, June, Milwaukee (June 1995).

45. A. Hirano, M. Yamamoto, K. Sakaguchi, K. Iida, and T. Shoji, *Effects of Water Flow Rate on Fatigue Life of Carbon Steel in High Temperature Pure Water Environment*, in Assessment Methodologies for Predicting Failure: Service Experience and Environmental Considerations, PVP Vol. 410-2, R. Mohan, ed., American Society of Mechanical Engineers, New York, pp. 13–18 (2000).

46. E. Lenz, N. Wieling, and H. Muenster, *Influence of Variation of Flow Rates and Temperature on the Cyclic Crack Growth Rate under BWR Conditions*, in Environmental Degradation of Materials in Nuclear Power Systems – Water Reactors, Metallurgical Society, Warrendale, PA (1988).

47. S. Yukawa, *Meeting of the Steering Committee for Cyclic Life and Environmental Effects (CLEE)*, the Pressure Vessel Research Council, Columbus, OH (June 1999).

48. NRC Bulletin No. 88–11, *Pressurizer Surge Line Thermal Stratification*, U.S. Nuclear Regulatory Commission, Washington, DC (Dec. 20, 1988).

49. NRC IE Bulletin No. 79–13, *Cracking in Feedwater System Piping*, U.S. Nuclear Regulatory Commission, Washington, DC (June 25, 1979).

50. NRC Information Notice 93–20, *Thermal Fatigue Cracking of Feedwater Piping to Steam Generators*, U.S. Nuclear Regulatory Commission, Washington, DC (March 24, 1993).

51. R. B. Dooley and R. S. Pathania, *Corrosion Fatigue of Water Touched Pressure Retaining Components in Power Plants*, EPRI TR–106696, Electric Power Research Institute, Palo Alto, CA (1997).

52. H. Watanabe, *Boiling Water Reactor Feedwater Nozzle/Sparger, Final Report*, NEDO–21821–A, General Electric Co., San Jose, CA (1980).

53. B. M. Gordon, D. E. Delwiche, and G. M. Gordon, *Service Experience of BWR Pressure Vessels*, in Performance and Evaluation of Light Water Reactor Pressure Vessels, PVP Vol.–119, American Society of Mechanical Engineers, New York, pp. 9–17 (1987).

54. E. Lenz, B. Stellwag, and N. Wieling, *The Influence of Strain–Induced Corrosion Cracking on the Crack Initiation in Low–Alloy Steels in HT–Water – A Relation Between Monotonic and Cyclic Crack Initiation Behavior*, in IAEA Specialists Meeting Corrosion and Stress Corrosion of Steel Pressure Boundary Components and Steam Turbines, VTT Symp. 43, Espoo, Finland, pp. 243–267 (1983).

55. J. Hickling and D. Blind, *Strain–Induced Corrosion Cracking of Low–Alloy Steels in LWR Systems – Case Histories and Identification of Conditions Leading to Susceptibility*, Nucl. Eng. Des. **91**, 305–330 (1986).

56. F. P. Ford, S. Ranganath, and D. Weinstein, *Environmentally Assisted Fatigue Crack Initiation in Low–Alloy Steels – A Review of the Literature and the ASME Code Requirements*, EPRI TR–102765, Electric Power Research Institute, Palo Alto, CA (1993).

57. J.-M. Stephan and J. C. Masson, *Auxiliary Feedwater Line Stratification and COUFAST Simulation*, Proc. Int. Conf. on Fatigue of Reactor Components, Napa CA, July 31–August 2, 2000.

58. J. F. Enrietto, W. H. Bamford, and D. F. White, *Preliminary Investigation of PWR Feedwater Nozzle Cracking*, Intl. J. Pressure Vessels and Piping **9**, 421–443 (1981).

59. G. Katzenmeier, K. Kussmaul, E. Roos, and H. Diem, *Component Testing at the HDR-Facility for Validating the Calculation Procedures and the Transferability of the Test Results from Specimen to Component*, Nucl. Eng. Des. **119**, 317-327 (1990).

60. W. J. Foley, R. S. Dean, and A. Hennick, *Closeout of IE Bulletin 79–13: Cracking in Feedwater System Piping*, NUREG/CR–5258, U.S. Nuclear Regulatory Commission, Washington, DC (1991).

61. W. H. Bamford, G. V. Rao, and J. L. Houtman, *Investigation of Service–Induced Degradation of Steam Generator Shell*, in Proc. 5th Intl. Symp. on Environmental Degradation of Materials in Nuclear Power Systems – Water Reactors, American Nuclear Society, La Grange Park, IL (1982).

62. NRC Information Notice 88–01, *Safety Injection Pipe Failure*, U.S. Nuclear Regulatory Commission, Washington, DC (Jan. 27, 1988).

63. NRC Bulletin No. 88–08, *Thermal Stresses in Piping Connected to Reactor Coolant Systems*, U.S. Nuclear Regulatory Commission, Washington, DC (June 22; Suppl. 1, June 24; Suppl. 2, Aug. 4, 1988; Suppl. 3, April 1989).

64. V. N. Shah, M. B. Sattison, C. L. Atwood, A. G. Ware, G. M. Grant, and R. S. Hartley, *Assessment of Pressurized Water Reactor Primary System Leaks*, NUREG/CR–6582, INEEL/EXT–97–01068 (Dec. 1998).

65. T. Sakai, *Leakage from CVCS Pipe of Regenerative Heat Exchanger Induced by High–Cycle Thermal Fatigue at Tsuruga Nuclear Power Station Unit 2*, Int. Conf. on Fatigue of Reactor Components, Napa, CA, July 31–August 2, 2000.

66. C. Faidy, T. Le Courtois, E. de Fraguier, J. A. Leduff, A. Lefrancois, and J. Dechelotte, *Thermal Fatigue in French RHR System*, Int. Conf. on Fatigue of Reactor Components, Napa, CA, July 31–August 2, 2000.

67. E. Lenz, A. Liebert, and N. Wieling, *Thermal Stratification Tests to Confirm the Applicability of Laboratory Data on Strain–Induced Corrosion Cracking to Component Behavior*, in 3rd IAEA Specialists Meeting on Sub–Critical Crack Growth, Moscow, pp. 67–91 (1990).

68. H. S. Mehta, *An Update on the EPRI/GE Environmental Fatigue Evaluation Methodology and its Applications*, Probabilistic and Environmental Aspects of Fracture and Fatigues, PVP Vol. 386, S. Rahman, ed., American Society of Mechanical Engineers, New York, pp. 183–193 (1999).

69. M. E. Indig, J. L. Nelson, and G. P. Wozadlo, *Investigation of Protection Potential against IASCC*, in Proc. 5th Intl. Symp. on Environmental Degradation of Materials in Nuclear Power Systems – Water Reactors, D. Cubicciotti, E. P. Simonen, and R. Gold, eds., American Nuclear Society, La Grange Park, IL, pp. 941-947 (1992).

70. M. Kodama, S. Nishimura, J. Morisawa, S. Shima, S. Suzuki, and M. Yamamoto, *Effects of Fluence and Dissolved Oxygen on IASCC in Austenitic Stainless Steels*, in Proc. 5th Intl. Symp. on Environmental Degradation of Materials in Nuclear Power Systems – Water Reactors, D. Cubicciotti, E. P. Simonen, and R. Gold, eds., American Nuclear Society, La Grange Park, IL, pp. 948-954 (1992).

71. H. M. Chung, W. E. Ruther, J. E. Sanecki, A. G. Hins, and T. F. Kassner, *Effects of Water Chemistry on Intergranular Cracking of Irradiated Austenitic Stainless Steels*, in Proc. 7th Intl. Symp. on Environmental Degradation of Materials in Nuclear Power Systems - Water Reactors, G. Airey et al., eds., NACE International, Houston, pp. 1133-1143 (1995).

72. F. Garzarolli, P. Dewes, R. Hahn, and J. L. Nelson, *Deformability of High-Purity Stainless Steels and Ni-Base Alloys in the Core of a PWR*, in Proc. 6th Intl. Symp. on Environmental Degradation of Materials in Nuclear Power Systems - Water Reactors, R. E. Gold and E. P. Simonen, eds., Minerals, Metals, and Materials Society, Warrendale, PA, pp. 607-613 (1993).

73. H. Kanasaki, T. Okubo, I. Satoh, M. Koyama, T. R. Mager, and R. G. Lott, *Fatigue and Stress Corrosion Cracking Behavior of Irradiated Stainless Steels in PWR Primary Water*, in Proc. 5th Intl. Conf. on Nuclear Engineering, March 26-30, Nice, France (1997).

74. A. J. Jacobs, G. P. Wozadlo, K. Nakata, T. Yoshida, and I. Masaoka, *Radiation Effects on the Stress Corrosion and Other Selected Properties of Type-304 and Type-316 Stainless Steels*, in Proc. 3rd Intl. Symp. on Environmental Degradation of Materials in Nuclear Power Systems – Water Reactors, G. J. Theus and J. R. Weeks, eds., Metallurgical Society, Warrendale, PA, pp. 673-680 (1988).

75. K. Fukuya, K. Nakata, and A. Horie, *An IASCC Study Using High Energy Ion Irradiation*, in Proc. 5th Intl. Symp. on Environmental Degradation of Materials in Nuclear Power Systems – Water Reactors, D. Cubicciotti, E. P. Simonen, and R. Gold, eds., American Nuclear Society, La Grange Park, IL, pp. 814–820 (1992).

76. H. M. Chung, W. E. Ruther, J. E. Sanecki, A. G. Hins, and T. F. Kassner, *Stress Corrosion Cracking Susceptibility of Irradiated Type 304 Stainless Steels*, in Effects of Radiation on Materials, 16th Int. Symp., ASTM STP 1175, A. S. Kumar, D. S. Gelles, R. K. Nanstad, and T. A. Little, eds., American Society for Testing and Materials, Philadelphia, pp. 851-869 (1993).

77. H. M. Chung, W. E. Ruther, J. E. Sanecki, and T. F. Kassner, *Grain-Boundary Microchemistry and Intergranular Cracking of Irradiated Austenitic Stainless Steels*, in Proc. 6th Intl. Symp. on Environmental Degradation of Materials in Nuclear Power Systems - Water Reactors, R. E. Gold and E. P. Simonen, eds., Minerals, Metals, and Materials Society, Warrendale, PA, pp. 511-519 (1993).

78. J. M. Cookson, D. L. Damcott, G. S. Was, and P. L. Anderson, *The Role of Microchemical and Microstructural Effects in the IASCC of High-Purity Austenitic Stainless Steels*, ibid., pp. 573-580 (1993).

79. M. Kodama, J. Morisawa, S. Nishimura, K. Asano, S. Shima, and K. Nakata, J. Nucl. Mater. **212–215**, 1509 (1994).

80. T. Tsukada and Y. Miwa, *Stress Corrosion Cracking of Neutron Irradiated Stainless Steels*, in Proc. 7th Int. Symp. on Environmental Degradation of Materials in Nuclear Power Systems - Water Reactors, NACE International, Houston, pp. 1009–1018 (1995).

81. F. Garzarolli, P. Dewes, R. Hahn, and J. L. Nelson, *In-Reactor Testing of IASCC Resistant Stainless Steels*, ibid., pp. 1055–1065 (1995).

82. H. M. Chung, W. E. Ruther, J. E. Sanecki, A. G. Hins, N. J. Zaluzec, and T. F. Kassner, J. Nucl. Mater. **239**, 61 (1996).

83. J. M. Cookson, G. S. Was, and P. L. Anderson, Corrosion **54**, 299 (1998).

84. S. Kasahara, K. Nakata, K. Fukuya, S. Shima, A. J. Jacobs, G. P. Wozadlo, and S. Suzuki, *The Effects of Minor Elements on IASCC Susceptibility in Austenitic Stainless Steels Irradiated with Neutrons*, in Proc. 6th Intl. Symp. on Environmental Degradation of Materials in Nuclear Power Systems - Water Reactors, R. E. Gold and E. P. Simonen, eds., Minerals, Metals, and Materials Society, Warrendale, PA, pp. 615-623 (1993).

85. A. Jenssen and L. G. Ljungberg, *Irradiation Assisted Stress Corrosion Cracking - Postirradiation CERT Tests of Stainless Steels in a BWR Test Loop*, in Proc. 7th Intl. Symp. on Environmental Degradation of Materials in Nuclear Power Systems - Water Reactors, G. Airey et al., eds., NACE International, Houston, pp. 1043–1052 (1995).

86. H. M. Chung, W. E. Ruther, R. V. Strain, W. J. Shack, and T. M. Karlsen, *Irradiation-Assisted Stress Corrosion Cracking of Model Austenitic Stainless Steels*, in Proc. 9th Intl. Conf. on Environmental Degradation of Materials in Nuclear Power Systems - Water Reactors, eds. S. Bruemmer, P. Ford, and G. Was, Minerals, Metals, and Material Society, Warrendale, PA, pp. 931-939 (1999).

87. T. Tsukada, Y. Miwa, H. Nakajima, and T. Kondo, *Effects of Minor Elements on IASCC of Type 316 Model Stainless Steels*, in Proc. 8th Int. Symp. on Environmental Degradation of Materials in Nuclear Power Systems - Water Reactors, Aug. 10-14, 1997, Amelia Island, FL, S. M. Bruemmer, ed., American Nuclear Society, La Grange Park, IL, pp. 795-802 (1997).

88. J. J. de Barbadillo and E. Snape, eds., *Sulfide Inclusions in Steel*, Proc. Intl. Symp., November 7-8, 1974, Port Chester, New York, American Society of Metals (1975).

89. H. M. Chung, J. E. Sanecki, and F. A. Garner, *Radiation–Induced Instability of MnS Precipitates and Its Possible Consequences on Irradiation–Induced Stress Corrosion Cracking of Austenitic Stainless Steels*, in Effects of Radiation on Materials: 18th Intl. Symp., ASTM STP 1325, R. K. Nanstad, M. L. Hamilton, A. S. Kumar, and F. A. Garner, eds., American Society for Testing and Material, pp. 647-658 (1999).

90. P. L. Andresen and C. L. Briant, *Role of S, P, and N Segregation on Intergranular Environmental Cracking of Stainless Steels in High Temperature Water*, in Proc. 3rd Intl. Symp. on Environmental Degradation of Materials in Nuclear Power Systems – Water Reactors, G. J. Theus and J. R. Weeks, eds., Metallurgical Society, Warrendale, PA, pp. 371-381 (1988).

91. H. M. Chung, W. E. Ruther, and R. V. Strain, *Irradiation Assisted Stress Corrosion Cracking of Austenitic SS*, in Environmentally Assisted Cracking in Light Water Reactors, Semiannual Report, January 1999-June 1999, NUREG/CR-4667, Vol. 28, ANL-00/7, pp. 13-27 (July 2000).

92. H. M. Chung, W. E. Ruther, and R. V. Strain, *Irradiation Assisted Stress Corrosion Cracking of Austenitic SS*, in Environmentally Assisted Cracking in Light Water Reactors, Semiannual Report, July–December 1999, NUREG/CR-4667, Vol. 29, ANL-00/23, pp. 17-29 (Nov. 2000).

93. H. M. Chung, D. Perkins, and R. V. Strain, *Irradiation Assisted Stress Corrosion Cracking of Austenitic SS*, in Environmentally Assisted Cracking in Light Water Reactors, Semiannual Report, January 2000-June 2000, NUREG/CR-4667, Vol. 30, ANL-01/08, pp. 17-33 (June 2001).

94. S. M. Bruemmer et al., *Critical Issue Reviews for the Understanding and Evaluation of Irradiation-Assisted Stress Corrosion Cracking*, EPRI TR-107159, Electric Power Research Institute, Palo Alto, CA (1996).

95. M. L. Herrera, et al., *Evaluation of the Effects of Irradiation on the Fracture Toughness of BWR Internal Components*, in Proc. ASME/JSME 4th Intl. Conf. on Nucl. Eng. (ICONE-4), Vol. 5, A. S. Rao, R. M. Duffey, and D. Elias, eds., American Society of Mechanical Engineers, New York, pp. 245–251 (1996).

96. W. J. Mills, *Fracture Toughness of Type 304 and 316 Stainless Steels and their Welds*, Intl. Mater. Rev. **42**, 45–82 (1997).

97. P. J. Maziasz and C. J. McHargue, *Microstructural Evolution in Annealed Austenitic Steels during Neutron Irradiation*, Int. Met. Rev. **32**, 190 (1987).

98. P. J. Maziasz, *Overview of Microstructural Evolution in Neutron-Irradiated Austenitic Stainless Steels*, J. Nucl. Mater. **205**, 118–145 (1993).

99. F. A. Garner, *Evolution of Microstructures in Face-Centered Cubic Metals during Neutron Irradiation*, J. Nucl. Mater. **205**, 98–111 (1993).

100. J. Dufresne, B. Henry, and H. Larsson, *Fracture Toughness of Irradiated AISI 304 and 316L Stainless Steels*, in Effects of Radiation on Structural Materials, ASTM STP 683, J. A. Sprague and D. Kramer, eds., American Society for Testing and Materials, Philadelphia, pp. 511–528 (1979).

101. C. Picker, A. L. Stott, and H. Cocks, *Effects of Low-Dose Fast Neutron Irradiation on the Fracture Toughness of Type 316 Stainless Steel and Weld Metal*, in Proc. Specialists Meeting on Mechanical Properties of Fast Reactor Structural Materials, Chester, UK, Paper IWGFR 49/440–4 (1983).

102. F. H. Huang, *The Fracture Characterization of Highly Irradiated Type 316 Stainless Steel*, Int. J. Fracture **25**, 181–193 (1984).

103. J. Bernard and G. Verzeletti, *Elasto-Plastic Fracture Mechanics Characterization of Type 316H Irradiated Stainless Steel up to 1 dpa*, in Effects of Radiation on Materials, 12th Intl. Symp., ASTM STP 870, F. A. Garner and J. S. Perrin, eds., American Society for Testing and Materials, Philadelphia, pp. 619–641 (1985).

104. W. J. Mills, L. A. James, and L. D. Blackburn, *Results of Fracture Mechanics Tests on PNC SU 304 Plate*, Westinghouse Hanford Report HEDL-7544, Hanford Engineering Development Laboratory, Richland, WA (1985).

105. W. J. Mills, *Fracture Toughness of Irradiated Stainless Steel Alloys*, Nucl. Technol. **82**, 290–303 (1988).

106. D. J. Michel and R. A. Gray, *Effects of Irradiation on the Fracture Toughness of FBR Structural Materials*, J. Nucl. Mater. **148**, 194–203 (1987).

107. P. Ould, P. Balladon, and Y. Meyzaud, *Bull. Cercle Etud. Metaux* **15**, 31.1–31.12 (1988).

108. E. V. Van Osch, M. G. Horsten, and M. I. De Vries, *Fracture Toughness of PWR Internals*, ECN Contribution to CEC Contract on PWR Internals–Part 2 (ETNU/CT/94/0136–F), ECN–I–97–010 (71747/NUC/EvO/mh/006274), Netherlands Energy Research Foundation ECN, Petten, Netherlands (1997).

109. O. K. Chopra, E. E. Gruber, and W. J. Shack, *Fracture Toughness Characterization of Type 304 Stainless Steel Irradiated in the Halden Reactor*, in Proc. 8th Intl. Conference on Nuclear Engineering, 2.02, Aging and Modeling of Component Aging Including Corrosion of Metals and Welds, Paper 8301, American Society of Mechanical Engineers, New York (2000).

110. E. E. Gruber and O. K. Chopra, *Fracture Toughness J–R Test of Austenitic Stainless Steels Irradiated in the Halden Reactor*, in Environmentally Assisted Cracking in Light Water Reactors, Semiannual Report, July–December 1999, NUREG/CR-4667, Vol. 29, ANL-00/23, pp. 30–38 (November 2000).

111. T. H. Hughes and E. E. Gruber, *Development of Hot-Cell J–R Test Facility*, in Environmentally Assisted Cracking in Light Water Reactors Semiannual Report, July 1996–December 1996, NUREG/CR–4667, Vol. 23, ANL–97/10, pp. 42–52 (1997).

112. E. E. Gruber and O. K. Chopra, *Fracture Toughness J–R Test of Austenitic Stainless Steels Irradiated in Halden Reactor*, in Environmentally Assisted Cracking in Light Water Reactors Semiannual Report, July 1998–December 1998, NUREG/CR–4667, Vol. 27, ANL–99/11, pp. 39–45 (Oct. 1999).

113. W. E. Ruther, W. K. Soppet, and T. F. Kassner, *Corrosion Fatigue of Alloys 600 and 690 in Simulated LWR Environments*, NUREG/CR-6383, ANL-95/37 (April 1996).

114. W. E. Ruther, W. K. Soppet, and T. F. Kassner, *Environmentally Assisted Cracking of Alloys 600 and 690 in Simulated LWR Water*, in Environmentally Assisted Cracking in Light Water Reactors, Semiannual Report, July 1997–December 1997, NUREG/CR-4667 Vol. 25, ANL-98/18, pp. 42–75 (Sept. 1998).

115. W. E. Ruther, W. K. Soppet, T. F. Kassner, and W. J. Shack, *Environmentally Assisted Cracking of Alloys 600 and 690 in Simulated LWR Water*, in Environmentally Assisted Cracking in Light Water Reactors, Semiannual Report, January 1998–July 1998, NUREG/CR-4667 Vol. 26, ANL-98/18, pp. 25–32 (March 1999).

116. W. E. Ruther, W. K. Soppet, T. F. Kassner, and W. J. Shack, *Environmentally Assisted Cracking of Alloys 600 and 690 in Simulated LWR Water*, in Environmentally Assisted Cracking in Light Water Reactors, Semiannual Report, July 1998–December 1998, NUREG/CR-4667 Vol. 27, ANL-99/11, pp. 45-54 (October 1999).

117. W. K. Soppet, O. K. Chopra, and W. J. Shack, *Environmentally Assisted Cracking of Alloys 600 and 690 in Simulated LWR Water*, in Environmentally Assisted Cracking in Light Water Reactors, Semiannual Report, July 1999–December 1999, NUREG/CR-4667 Vol. 29, ANL-00/23, pp. 39-45 (November 2000).

118. F. P. Ford, *Overview of Collaborative Research into the Mechanisms of Environmentally Controlled Cracking in the Low Alloy Pressure Vessel Steel/Water System*, Proc. 2nd Int. Atomic Energy Agency Specialists' Meeting on Subcritical Crack Growth, NUREG/CP-0067, MEA-2090, Vol. 2, pp. 3–71 (1986).

119. H. Hänninen, K. Törrönen, and W. H. Cullen, *Comparison of Proposed Cyclic Crack Growth Mechanisms of Low Alloy Steels in LWR Environments*, Proc. 2nd Int. Atomic Energy Agency Specialists' Meeting on Subcritical Crack Growth, NUREG/CP-0067, MEA-2090, Vol. 2, pp. 73–97 (1986).

Appendix A: Fatigue Test Results

Table A1. Fatigue test results for A106–Gr B carbon steel at 288°C

Test Number	Specimen Number	Environ -ment[a]	Dissolved Oxygen[b] (ppb)	pH at RT	Conduc- tivity (μS/cm)	ECP[b] Pt mV (SHE)	ECP[b] Steel mV (SHE)	Tensile Rate (%/s)	Compres- sive Rate (%/s)	Stress Range (MPa)	Strain Range (%)	Life N_{25} (Cycles)
1498	J7-02	Air	–	–	–	–	–	0.4	0.4	1001.4	1.00	1,048
1546	J7-05	Air	–	–	–	–	–	0.4	0.4	975.7	0.92	1,365
1553	J7-12	Air	–	–	–	–	–	0.4	0.4	921.1	0.76	3,253
1554	J7-13	Air	–	–	–	–	–	0.4	0.4	896.8	0.73	3,753
1674[c]	J7-41	Air	–	–	–	–	–	0.4	0.4	1003.6	0.76	6,275
1686[c]	J7-58	Air	–	–	–	–	–	0.4	0.4	1017.2	0.80	2,592
1731	J7-74	Air	–	–	–	–	–	0.4	0.004	1005.5	0.76	3,485
1615	J7-19	Air	–	–	–	–	–	0.04	0.4	959.8	0.76	3,873
1609	J7-09	Air	–	–	–	–	–	0.004	0.4	1026.0	0.76	3,721
1612	J7-17	Air	–	–	–	–	–	0.004	0.4	1008.2	0.78	3,424
1673	J7-40	Air	–	–	–	–	–	0.004	0.4	1003.6	0.76	6,275
1548	J7-07	Air	–	–	–	–	–	0.4	0.4	831.9	0.55	10,632
1543	J7-03	Air	–	–	–	–	–	0.4	0.4	818.2	0.50	14,525
1619	J7-21	Air	–	–	–	–	–	0.4	0.4	741.7	0.40	37,142
1636[d]	J7-29	Air	–	–	–	–	–	0.4	0.4	749.6	0.40	34,829
1621	J7-24	Air	–	–	–	–	–	0.01	0.4	787.1	0.40	38,128
1550	J7-08	Air	–	–	–	–	–	0.4	0.4	681.7	0.35	66,768
1552	J7-11	Air	–	–	–	–	–	0.4	0.4	680.6	0.35	93,322
1555	J7-18	Air	–	–	–	–	–	0.4	0.4	676.3	0.34	98,456
1644	J7-37	Air	–	–	–	–	–	0.004	0.4	702.0	0.36	>94,657
1744[d]	J7-81	DI	<1	6.5	0.082	-452	-597	0.4	0.4	760.5	0.41	19,860
1738[d]	J7-76	DI	1	6.5	0.092	-441	-592	0.004	0.4	976.2	0.78	1,350
1547	J7-04	PWR	8	6.7	23.260	-676	-761	0.4	0.4	1010.9	0.99	692
1564	J7-14	PWR	12	6.6	21.740	-630	-720	0.4	0.4	942.0	0.77	1,525
1676	J7-36	PWR	2	6.5	20.830	-703	-667	0.4	0.4	926.7	0.74	2,230
1679	J7-44	PWR	3	6.5	20.410	-687	-694	0.004	0.4	1005.8	0.76	2,141
1681	J7-53	PWR	1	6.5	20.000	-705	-714	0.0004	0.4	1015.7	0.76	2,672
1549	J7-06	PWR	8	6.7	25.640	-681	-725	0.4	0.4	827.0	0.53	9,396
1560	J7-20	PWR	12	6.6	23.730	-645	-721	0.4	0.4	701.3	0.36	35,190
1556	J7-10	PWR	8	6.6	22.730	-605	-711	0.4	0.4	710.9	0.36	38,632
1632	J7-27	Hi DO	800	5.8	0.110	230	193	0.4	0.4	913.3	0.74	2,077
1705	J7-68	Hi DO	650	5.9	0.150	195	178	0.4	0.4	947.9	0.77	1,756
1680[c]	J7-45	Hi DO	700	6.0	0.080	183	175	0.4	0.4	999.6	0.82	1,007
1690[c]	J7-60	Hi DO	700	6.0	0.080	185	165	0.4	0.4	1002.2	0.82	1,092
1687[e]	J7-55	Hi DO	700	6.0	0.100	207	186	0.4	0.4	1020.0	0.81	840
1757	J7-85	Hi DO	670	5.9	0.072	264	156	0.4	0.0	942.2	0.74	1,195
1693	J7-57	Hi DO	650	6.0	0.100	210	193	0.04	0.4	920.0	0.74	1,125
1694[f]	J7-61	Hi DO	650	6.0	0.080	183	175	0.04	0.4	935.7	0.75	980
1614	J7-16	Hi DO	400	5.9	0.110	155	80	0.004	0.4	930.4	0.79	303
1682	J7-54	Hi DO	700	6.0	0.090	190	181	0.004	0.4	921.1	0.75	469
1725	J7-72	DI	20	5.8	0.150	-235	54	0.004	0.4	926.3	0.74	548
1733	J7-75	DI	2	6.4	0.106	-388	-573	0.004	0.4	1020.7	0.80	2,415
1836	J7-97	Hi DO	880	6.0	0.061	232	197	0.004	0.4	903.1	0.77	470
1696[f]	J7-62	Hi DO	610	5.9	0.070	185	186	0.004	0.4	923.3	0.75	363
1623	J7-25	Hi DO	800	5.9	0.080	209	156	0.004	0.004	943.8	0.79	338
1616	J7-22	Hi DO	800	5.8	0.080	195	155	0.0004	0.4	912.8	0.80	153
1620	J7-23	Hi DO	900	5.9	0.110	225	160	0.00004	0.004	943.1	0.79	161
1706	J7-69	Hi DO	600	5.9	0.070	212	197	0.4	0.4	825.2	0.53	7,858
1634	J7-28	Hi DO	800	5.8	0.160	232	197	0.4	0.4	733.2	0.40	19,318
1624	J7-26	Hi DO	800	5.9	0.100	210	185	0.004	0.4	775.7	0.46	2,276
1639	J7-32	Hi DO	800	5.9	0.090	230	210	0.004	0.4	751.6	0.42	2,951
1643	J7-33	Hi DO	800	6.0	0.110	195	177	0.004	0.4	698.5	0.36	>65,000

[a]DI = deionized water and PWR = simulated PWR water with 2 ppm lithium and 1000 ppm boron.
[b]Represents DO levels and ECP values in effluent water.
[c]Tested with 5–min hold period at peak tensile strain.
[d]Specimen preoxidized in water with 600 ppb DO for 100 h at 288°C.
[e]Tested with 30–min hold period at peak tensile strain.
[f]Tested with sine waveform.

Table A2. Fatigue test results for A533–Gr B low–alloy steel at 288°C

Test Number	Specimen Number	Environ –ment[a]	Dissolved Oxygen[b] (ppb)	pH at RT	Conduc- tivity (μS/cm)	ECP[b] Pt mV (SHE)	ECP[b] Steel mV (SHE)	Tensile Rate (%/s)	Compres- sive Rate (%/s)	Stress Range (MPa)	Strain Range (%)	Life N_{25} (Cycles)
1508	44-02	Air	–	–	–	–	–	0.4	0.4	910.9	1.002	3,305
1524	44-09	Air	–	–	–	–	–	0.4	0.4	892.3	0.950	3,714
1523	44-08	Air	–	–	–	–	–	0.4	0.4	898.6	0.917	2,206
1521	44-06	Air	–	–	–	–	–	0.4	0.4	889.4	0.910	3,219
1522	44-07	Air	–	–	–	–	–	0.4	0.4	905.4	0.899	3,398
1515	44-03	Air	–	–	–	–	–	0.4	0.4	866.1	0.752	6,792
1749[c]	44-61	Air	–	–	–	–	–	0.4	0.4	–	–	6,372
1717	44-51	Air	–	–	–	–	–	0.4	0.004	884.6	0.758	6,217
1625	44-25	Air	–	–	–	–	–	0.004	0.4	887.7	0.757	4,592
1865	44-82	Air	–	–	–	–	–	0.0004	0.4	907.5	0.749	5,930
1629[d]	44-28	Air	–	–	–	–	–	0.4	0.4	782.9	0.503	31,243
1590	44-24	Air	–	–	–	–	–	0.4	0.004	821.1	0.503	24,471
1576	44-19	Air	–	–	–	–	–	0.004	0.4	805.8	0.503	28,129
1505	44-01	Air	–	–	–	–	–	0.4	0.4	767.6	0.501	31,200
1525	44-10	Air	–	–	–	–	–	0.4	0.4	743.6	0.452	65,758
1640	44-29	Air	–	–	–	–	–	0.4	0.4	710.9	0.402	65,880
1798	44-73	Air	–	–	–	–	–	0.4	0.4	715.6	0.399	115,119
1538	44-17	Air	–	–	–	–	–	0.4	0.4	708.0	0.387	>1,000,000
1517	44-05	Air	–	–	–	–	–	0.4	0.4	692.5	0.353	2,053,295
1659	44-46	Air	–	–	–	–	–	0.004	0.4	656.2	0.343	>114,294
1526	44-11	DI	–	–	–	–	–	0.4	0.4	876.4	0.873	3,332
1527	44-12	DI	–	6.0	–	–	–	0.4	0.4	752.8	0.493	10,292
1528	44-13	DI	5	5.8	–	–	–	0.4	0.4	744.1	0.488	25,815
1743[e]	44-59	DI	<1	6.5	0.08	-405	-465	0.4	0.4	712.6	0.386	84,700
1530	44-15	PWR	3	6.9	41.67	-716	-730	0.4	0.4	885.5	0.894	1,355
1545	44-21	PWR	8	6.9	22.73	-684	-729	0.4	0.4	889.7	0.886	3,273
1533	44-16	PWR	4	6.9	45.45	-722	-764	0.004	0.4	916.0	0.774	3,416
1529	44-14	PWR	3	6.9	45.45	-718	-737	0.4	0.4	743.4	0.484	31,676
1605	44-22	PWR	9	6.5	23.81	-678	-689	0.4	0.004	785.2	0.460	>57,443
1588	44-23	PWR	6	6.5	23.26	-675	-668	0.004	0.4	828.7	0.514	15,321
1539	44-18	PWR	6	6.8	38.46	-645	-670	0.4	0.4	690.9	0.373	136,570
1542	44-20	PWR	6	6.6	27.03	-700	-740	0.4	0.4	631.8	0.354	>1,154,892
1645	44-31	Hi DO	800	6.1	0.07	-697	-697	0.4	0.4	831.1	0.721	2,736
1768	44-63	Hi DO	600	6.0	0.07	248	206	0.4	0.004	907.3	0.755	1,350
1626	44-26	Hi DO	900	5.9	0.13	225	200	0.004	0.4	910.1	0.788	247
1715	44-41	Hi DO	600	5.9	0.08	198	182	0.004	0.4	904.1	0.813	381
1864	44-81	Hi DO	630	6.5	0.083	343	202	0.004	0.4	895.8	0.746	340
1866	44-83	Hi DO	730	6.3	0.063	361	263	0.0004	0.4	889.9	0.748	137
1867	44-84	Hi DO	780	6.5	0.061	337	229	0.00004	0.4	897.0	0.738	123
1718	44-47	Hi DO	240	6.1	0.390	124	127	0.004	0.4	904.3	0.807	346
1720	44-52	Hi DO	45	5.8	0.095	-58	116	0.004	0.4	905.9	0.806	330
1735	44-56	Hi DO	25	6.1	0.188	25	212	0.004	0.4	909.7	0.812	502
1723	44-53	Hi DO	20	5.9	0.080	-249	82	0.004	0.4	907.2	0.807	371
1730	44-55	Hi DO	5	6.6	0.088	-368	-551	0.004	0.4	911.7	0.803	1,900
1736	44-58	Hi DO	1	6.1	0.073	-381	-151	0.004	0.4	934.2	0.810	1,447
1711	44-45	Hi DO	630	5.8	0.31	234	220	0.4	0.4	772.1	0.542	5,850
1707	44-42	Hi DO	650	5.9	0.08	155	140	0.4	0.004	803.0	0.488	3,942
1709	44-44	Hi DO	650	5.9	0.11	195	180	0.4	0.004	805.1	0.501	3,510
1627	44-27	Hi DO	800	5.9	0.10	229	210	0.004	0.4	826.8	0.534	769
1641	44-30	Hi DO	800	5.9	0.09	176	160	0.4	0.4	693.0	0.385	17,367
1665	44-38	Hi DO	800	6.1	0.08	200	189	0.004	0.4	717.0	0.376	3,455
1666	44-40	Hi DO	750	6.1	0.09	195	187	0.0004	0.4	729.6	0.376	>7,380
1647	44-32	Hi DO	800	6.1	0.09	215	201	0.4	0.4	688.0	0.380	26,165
1660	44-37	Hi DO	750	6.1	0.11	200	185	0.004	0.4	689.6	0.360	>83,024
1649	44-33	Hi DO	700	6.3	0.08	208	196	0.4	0.4	673.4	0.352	28,710
1652	44-34	Hi DO	700	6.1	0.09	214	202	0.4	0.4	638.1	0.328	56,923
1655	44-36	Hi DO	750	6.1	0.10	191	179	0.4	0.4	567.6	0.289	>1,673,954

[a]DI = deionized water and PWR = simulated PWR water with 2 ppm lithium and 1000 ppm boron.
[b]Represents DO levels and ECP values in effluent water.
[c]Tested with 5–min hold period at peak tensile strain.
[d]Specimen preoxidized in water with 600 ppb DO for 100 h at 288°C.
[e]Specimen preoxidized in water with 600 ppb DO for 30 h at 288°C.

Table A3. Fatigue test results for A106–Gr B and A533–Gr B steels at room temperature

Test Number	Specimen Number	Environ -ment[a]	Dissolved Oxygen[b] (ppb)	pH at RT	Conduc- tivity (μS/cm)	ECP[b] Pt mV (SHE)	ECP[b] Steel mV (SHE)	Tensile Rate (%/s)	Compres- sive Rate (%/s)	Stress Range (MPa)	Strain Range (%)	Life N_{25} (Cycles)
A106 Gr B												
1700	J7-67	Air	–	–	–	–	–	0.4	0.4	715.2	0.76	6,574
1766	J7-86	Air	–	–	–	–	–	0.4	0.4	719.7	0.76	7,120
1770	J7-92	Air	–	–	–	–	–	0.4	0.4	608.5	0.40	37,379
1699	J7-66	Hi DO	850	6.0	0.070	–	–	0.4	0.4	728.7	0.75	4,794
1772	J7-89	Hi DO	745	6.2	0.074	–	–	0.4	0.4	618.7	0.40	23,300
A533 Gr B												
1727	44-54	Air	–	–	–	–	–	0.4	0.4	766.7	0.76	9,145
1785	44-68	Air	–	–	–	–	–	0.4	0.4	763.7	0.76	8,840
1779	44-67	Air	–	–	–	–	–	0.004	0.4	759.8	0.76	5,960
1729	44-57	Air	–	–	–	–	–	0.4	0.4	677.5	0.41	77,759
1786	44-71	Air	–	–	–	–	–	0.4	0.4	687.7	0.40	61,100
1795	44-54	Air	–	–	–	–	–	0.4	0.4	694.6	0.40	82,050
1759	44-60	Hi DO	610	6.1	0.068	–	–	0.4	0.4	774.7	0.75	6,250
1761	44-62	Hi DO	770	6.1	0.080	–	–	0.4	0.4	694.5	0.40	46,500

[a]DI = deionized water and PWR = simulated PWR water with 2 ppm lithium and 1000 ppm boron.
[b]Represents DO levels and ECP values in effluent water.

Table A4. Fatigue test results for A302–Gr B low–alloy steel at 288°C

Test Number	Specimen Number[a]	Environ -ment[b]	Dissolved Oxygen[c] (ppb)	pH at RT	Conduc- tivity (μS/cm)	ECP[c] Pt mV (SHE)	ECP[c] Steel mV (SHE)	Tensile Rate (%/s)	Compres- sive Rate (%/s)	Stress Range (MPa)	Strain Range (%)	Life N_{25} (Cycles)
1697	214-C01	Air	–	–	–	–	–	0.4	0.4	944.5	0.76	8,070
1780	214-R03	Air	–	–	–	–	–	0.4	0.4	908.6	0.76	1,598
1809	214-A03	Air	–	–	–	–	–	0.4	0.4	938.8	0.76	7,220
1701	214-C02	Air	–	–	–	–	–	0.004	0.4	1021.4	0.76	4,936
1828	214-C15	Air	–	–	–	–	–	0.004	0.4	1019.5	0.76	3,945
1781	214-R04	Air	–	–	–	–	–	0.004	0.4	952.4	0.76	375
1830	214-A08	Air	–	–	–	–	–	0.004	0.4	1014.2	0.76	4,650
1712[d]	214-C07	Air	–	–	–	–	–	0.0004	0.4	1041.9	0.76	5,350
1789	214-C09	Air	–	–	–	–	–	0.4	0.4	859.5	0.51	46,405
1783	214-C08	Air	–	–	–	–	–	0.4	0.4	796.1	0.41	1,044,000
1782	214-R05	Air	–	–	–	–	–	0.4	0.4	752.8	0.40	33,650
1811	214-A04	Air	–	–	–	–	–	0.4	0.4	770.1	0.40	1,300,000
1787	214-R07	Air	–	–	–	–	–	0.4	0.4	667.5	0.34	431,150
1702	214-C03	PWR	3	6.5	20.0	-682	-700	0.4	0.4	921.2	0.74	6,212
1776	214-R02	PWR	1	6.4	18.4	-707	-625	0.4	0.4	887.1	0.77	1,244
1777	214-A02	PWR	1	6.4	19.2	-701	-735	0.4	0.4	913.8	0.77	4,366
1704	214-C04	PWR	3	6.5	19.2	-695	-710	0.004	0.4	1022.6	0.75	3,860
1774	214-R01	PWR	2	6.4	19.4	-747	-774	0.004	0.4	949.7	0.76	348
1775	214-A01	PWR	1	6.5	19.4	-722	-752	0.004	0.4	995.6	0.75	1,458
1837	214-A09	PWR	3	6.5	18.2	-654	-644	0.004	0.4	1005.7	0.75	4,070
1716[d]	214-C05	PWR	5	6.5	19.2	-693	-717	0.0004	0.4	1042.3	0.74	3,718
1833	214-C12	Hi DO	345	6.4	0.06	–	–	0.004	0.4	959.8	0.75	330
1788	214-C06	Hi DO	650	5.9	0.10	-97	197	0.004	0.4	957.0	0.75	317
1784	214-R06	Hi DO	510	6.0	0.07	257	214	0.004	0.4	937.6	0.75	111
1813	214-A05	Hi DO	880	6.0	0.12	250	209	0.004	0.4	963.4	0.76	238
1822	214-C10	Hi DO	600	5.9	0.07	207	192	0.004	0.4	848.6	0.49	550
1820	214-R08	Hi DO	660	6.0	0.07	240	196	0.004	0.4	847.3	0.48	360
1819	214-A06	Hi DO	700	6.0	0.08	259	178	0.004	0.4	868.0	0.48	755

[a]Specimen ID numbers with C = rolling direction, R = radial direction, and A = transverse direction.
[b]DI = deionized water and PWR = simulated PWR water with 2 ppm lithium and 1000 ppm boron.
[c]Represents DO levels and ECP values in effluent water.
[d]Slow strain rate applied only during 1/8 cycle near peak tensile strain.

Table A5. Fatigue test results for Type 316NG austenitic stainless steel

Test Number	Specimen Number	Environ -ment[a]	Dissolved Oxygen[b] (ppb)	pH at RT	Conduc- tivity[c] (μS/cm)	ECP[b] Pt mV (SHE)	ECP[b] Steel mV (SHE)	Tensile Rate (%/s)	Compres- sive Rate (%/s)	Stress Range (MPa)	Strain Range (%)	Life N_{25} (Cycles)
25°C												
1394	S-12	Air	–	–	–	–	–	0.99	0.99	694.7	1.51	4,649
1391	S-08	Air	–	–	–	–	–	0.66	0.66	554.8	1.00	13,561
1390	S-01	Air	–	–	–	–	–	0.50	0.50	518.1	0.75	25,736
1396	S-07	Air	–	–	–	–	–	0.50	0.50	506.7	0.76	30,000
1420	S-30	Air	–	–	–	–	–	0.49	0.49	495.3	0.49	54,249
1392	S-09	Air	–	–	–	–	–	0.33	0.33	475.9	0.51	60,741
1393	S-10	Air	–	–	–	–	–	0.27	0.27	464.7	0.41	127,386
1395	S-13	Air	–	–	–	–	–	0.23	0.23	456.7	0.35	183,979
1397	S-21	Air	–	–	–	–	–	0.20	0.20	446.0	0.30	347,991
1398	S-15	Air	–	–	–	–	–	0.18	0.18	436.7	0.27	666,000
1399	S-16	Air	–	–	–	–	–	0.17	0.17	431.8	0.25	>1,900,000
1400	S-17	Air	–	–	–	–	–	0.17	0.17	427.4	0.25	1,775,000
288°C												
1408	S-22	Air	–	–	–	–	–	0.50	0.50	416.6	0.76	21,548
1790	S-46	Air	–	–	–	–	–	0.005	0.50	452.8	0.75	16,765
1409	S-23	Air	–	–	–	–	–	0.50	0.50	377.2	0.50	53,144
1410	S-25	Air	–	–	–	–	–	0.50	0.50	377.6	0.50	51,194
1792	S-49	Air				-20.3	-20.3	0.005	0.50	413.4	0.51	35,710
1407	S-24	Air	–	–	–	–	–	0.27	0.27	364.4	0.40	82,691
1430	S-36	Air	–	–	–	–	–	0.20	0.20	348.3	0.30	168,852
1435	S-38	Air	–	–	–	–	–	0.17	0.17	342.0	0.25	314,352
1480	S-40	Air	–	–	–	–	–	0.16	0.16	340.1	0.25	319,308
1485	S-41	Air	–	–	–	–	–	0.17	0.17	340.4	0.25	369,206
320°C												
1405	S-19	Air	–	–	–	–	–	0.50	0.50	426.0	0.75	20,425
1404	S-18	Air	–	–	–	–	–	0.50	0.50	387.4	0.50	47,011
1406	S-20	Air	–	–	–	–	–	0.50	0.50	371.6	0.40	82,691
288°C												
1796	S-47	PWR	5	6.40	20.202	-681	-677	0.50	0.50	403.6	0.80	12,500
1812	S-45	PWR	2	6.48	20.000	-693	-690	0.05	0.50	413.9	0.80	6,375
1791	S-51	PWR	4	6.45	19.230	-701	-701	0.005	0.50	441.9	0.77	3,040
1793	S-50	PWR	4	6.41	19.230	-703	-704	0.005	0.50	434.3	0.80	3,020
1794	S-48	PWR	4	6.40	20.000	-694	-693	0.005	0.50	390.9	0.50	7,370
1814	S-44	PWR	1	6.50	20.000	-698	-695	0.05	0.50	348.7	0.29	33,200
1426	S-32	Hi DO	>200	–	–	-8	-18	0.80	0.80	405.1	0.80	12,069
1427	S-33	Hi DO	>200	–	–	-8	–	0.08	0.08	421.7	0.82	6,679
1428	S-34	Hi DO	>200	–	–	-4	-18	0.007	0.007	441.4	0.74	5,897
1797	S-43	Hi DO	750	5.90	0.076	195	60	0.005	0.50	437.3	0.78	4,520
1414	S-26	Hi DO	>200	–	–	–	–	0.50	0.50	375.3	0.50	26,230
1418	S-28	Hi DO	>200	–	–	–	–	0.50	0.50	375.5	0.50	25,714
1423	S-29	Hi DO	>200	–	–	-63	25	0.05	0.05	378.8	0.50	17,812
1425	S-31	Hi DO	>200	–	–	-37	-15	0.00	0.00	393.2	0.49	13,684
1431	S-35	Hi DO	>200	–	–	-26	-22	0.29	0.29	356.5	0.29	116,754
1434	S-37	Hi DO	>200	–	–	-5	-18	0.03	0.03	350.0	0.29	40,643
1436	S-39	Hi DO	>200	–	–	-5	-13	0.25	0.25	354.0	0.25	>1,719,851
1512	S-42	Hi DO	>200	–	–	35	90	0.24	0.24	361.2	0.24	2,633,954

[a]DI = deionized water and PWR = simulated PWR water with 2 ppm lithium and 1000 ppm boron. Specimens tested in high DO water were soaked only for 24 h; the ECP values had not stabilized at the start of the test.

[b]Represents DO levels and ECP values in effluent water.

[c]Conductivity of water measured in feedwater supply tank.

Table A6. Fatigue test results for Type 304 austenitic stainless steel at 288°C

Test Number	Specimen Number	Environ -ment[a]	Dissolved Oxygen[b] (ppb)	pH at RT	Conduc- tivity[c] (μS/cm)	ECP[b] Pt mV (SHE)	ECP[b] Steel mV (SHE)	Tensile Rate (%/s)	Compres- sive Rate (%/s)	Stress Range (MPa)	Strain Range (%)	Life N_{25} (Cycles)
1801	309-01	Air	–	–	–	–	–	0.4	0.4	419.2	0.76	24,500
1805	309-03	Air	–	–	–	–	–	0.004	0.4	467.9	0.76	14,410
1804	309-02	Air	–	–	–	–	–	0.4	0.4	382.8	0.51	61,680
1817	309-12	Air	–	–	–	–	–	0.004	0.4	421.7	0.51	42,180
1825	309-08	Air	–	–	–	–	–	0.04	0.4	394.4	0.30	>625,860[d]
1846	309-16	Air	–	–	–	–	–	0.04	0.4	396.4	0.32	>316,000
1806	309-04	PWR	4	6.0	18.867	-682	-679	0.4	0.4	428.9	0.73	11,500
1810	309-07	PWR	5	6.4	18.887	-688	-685	0.04	0.4	447.6	0.77	5,800
1808	309-06	PWR	4	6.4	18.868	-693	-690	0.004	0.4	468.3	0.77	2,850
1821	309-09	PWR	2	6.5	22.222	-700	-697	0.004	0.4	474.3	0.76	2,420
1859	309-28	PWR	2	6.5	18.692	-699	-696	0.004	0.4	471.7	0.77	2,420
1861	309-36	DI	1	6.2	0.059	-601	-614	0.004	0.4	463.0	0.79	2,620
1862	309-27	DI	2	6.2	0.058	-608	-607	0.004	0.4	466.1	0.78	2,450
1863	309-31	DI	1	6.3	0.061	-446	-540	0.004	0.4	476.5	0.77	2,250
1829	309-15	PWR	2	6.5	18.182	-705	-705	0.0004	0.4	493.6	0.73	1,560
1834	309-19	PWR	2	6.5	18.182	-711	-712	0.0001	0.4	535.9	0.69	1,415
1807	309-05	PWR	4	6.5	18.868	-685	-682	0.4	0.4	374.6	0.51	25,900
1823	309-10	PWR	3	6.6	23.055	-701	-699	0.004	0.4	408.2	0.51	6,900
1826	309-13	PWR	2	6.5	18.762	-711	-710	0.01	0.4	375.8	0.29	>89,860[e]
1847	309-17	PWR	5	6.5	18.868	-700	-696	0.01	0.4	388.9	0.32	>165,300[f]
1827[g]	309-14	Hi DO	850	6.0	0.086	254	76	0.004	0.4	475.8	0.75	3,650
1860[g]	309-29	Hi DO	810	6.1	0.560	273	125	0.004	0.4	468.3	0.77	3,050
1852	309-18	Hi DO	790	6.1	0.061	235	149	0.4	0.4	429.1	0.74	10,800
1853	309-22	Hi DO	880	6.1	0.059	248	155	0.004	0.4	466.5	0.76	12,300
1855	309-23	Hi DO	890	6.0	0.115	275	150	0.004	0.4	464.4	0.77	8,080
1856	309-24	Hi DO	870	6.2	0.074	272	163	0.004	0.4	473.6	0.75	10,450
1857	309-30	Hi DO	790	6.1	0.420	254	143	0.004	0.4	461.9	0.78	5,300
1845	309-21	Hi DO	870	6.0	0.063	270	181	0.0004	0.4	488.7	0.71	>7,310
1869	309-33	Hi DO	720	6.1	0.059	253	201	0.4	0.4	375.0	0.51	24,100
1868	309-32	Hi DO	760	6.1	0.059	261	126	0.004	0.4	419.4	0.50	33,900

[a]DI = deionized water and PWR = simulated PWR water with 2 ppm lithium and 1000 ppm boron. Specimens tested in high DO water were soaked for ≈120 h for the ECP values to stabilize.

[b]Represents DO levels and ECP values in effluent water.

[c]Conductivity of water measured in feedwater supply tank.

[d]Specimen failed after additional 331,300 cycles at 0.322% strain range.

[e]Specimen failed after additional 41,240 cycles at 0.315% strain range.

[f]Specimen failed after additional 50,700 cycles at 0.343% strain range.

[g]Specimens were soaked only for 24 h; the ECP values had not stabilized at the start of the test.

Table A7. Fatigue test results for CF–8M cast stainless steels at 288°C

Test Number	Specimen Number	Environ -ment[a]	Dissolved Oxygen[b] (ppb)	pH at RT	Conduc- tivity[c] (μS/cm)	ECP[b] Pt mV (SHE)	ECP[b] Steel mV (SHE)	Tensile Rate (%/s)	Compres- sive Rate (%/s)	Stress Range (MPa)	Strain Range (%)	Life N_{25} (Cycles)
Unaged Heat #74												
1831	U74–01	Air	–	–	–	–	–	0.4	0.4	429.7	0.76	26,500
1832	U74–05	Air	–	–	–	–	–	0.004	0.4	534.0	0.76	9,050
1848	U74–06	Air	–	–	–	–	–	0.004	0.4	440.7	0.76	17,900
1850	U74–02	PWR	5	6.5	17.241	-695	-693	0.004	0.4	419.5	0.76	10,700
1854	U74–03	PWR	2	6.5	18.692	-699	-695	0.004	0.4	448.4	0.75	4,720
Aged Heat #74												
1839	A74–01	Air	–	–	–	–	–	0.4	0.4	474.2	0.76	15,293
1840	A74–05	Air	–	–	–	–	–	0.004	0.4	534.8	0.75	19,800
1851	A74–04	PWR	4	6.5	18.182	-700	-699	0.4	0.4	482.1	0.75	6,420
1844	A74–03	PWR	2	6.5	18.182	-671	-690	0.004	0.4	527.7	0.72	2,180
1842	A74–02	BWR	820	6.1	0.063	267	141	0.004	0.4	508.5	0.75	1,375
Aged Heat #75												
1835	A75–01	Air	–	–	–	–	–	0.004	0.4	631.2	0.76	7,200
1843	A75–03	PWR	2	6.5	18.182	-572	-580	0.004	0.4	625.3	0.80	1,464
1838	A75–02	BWR	870	6.5	0.061	257	109	0.004	0.4	636.1	0.78	1,320

[a]DI = deionized water and PWR = simulated PWR water with 2 ppm lithium and 1000 ppm boron.
[b]Represents DO levels and ECP values in effluent water.
[c]Conductivity of water measured in feedwater supply tank.

NRC FORM 335 (2-89) NRCM 1102, 3201, 3202

U.S. NUCLEAR REGULATORY COMMISSION

BIBLIOGRAPHIC DATA SHEET

(See instructions on the reverse)

1. REPORT NUMBER (Assigned by NRC, Add Vol., Supp., Rev., and Addendum Numbers, if any.)

NUREG/CR-4667, Vol 31
ANL-01/09

2. TITLE AND SUBTITLE

Environmentally Assisted Cracking in Light Water Reactors

Semiannual Report
July 2000 - December 2000

3. DATE REPORT PUBLISHED

MONTH	YEAR
April	2002

4. FIN OR GRANT NUMBER

N/A

5. AUTHOR(S)

O.K. Chopra, H.M. Chung, E.E. Gruber,
W.J. Shack, W.K. Soppett, and R.V. Strain

6. TYPE OF REPORT

Technical (Semiannual)

7. PERIOD COVERED *(Inclusive Dates)*

July - December 2000

8. PERFORMING ORGANIZATION - NAME AND ADDRESS *(If NRC, provide Division, Office or Region, U.S. Nuclear Regulatory Commission, and mailing address; if contractor, provide name and mailing address.)*

Argonne National Laboratory
9700 South Cass Avenue
Argonne, IL 60439

9. SPONSORING ORGANIZATION - NAME AND ADDRESS *(If NRC, type "Same as above"; if contractor, provide NRC Division, Office or Region, U.S. Nuclear Regulatory Commission, and mailing address.)*

Division of Engineering Technology
Office of Nuclear Regulatory Research
U.S. Nuclear Regulatory Commission
Washington, DC 20555-0001

10. SUPPLEMENTARY NOTES

M.B. McNeil, NRC Project Manager

11. ABSTRACT *(200 words or less)*

This report summarizes work performed by Argonne National Laboratory on fatigue and environmentally assisted cracking (EAC) in light water reactors (LWRs) from July 2000 through December 2000. Topics that have been investigated include (a) environmental effects on fatigue S-N behavior of primary pressure boundary materials, (b) irradiation-assisted stress corrosion cracking (IASCC) of austenitic stainless steels (SSs), and (c) EAC of Alloys 600 and 690. The fatigue strain-vs.-life data are summarized for the effectos of various material, loading, and environmental parameters on the fatigue lives of carbon and low-alloy steels and austenitic SSs. Slow-strain-rate tensile tests and post-test fractographic analyses have been conducted on several irradiated SS alloys to determine the influence of alloying and impurity elements on the susceptibility of these steels to IASCC. Fracture toughness J-R curve test was performed on a commercial heat of Type 304 SS that was irradiated to $\approx 2.0 \times 10^{21}$ n·cm^{-2}, the results were compared with the data obtained earlier on steels irradiated to 0.3 and 0.9×10^{21} n·cm^{-2}. Tests were also conducted on compact-tension specimens of Alloy 600 under cyclic loading to evaluate the enhancement of crack growth rates in LWR environments.

12. KEY WORDS/DESCRIPTORS *(List words or phrases that will assist researchers in locating the report.)*

Corrosion Fatigue
Crack Growth
Irradiation-Assisted Stress Corrosion Cracking
Radiation-Induced Segregation
Stress Corrosion Cracking
Carbon and Low-Alloy Steels
Types 304, 304L, 316, and 316NG Stainless Steel
Alloys 600 and 690

13. AVAILABILITY STATEMENT

unlimited

14. SECURITY CLASSIFICATION

(This Page)
unclassified

(This Report)
unclassified

15. NUMBER OF PAGES

16. PRICE

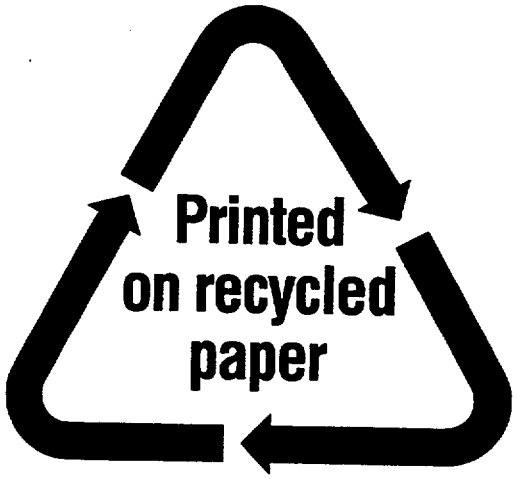

Federal Recycling Program